

PhD degree in Systems Medicine
Curriculum in Molecular Oncology
European School of Molecular Medicine (SEMM),
University of Milan and University of Naples “Federico II”
Settore disciplinare: MED/04



UNIVERSITÀ
DEGLI STUDI
DI MILANO

Intra-tumoral infiltration of GZMK^{high} CD8⁺ T effector
memory cells is associated with poor clinical outcome in
non-metastatic colorectal cancer.

Silvia Tiberti

European Institute of Oncology (IEO)

Tutor: Dr. Teresa Manzo

Co-tutor: Dr. Stefano Santaguida

PhD Coordinator: Prof. Saverio Minucci

Academic year: 2021-2022

Table of Contents

Abbreviations	3
List of the tables	7
List of the figures	7
Abstract	9
Introduction	10
1. Colorectal Cancer and its classification	10
2. Heterogeneity of CRC TME	13
3. CD8 ⁺ T cells and anti-tumor response	15
a. CD8 ⁺ T cells and tumor reactivity	15
b. CD8 ⁺ T cell dysfunction in solid tumors	16
4. CD8 ⁺ T cells crosstalk with tumor immune compartment	19
a. CD4 ⁺ T cells	19
b. B cells	21
c. Dendritic cells	22
d. Macrophages	23
e. Granulocytes	24
f. Neutrophils	26
i. Neutrophils in solid tumor	26
ii. Neutrophils-T cells interaction	28
5. Multiomics approaches to dissect tumor heterogeneity	30
Methods	32
1. Ethics approval for the research	32
2. Cell lines	33
3. Tissue dissociation and cells isolation	33
4. Multiparametric flow cytometry (MPFC) and sorting	35
5. MPFC data analysis	36
6. Immunohistochemistry (IHC), Immunofluorescence (IF), and GIEMSA staining	37
7. Imaging analysis	37
8. <i>In vitro</i> CD8 ⁺ T Cells and Neutrophils co-culture and treatment with Interstitial fluid (InF)	39
9. <i>In vitro</i> GZMK and SDF1 treatment	39
10. Neutrophils migration assay	40
11. Neutrophils gelatinase assay	41

12.	Neutrophils adhesion assay	41
13.	<i>In vivo</i> animal experiments	41
14.	Bead-based multiplexed ELISA	42
15.	Single cell RNA sequencing (scRNAseq)	43
16.	RNA sequencing	43
17.	RNA data analysis ²¹⁹	43
18.	Survival analysis methods ²¹⁹	44
19.	Statistics and Data visualization.	44
	Results	45
1.	Immune-profile in non-metastatic CRC patients	45
2.	CRC TME is mainly infiltrated by CD8 ⁺ effector memory T (T _{EM}) cells	46
3.	The TME of CRC is infiltrated by two main CD8 ⁺ T cell populations identified by differential expression of CD39 and GZMK	50
4.	GZMK expression correlates with a distinct transcriptional program in CD8 ⁺ T _{EM}	54
5.	The transcriptional signature of GZMK ⁺ CD8 ⁺ T _{EM} predicts prognosis in CRC patients	60
6.	GZMK produced by infiltrating CD8 ⁺ T _{EM} is associated with early relapse in CRC	63
7.	CRC tumors are highly infiltrated by neutrophils	64
8.	CRC patients can be stratified based on the abundance of CD15 ^{high} neutrophils in the TME	65
9.	CD15 ^{high} neutrophils accumulating in HN tumors hold a N2-like pro-tumoral phenotype	67
10.	CD15 ^{high} neutrophils are retained in the TME of HN CRC tumors	68
11.	Stromal cell-derived factor 1 (SDF-1) reshape the functional state of infiltrating neutrophils, promoting their differentiation and retention within the TME	71
12.	CD15 ^{high} neutrophils abundance directly correlates with GZMK expression of CD8 ⁺ T cells	73
13.	Neutrophil/CD8 ⁺ T cell interaction influences tumor control in an <i>in vivo</i> mouse model of CRC	78
14.	Direct neutrophil/CD8 ⁺ T cell interaction is required for skewing CD8 ⁺ T cell to produce high levels of GZMK	81
15.	The GZMK produced by infiltrating CD8 ⁺ T _{EM} promotes relapse by reducing E-Cadherin expression in CRC tumors	84
	Discussion	87
	Conclusions	92
	Bibliography	94
	Appendix: List of papers published or submitted during the PhD	114

Abbreviations

MPFC: Multiparametric flow cytometry
ELISA: multiplex enzyme-linked immunosorbent assay
scRNAseq: single cell RNA sequencing
CRC: Colorectal cancer
TME: tumor micro-environment
GZMK: Granzyme K
T_{EM}: T effector memory
SDF-1: stromal cell-derived factor 1
TCGA-COAD: the Cancer Genome Atlas Colon Adenocarcinoma
EMT: epithelial to mesenchymal transition
TNM: Tumor-node-metastasis
dMMR: DNA mismatch repair
MSI microsatellite-unstable
MSS microsatellite-stable
PD1: programmed cell death protein 1
CTLA4: cytotoxic T lymphocyte-associated antigen 4
LAG3: Lymphocyte-activation gene 3
CMS: Consensus Molecular Subtypes
CAF: cancer-associated fibroblast
CXCL12: C-X-C Motif Chemokine Ligand 12
TIME: tumor immune microenvironment
I-E: infiltrated–excluded
I-I: infiltrated–inflamed
I-TLS: infiltrated-TLS
TLS: Tertiary Lymphoid Structures
DC: dendritic cell
TIL: tumor infiltrating lymphocyte
Treg: T regulatory cell
MDSC: Myeloid derived suppressor cell
TAM: tumor associated macrophage
NSCLC: non-small cell lung cancer
TRACERx: TRACKing non-small cell lung Cancer Evolution through therapy [Rx]
LCFA: long chain fatty acid
TCR: T cell receptor

CTL: cytotoxic T cell
PRF: perforin
GZM: granzyme
GNLY: granulysin1
ILC: Innate lymphoid cell
ICB: immune checkpoint blockade
TF: transcription factors
TMB Tumor Mutational Burden
ADCC: antibody-dependent cellular cytotoxicity
PB: peripheral blood
TME: tumor microenvironment
GM-CSF: Granulocyte-macrophage colony-stimulating factor
FLT3L: Fms Related Receptor Tyrosine Kinase 3 Ligand
ROS: Reactive Oxygen Species
TAN: Tumor-Associated Neutrophils
CR3: Complement Receptor 3
NO: Nitric Oxide
G-CSF: granulocyte colony-stimulating factor
CXCL8: CXC-chemokine ligand 8
CXCL5: CXC-chemokine ligand 5
CCL2: CC-chemokine ligand 2
LPS: lipopolysaccharide
IFN β : interferon β
H₂O₂: hydrogen peroxide
IgG: immunoglobulin G
Fc γ R: Fc γ receptor
Fc α RI: IgA Fc receptor
MPO: myeloperoxidase
NET: Neutrophils Extracellular Trap
ECM: extracellular matrix
MMP-9: Matrix metalloproteinase 9
NE: neutrophil elastase
TGF β R: transforming growth factor- β receptor
ROS: reactive oxygen species
PGE2: prostaglandin E2
UTC $\alpha\beta$: unconventional $\alpha\beta$ T cell

$\gamma\delta$ T: Gamma delta T cells
IFN γ : interferon- γ
GM-CSF: granulocyte–macrophage colony-stimulating factor
Cytof: cytometry by time of flight
mIF: multiplex immunofluorescence
DEG: differentially expressed genes
scATACseq: single cell Assay for Transposase-Accessible Chromatin using sequencing
scChIP–seq: single cell chromatin immunoprecipitation sequencing
sn-m3C-seq: single-nucleus methyl-3C sequencing
scHi-C-seq: single cell high-throughput chromosome sequencing
t-SNE: t-distributed Stochastic Neighbor Embedding
UMAP: Uniform Manifold Approximation and Projection
IEO: European Institute of Oncology
ATCC: American Type Culture Collection
HMEC-1: Human Microvascular Endothelial Cells
CDC: Center for Disease Control and Prevention
EGF: epidermal growth factor
FBS: fetal bovine serum
T: Tumor
NAT: Normal Adjacent Tissue
InF: interstitial fluid
HBSS: Hank's Balanced Salt Solution
PBMC: Peripheral blood mononuclear cell
DMSO: dimethyl sulfoxide
PMN: polymorphonuclear leukocyte
BM: Bone marrow
TEER: trans-epithelial electrical resistance
PDMS: Polydimethylsiloxane
FFPE: formalin-fixed paraffin embedded
RNAseq: RNA sequencing
BMI: Body Mass Index
Th: Helper T cells
T_N: Naïve cells
T_{CM}: central memory cells
T_{EM}: effector memory cells
T_{EMRA}: effector cells re-expressing CD45RA

MFI: mean fluorescence intensity
T_{RM}: tissue-resident memory T cells
Treact: tumor reactive T cells
MAIT: mucosal associated invariant T
TAN: tumor-associated neutrophil
E-Cad: E-Cadherin
LN: Low CD15^{high} neutrophils patient
HN: Low CD15^{high} neutrophils patient
tROS: total Ros
PCA: principal component analysis
IHC: Immune histochemistry
OS: overall survival
DFS: disease-free survival
CL: cluster

List of the tables

Table 1 Definition of Tumor-Node-Metastasis (TNM). ⁹	11
Table 2. List of antibodies applied for the multiparametric flow cytometry analysis.	35
Table 3. Characteristics of CRC patients.	46
Table 4. Multiparametric flow cytometry panel.	48

List of the figures

Figure 1. Consensus Molecular Subtypes (CMSs) classification.	13
Figure 2. Tumor immune microenvironment (TIME) subtypes.	14
Figure 3. Mechanism leading to T cells dysfunction and impaired anti-cancer response.	17
Figure 4. Progressive dysfunctional state of CD8 ⁺ T cells during tumor progression.	18
Figure 5. Mechanisms of immunosuppression operated by Treg.	20
Figure 6. Tertiary Lymphoid structure (TLS) within tumors.	22
Figure 7. Dendritic cells (DCs) molecules regulating CD8 ⁺ T cells activity.	23
Figure 8. Neutrophils phenotype during maturation.	25
Figure 9. Neutrophils in anticancer response.	27
Figure 10. Schematic overview of neutrophils migration-on-Chip.	40
Figure 11. Study design.	45
Figure 12. Cytolytic activity is not able to predict Overall survival (OS) in early-stage colorectal cancer (CRC) patients.	47
Figure 13. T lymphocytes are the main component of CRC infiltrate.	47
Figure 14. CD8 ⁺ T cells within colorectal cancer (CRC) tumor are mainly effector memory cells (T _{EM}).	49
Figure 15. CD8 ⁺ T cells within colorectal cancer (CRC) are not exhausted.	49
Figure 16. Clustering analysis reveals high heterogeneity among CD8 ⁺ T cells in early-stage colorectal cancer (CRC) patients within different compartments.	50
Figure 17. CD8 ⁺ T cells phenotype is described by 18 clusters.	51
Figure 18. CD8 ⁺ T cells clusters are differentially distributed across tissues.	52
Figure 19. Colorectal cancer (CRC) is mainly infiltrate by two clusters of CD8 ⁺ T _{EM} characterized for the differential expression of CD39 and GZMK.	52
Figure 20. Colorectal cancer (CRC) is mainly infiltrate by CD39 ⁻ GZMK ^{high} CD8 ⁺ effector memory T cells (T _{EM}).	53
Figure 21. CD39 ⁻ GZMK ^{high} CD8 ⁺ T _{EM} are resident activated cells.	53
Figure 22. CD39 ⁻ CD8 ⁺ T _{EM} have a high cytotoxic activity.	54
Figure 23. Single cell RNA sequencing (scRNAseq) analysis confirm the high abundance of T cells within the tumor (T).	55
Figure 24. GZMK is mainly express by the CD8 ⁺ T cells cluster.	56
Figure 25. CD8 ⁺ T are mainly effector memory cells T _{EM} expressing GZMK.	57
Figure 26. Pseudotime analysis describes CD8 ⁺ effector memory (T _{EM}) T cells in between naïve and terminally differentiated/exhausted cells.	58
Figure 27. CD8 ⁺ effector memory (T _{EM}) cells are characterized by cytolytic and alloreactive signatures.	58
Figure 28. GZMK CD8 ⁺ effector memory (T _{EM}) cells express also TNF α .	59
Figure 29. Peculiar transcription factors (TF) are drivers for the cytotoxic phenotype of GZMK CD8 ⁺ effector memory (T _{EM}) cells.	59
Figure 30. CD8 ⁺ effector memory (T _{EM}) expressing GZMK predict Overall survival (OS) in early-stage colorectal cancer (CRC) patients.	62

Figure 31. CD8 ⁺ effector memory (T _{EM}) expressing GZMK predict Overall survival (OS) in lung adenocarcinoma patients.	62
Figure 32. CD39 ⁻ GZMK ^{high} CD8 ⁺ T _{EM} are accumulated within tumor (T) of colorectal cancer (CRC) patients which experienced early-relapse.	63
Figure 33. GZMB is not subject to remodulation within the tumor.	64
Figure 34. Neutrophils are strongly enriched within colorectal cancer (CRC).	65
Figure 35. Neutrophils' CD15 expression is modulated within the tumor microenvironment (TME).	66
Figure 36. Neutrophils can lose CD15 expression.	67
Figure 37. CD15 ^{high} neutrophils present an N2-like phenotype.	68
Figure 38. A different clearance characterized high (HN) and low (LN) neutrophils patients.	69
Figure 39. Soluble components of the tumor microenvironment (TME) favor neutrophils retention into the tumor of high neutrophils (HN) patients.	70
Figure 40. High neutrophils (HN) patients present a peculiar pro-tumoral milieu.	71
Figure 41. Cancer-associated fibroblasts (CAFs) produce stromal cell-derived factor 1 (SDF-1) in high neutrophils (HN) patients.	72
Figure 42. Stromal cell-derived factor 1 (SDF-1) induces an N2-like phenotype in neutrophils.	72
Figure 43. Stromal cell-derived factor 1 (SDF-1) induces neutrophils retention within the tumor.	73
Figure 44. Neutrophils and CD8 ⁺ T cells infiltrate do not predict the overall survival per se.	74
Figure 45. CD15 ^{high} neutrophils correlate with GZMK expression in CD8 ⁺ T _{EM} .	75
Figure 46. CD15 ^{high} neutrophils have no effect on phenotypic markers on CD8 ⁺ T _{EM} .	75
Figure 47. CD15 ^{high} neutrophils induce GZMK expression within T $\gamma\delta$ while CD4 ⁺ T _{EM} are not affected.	76
Figure 48. High neutrophils (HN) patients accumulate GZMK ^{high} CD8 ⁺ T _{EM} .	76
Figure 49. GZMK expression within CD8 ⁺ T ^{EM} is negatively correlated with macrophages and Treg abundance in colorectal cancer (CRC).	77
Figure 50. GZMK expression is specifically upregulated in CD8 ⁺ T ^{EM} within tumors (T).	77
Figure 51. GZMK expression correlates with tumor growth in <i>in vivo</i> syngeneic MC38 mouse model of colon cancer.	78
Figure 52. G-CSF-induced neutrophils enrichment within the tumor (T) favor GZMK ^{high} CD39 ⁻ T cells accumulation.	79
Figure 53. Neutrophils depletion improve tumor control and reduces CD8 ⁺ T cells' GZMK expression.	79
Figure 54. CXCR4 inhibitor (ADM3100) control tumor growth by increasing CD8 ⁺ T cells infiltrate and reducing GZMK ^{high} CD39 ⁻ CD8 ⁺ T cells.	80
Figure 55. Neutrophils increase the basal production of GZMK in CD8 ⁺ T cells by direct contact in culture.	82
Figure 56. CD15 ^{high} neutrophils present within the tumor (T) induces higher production of GZMK in CD8 ⁺ T cells compared with peripheric neutrophils and the CD15 ^{low} counterpart.	83
Figure 57. Neutrophils modulates GZMK within CD8 ⁺ T cells in a contact mediated manner.	83
Figure 58. Coculture of CD8 ⁺ T cells and neutrophils induce a decrease in E-Cadherin (E-Cad) in an intestinal epithelial model.	84
Figure 59. GZMK is responsible for E-Cadherin (E-Cad) decrease in intestinal epithelial model.	85
Figure 60. GZMK modulate transcriptional profile of an intestinal epithelial model.	85
Figure 61. HN patients present lower E-Cadherin (E-Cad) expression.	86

Abstract

As with most solid tumor malignancies, CRC possess more than one major histological subtype that likely generate disparate immune responses. The heterogeneity in the immune cell response to CRC highlights the need to develop novel immune diagnostics that could predict the risk of disease relapse and devise a secondary strategy to address that risk. The purpose of this study was to prospectively provide a clear description of the patient-specific immune landscape present in CRC to target the dominant immune suppressive factors within a given tumor that may improve response rates while ushering in the age of personalized therapies for cancer patients. We described a functional interplay between neutrophils and CD8⁺ T cells that impacts on tumor immune escape and relapse. Specifically, we showed that tumor infiltrating neutrophils expressing high levels of CD15 interact with CD8⁺ T effector memory cells skewing them to produce GZMK, associated with tumor progression in CRC patients. Our findings identify a unique immune signature, which might inform therapeutic decision making, possibly leading to new immunotherapeutic targets.

Introduction

1. Colorectal Cancer and its classification

Colorectal cancer (CRC) is the third most common cancer worldwide with a high morbidity rate and poor prognosis. The five-year survival rate for patients with advanced CRC is around 14%, and metastasis occurs in more than 50% of patients with CRC¹⁻³.

CRC progresses from normal to atypical to carcinoma that includes the formation of precancerous polyps, which can subsequently develop into malignant invasive cancer CRCs. The inactivating mutations of the APC gene is detected in ~80% of the cases⁴⁻⁶, resulting in β -catenin stabilization and increased WNT signaling, leading to intestinal hyperplasia. Subsequent mutations in other cancer driver genes such as KRAS, TP53 and SMAD4 result in the transformation to carcinoma⁷. Despite these commonly detected alterations, the heterogeneity of the disease at genetic and molecular levels determines a different outcome and patient-dependent response to the therapies.

The Tumor-Node-Metastasis (TNM) classification, which classifies the extent of spread of cancer (Table 1), has been until now the main prognostic assessment tool for CRC patients⁸. However, even with favorable TNM staging, 30-40% of surgically resected CRC relapse, leading to metastasis formation and poor prognosis^{2,3}. These data suggest that the accuracy of prognostic assessments using TNM classification is not conclusive, especially for stage II and III CRC, calling for more effective patient stratification able to predict clinical outcome and, eventually, therapy response.

Stage	Definition
Primary tumor (T)	
TX	Primary tumor cannot be assessed
T0	No evidence of primary tumor
Tis	Carcinoma <i>in situ</i> : intraepithelial or invasion of lamina propria
T1	Tumor invades submucosa
T2	Tumor invades muscularis propria
T3	Tumor invades through muscularis propria into the subserosa or into nonperitonealized pericolic or perirectal tissues
T4	Tumor perforates visceral peritoneum or directly invades other organs or structures
Regional lymph nodes (N)†	
NX	Regional lymph nodes could not be assessed
N0	No regional lymph node metastases
N1	Metastases in one to three regional lymph nodes
N2	Metastases in four or more regional lymph nodes
Distant metastases (M)	
MX	Distant metastases could not be assessed
M0	No distant metastases
M1	Distant metastases
Extent of resection (R)‡	
RX	Presence of residual tumor cannot be assessed
R0	No residual tumor
R1	Microscopic residual tumor
R2	Macroscopic residual tumor

Table 1 Definition of Tumor-Node-Metastasis (TNM). ⁹

Multiple molecular subtypes and accumulation of various genetic alterations characterize the CRC TME¹⁰, generating high interpatient heterogeneity and making genomic approaches alone unable to conclusively delineate unique prognostic biomarkers.

CRC patients can be classified based on hypermutable phenotype. A deficient DNA mismatch repair (dMMR) activity is associated with a portion of CRC patients, leading to microsatellite instability (MSI) within cancer cells, as opposed to microsatellite stable (MSS) tumors. The MSS subtypes occupy a large proportion (85%) of CRC cases, whereas the dMMR/MSI patients account for only approximately 15% of all CRC patients¹¹. Gryfe et al. demonstrated in a cohort of 607 CRC patients that MSI predicts favorable outcomes¹². The mechanism by which MSI might influence prognosis has been underscored by Mlecnik et al., who demonstrate that a high frequency of frameshift mutations leads to increased neoantigen load, which favors immune cell infiltration within the tumor and effective antitumor response¹³. MSI CRC tumors display indeed high T cell infiltration, which has been reported as a valid prognostic too ¹⁴⁻²². Nevertheless, MSI-CRC has higher expression of co-inhibitory receptors, such as PD1 (programmed cell death protein 1), CTLA4 (cytotoxic T lymphocyte-associated antigen 4) and LAG3 (Lymphocyte-activation gene 3),

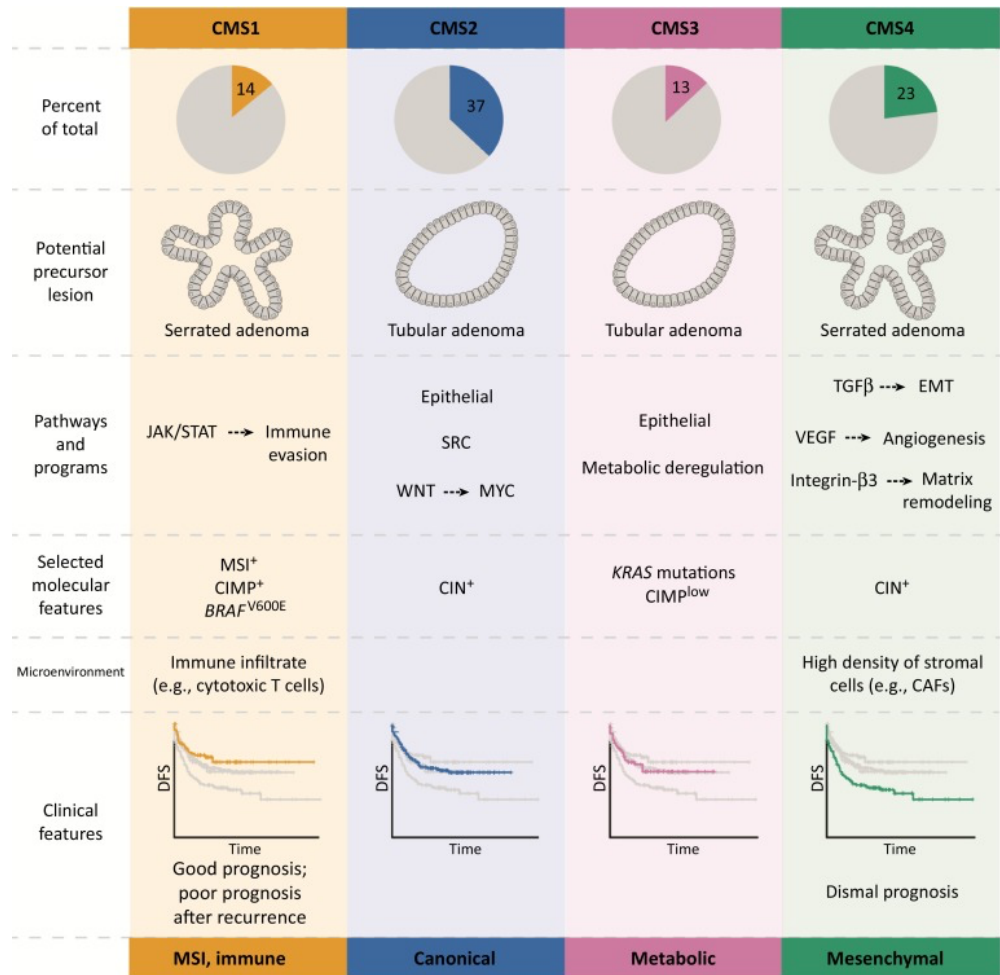
providing a potential explanation of why MSI CRC tumors are not rejected - despite high T cell infiltration²³. On the other hand, they further suggest that blockade of specific checkpoints might be efficacious for the treatment of the MSI subset of colorectal cancer. In this regard, a complete remission in an entire cohort of rectal cancer patients has been recently demonstrated²⁴. Thus, the diagnosis of MSI is now considered a positive prognostic factor for the efficiency of PD1 therapy, which has been approved as a therapeutic strategy to potentiate endogenous CTLs both within the TME and in periphery with the aim of counteracting tumor metastasis²⁵.

Several large CRC studies have demonstrated that T cell intratumoral abundance is significantly associated with better prognosis, even after adjusting for stage, lymph node count, and molecular biomarkers, including microsatellite instability²⁶⁻²⁸.

Thus, beyond MSI status, quantification of cytotoxic and memory T cells within TME is an indicator of tumor recurrence and survival demonstrating that tumor progression is not merely caused by genetic alterations as the TME composition also plays a central role¹⁵.

The evidence of endogenous immune system's intervention in the pathogenesis of the disease prompts a more complete characterization of the immune component of the TME and introduced the concept of "immunoscore" to quantify T cell infiltrate within solid tumors^{15,29-31}. Immunoscore has become a useful prognostic marker in several solid tumors, including but not limited to CRC^{14,16,30}, holding a stronger prediction value for survival than the TNM staging^{16,30,32}.

The most exhaustive classification of CRC patients is based on four Consensus Molecular Subtypes (CMSs) with peculiar molecular and clinical features. CMS1 contains MSI tumors with high mutational burden, which results in consistent CTL and Th1 CD4⁺ T cells immune infiltration. CMS2 (canonical) is the most common subtype and presents an epithelial differentiation, with a significant WNT and MYC pathways signaling activation. CMS3 is mainly characterized by a metabolic dysregulation due to KRAS mutation³³⁻³⁵. CMS4 is characterized by a strong TGFβ signaling, stromal invasion and neo-angiogenesis, which correlates with increased tumor aggressiveness and worst clinical outcome.¹⁰ The CMS4, which includes a large portion of CRC cases, present a stromal origin, with a huge component of cancer-associated fibroblasts (CAFs), and correlates with increase tumor aggressiveness and worst clinical outcome. Interestingly this subtype of cancer presents a pro-inflammatory immune phenotype associated with unfavorable prognosis and high C-X-C Motif Chemokine Ligand 12 (CXCL12), also known as stromal cell-derived factor 1 (SDF-1) expression levels¹⁰. The classification in one of the 4 CMS subtypes defines not only a cellular phenotype but could also predict the response to the therapy³⁶.



Trends in Cancer

Figure 1. Consensus Molecular Subtypes (CMSs) classification.

Clear definition based on diffusion (Percent of total), histological features (Potential precursor lesion), cellular processes involved in the development (Pathways and programs), driving genetic alterations (Selected molecular features), peculiarity of the tumor microenvironment (Microenvironment) and prognosis characteristics (Clinical features)³⁷

Since the transcriptomic and molecular classification of colorectal cancer is strongly associated with different immune and stromal contextures, the novel classifications of CRC tumors are based on the relationships between the phenotype of cancer cells and the corresponding immune and stromal profile of its microenvironment, potentially identifying the most appropriate treatments, including novel immunotherapies.

2. Heterogeneity of CRC TME

Recent studies of tumor-infiltrating immune cell populations in CRC and other tumor types provide evidence for a highly heterogeneous makeup of immune cell infiltrates, and this heterogeneity is likely to form a determining factor in therapy outcome³⁸⁻⁴⁵.

The development of new single cell technologies gave rise to many studies characterizing the heterogeneity of immune infiltrate in different types of cancer, including CRC, and shade

light on the tumor immune microenvironment (TIME). Three classes of TIME have been described: infiltrated–excluded (I–E), infiltrated–inflamed (I–I) and infiltrated-TLS (I-TLS)⁴⁶. I–E TIME is largely populated by immune cells but the number of CTLs is scarce in the tumor core with low activation and cytotoxic activity¹³. Here, the presence of other immune cells engaging long-lasting interactions with CTLs mediate lymphocyte trapping and dysfunction. For instance, it has been shown that macrophages limit anti-PD-1 treatment efficacy by dampening CD8⁺ T cell ability to reach the TME⁴⁷. This study suggested that strategies able to reduce macrophage-mediated T cell exclusion may increase tumor immunosurveillance and the efficiency of immunotherapies. I–I TIME are classified as “hot” tumors because of their high infiltration of immune cells and, in particular, CTLs with high expression of activation markers, effector molecules - such as IFN γ and GZM β - as well as checkpoint inhibitors. Importantly, the higher expression of co-inhibitory receptors in CTLs within this type of TIME correlates with a better response to immunotherapy⁴⁸. A peculiar type of TIME is the I-TLS where the immune infiltrate is able to aggregate in a well-defined architecture and give rise Tertiary Lymphoid Structures (TLS), with a composition similar to lymph nodes, with B cells, dendritic cells (DC) and Treg cells.

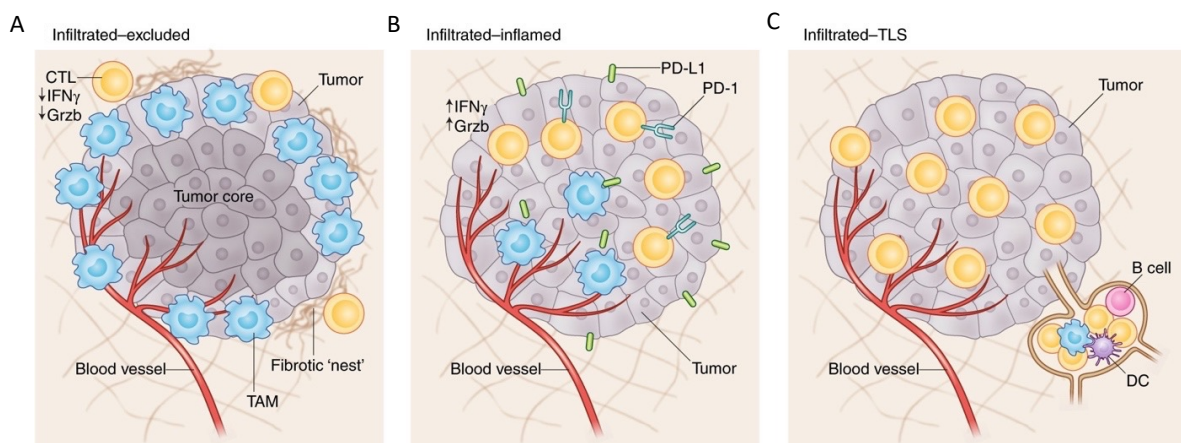


Figure 2. Tumor immune microenvironment (TIME) subtypes.

A. infiltrated-excluded: cytotoxic T cells (CTLs) express low levels of inflammatory cytokines (IFN γ and Gzmb) and are excluded from the tumor core due to their interaction with tumor associated macrophages (TAMs). **B.** infiltrated-inflamed: immune cells penetrate the tumor core and CTLs express both inflammatory molecules and inhibitory receptors (PD-1), accompanied by the expression of checkpoint inhibitors by cancer cells (PD-L1). **C.** infiltrated-TLS: present high CTLs infiltration and tertiary lymphoid structures (TLSs) of B cells and Dendritic Cells (DC).⁴⁶

Thus, immune cell function and type of TIME are key for an anti-tumor response, in which the type, abundance and location of tumor infiltrating immune cells influence survival in many types of cancer, included CRC^{32,49–51}. Nevertheless, in the TME there are few functional TILs and many immunosuppressive cells, mainly consisting of T regulatory cells (Tregs), Myeloid derived suppressor cells (MDSCs), and tumor associated macrophages

(TAMs), infiltrated in the TME, which influence TIL functionality and impact on clinical outcome.

In the last decade, a huge effort has been made with the aim of characterizing the tumor infiltrate and dissecting the role of the immune system in tumor progression.

The prospective study of non-small cell lung cancer (NSCLC) patients TRACERx (TRACKing non-small cell lung Cancer Evolution through therapy [Rx]), by integrating new single cell technologies, has led to a better understanding of cancer evolution⁵² and highlighted the existence of peculiar crosstalks between cancer and immune cells that deeply impact T cell activity within the tumor. Many other pioneering studies have allowed a deep comprehension of the immune infiltrate heterogeneity thanks also to the development of new single cell technologies.

3. CD8⁺ T cells and anti-tumor response

CTLs play a pivotal role in cancer immunity and cytotoxic CD8⁺ T cells have been associated with favorable prognosis in several types of solid tumors^{53,54}, including CRC^{21,22,32}.

CD8⁺ T cells recognize cancer cells through the T cell receptor (TCR) and differentiate into cytotoxic T cells (CTLs), whose primary role is to kill the target cell with remarkable precision and efficiency. Once conjugated to a target cell, the cytotoxic secretory granules traffic to the immunological synapse and release a cargo of deadly proteins, including perforin (PRF), granzymes (GZMs) and granulysin1 (GNLY), into the synaptic cleft; ultimately leading to apoptosis of target cells^{55,56}.

While the GZMB activity is well established, the activity of other GZMs is still under investigation⁵⁷. Recent works demonstrate a role of GZMA in chronic inflammation leading to CRC in an AOM/DSS mouse model of cancer development⁵⁸. Likewise, GZMK has been associated with different processes, like tissue damage, inflammatory process and aging^{59,60}. Interestingly, CD8⁺ GZMK⁺ populations have been described in different type of tumors and associated with a pre-dysfunctional state⁶¹⁻⁶³. However, the role of CD8⁺ GZMK⁺ populations in anti-tumor response has just recently begun to be elucidated.

a. CD8⁺ T cells and tumor reactivity

A high Tumor Mutational Burden (TMB) leads to high neoantigen load and is often associated with a stronger anti-tumor immune response since it could favor cancer cell recognition by CTLs. The prognostic significance of TMB status in predicting response to

immunotherapies corroborates this hypothesis. TCR specific CD8⁺ TILs able to reside in the TME are the main responsible for a better clinical outcome and ICB response^{64,65}. T cells with a tissue-resident memory phenotype contribute to immunosurveillance and are associated with improved prognosis⁴⁰. However, in the TME, the recurrent TCRs associated with cancer antigens reactivity are mainly detected on effector and dysfunctional T cell and are underrepresented on memory T cells, likely limiting a long-lasting anti-tumor response^{40,44,45,65,66}.

Tumor reactive CD8⁺ T cells are identified by the co-expression of CD103 and CD39⁶⁷. These cells have a tissue-resident memory phenotype, express high levels of exhaustion markers and are associated with improved overall survival⁶⁷. However, not all tumor-infiltrating T cells are specific for tumor antigens. Instead, human tumors are highly infiltrated by CD39^{neg} CD8⁺ T cells, which recognize a wide range of epitopes unrelated to cancer and lack hallmarks of chronic antigen stimulation at the tumor site, supporting their classification as bystanders^{64,68,69}. Bystanders CD8⁺ T cells comprised viral reactive T cells recalled in the TME by inflammatory molecules and chemokines such as CXCL9 and CXCL10^{69,70}, and CCL5.⁷¹ The role of these cells in cancer development is still controversial. In patients with stage III melanoma treated with adjuvant immunotherapy a low ratio between tumor reactive and bystanders T cells increase the probability of recurrence^{69,72,73}. However, *in vivo* studies in mice have demonstrated a possible beneficial role of reactivation of Virus-specific T cells enriched in the TME in cancer immunotherapy⁷⁴. The implications of bystander T cells in tumors are only at the beginning to be understood, however, their characteristics like abundance in the TME, lack of exhaustion, specificities to common pathogens, and innate-like killing capabilities could open new opportunities towards the development of new immunotherapeutic protocols.

b. CD8⁺ T cell dysfunction in solid tumors

Recent studies of tumor-infiltrating immune cell populations in melanoma and other tumor types provide evidence for a highly heterogeneous profile of immune cell infiltrates, and this heterogeneity is likely to form a determining factor in therapy outcome^{39,42,43,63,75,76}. Within the heterogeneous tumor microenvironment, T cells make up a considerable part of the immune infiltrate. The intratumoral T cell compartment comprises naïve-like, effector, memory, and regulatory T cells (Treg). In addition, a subset of CD8⁺ T cells that has acquired a state of “dysfunction” or “exhaustion” is frequently observed. Such dysfunctional T cells are characterized by a loss of classical CD8⁺ T cell effector functions, such as cytotoxicity

77–79. In addition, the dysfunctional T cells in human tumors display a unique T cell cytokine secretion signature^{40,41,63,80,81}.

The role and predictive potential of T cells with different levels of expression of exhaustion markers is still debated. In murine models, T cells with high expression of markers of T cell exhaustion appear refractory to reinvigoration by PD-1 blockade^{82–86}.

During the progression of the disease, the persistent exposure to neoantigens induces a dysfunctional state in antigen specific CD8⁺ and CD4⁺ T cells^{79,87}.

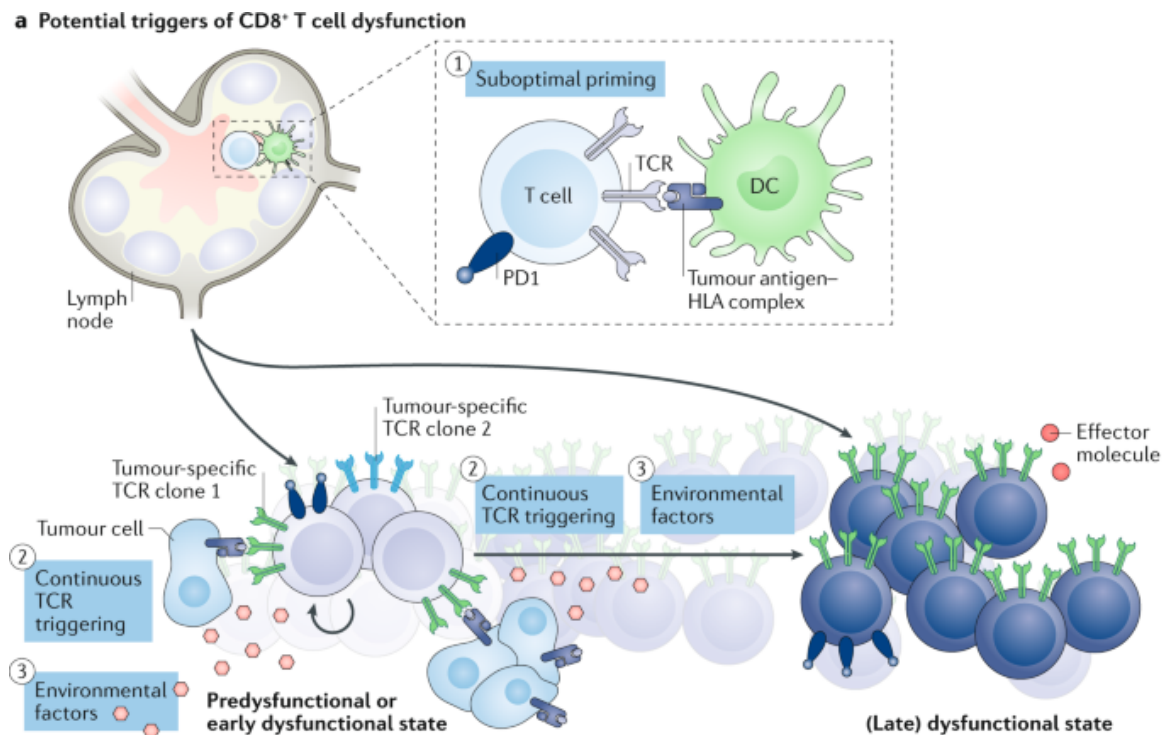


Figure 3. Mechanism leading to T cells dysfunction and impaired anti-cancer response.

The drivers of T cells dysfunction include: (1) the suboptimal priming of CD8⁺ T cells which could take place in lymph nodes or in tertiary lymphoid structures (TLSs) within the tumor, (2) continuous antigen exposure, thus T cells receptor (TCR) triggering, (3) in combination with factors present in the tumor microenvironment (TME) such as cytokines and metabolic conditions such as hypoxia, glucose deprivation, low pH and lipids accumulation.⁸¹

On the other hand, the pressure operated by the immune cells in the early stage of cancer development often limits neoantigens presentation by cancer cells, leading to the impairment in CTLs response, poor disease-free survival and a low sensibility to checkpoint blockade⁸⁸. Importantly, immune cells, despite their primary role in anti-cancer intervention, operate a pressure on tumor cells which modify their immunogenicity. This process called “cancer immunoediting” eventually leads to the emergence of tumor cells which have acquired the ability to circumvent immune recognition and ultimately promote tumor progression and resistance to immunotherapies⁸⁹.

In the last decade, the discovery of T cell checkpoint molecules expressed on the surface of CD8⁺ T cells-like PD1 and CTLA4 led to the breakthrough discovery of the use of immune checkpoint blockade (ICB) to reinvigorate CTLs cytotoxic response within the TME. ICBs have completely rewired cancer therapy demonstrating unprecedented clinical results in different types of cancer^{90,91}, remarking the fundamental role of CTLs in anti-tumor response.

Recently, studies integrating scRNAseq with TCR analysis have shed light on different populations of dysfunctional CD8⁺ T cells, have allowing to predict not only responsiveness to ICBs but also to dissect whether specific CTLs subsets were equally involved in mediating tumor control⁹². These studies have provided insight on the T cell dysfunction process. T cells within solid tumors experienced a progressive transition in their transcriptional profile by down-regulating proliferation and effector functions' related genes, while upregulating expression of checkpoints inhibitors such as TIGIT, PDCD1, LAG3, and CXCL13 as well as transcription factors (TF) associated with dysfunctional signatures⁶⁶. However, the proportion and the phenotype of exhausted cells is variable among different type of cancer and even interpatient^{39,44,66}. Thus, the higher complexity of intratumoral CD8⁺ T cell postulates the need of new and sophisticated approaches for patient stratification that will help to further understand the functional states and dynamics of T cells in cancer, and their impact on clinical outcome⁴⁵.

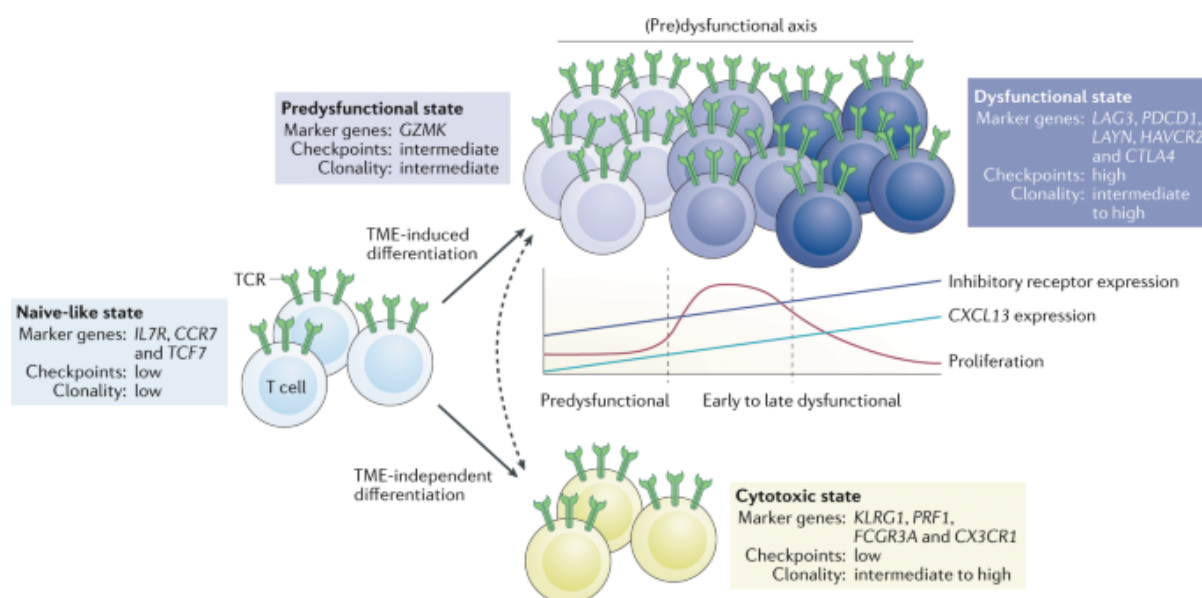


Figure 4. Progressive dysfunctional state of CD8⁺ T cells during tumor progression.

Representation of the progressive dysfunctional state developed by CD8⁺ T cells during tumor development. Naïve-like cells has been described in different type of solid tumor and normally differentiated in a functional cytotoxic state. However, into the tumor is common the development of a pre-dysfunctional state which progressively evolve in a final dysfunctional state. During this process there is an increase in inhibitory receptors expression, an increase up CXCL13 and a decrease in the proliferation capacity of the cells.⁸¹

Another important factor driving T cell dysfunction is the metabolic composition of the TME⁹³⁻⁹⁵. Cancer cells harbor different TME composition which can reshape the functionality of immune cells and hamper their anti-tumor response. An increasing body of evidence suggests that nutrients availability in the TME has a key influence on immune responses. For example, depletion of glucose and tryptophan and accumulation of lactate in the TME suppresses anti-tumor immunity⁹⁶⁻¹⁰¹. Nevertheless, glucose is a key factor for immune cells metabolism and aberrant aerobic glycolysis (Warburg effect) of tumor cells affects glucose availability dumping the CTLs responses and contributes to the recruitment of immune suppressive myeloid cells (MDSCs) into the tumor¹⁰⁴⁻¹⁰⁶. Another common metabolic alteration in the TME is increased lipid accumulation^{93,97,100,102}. The peculiar tumor milieu influences function and retention of the different types of infiltrating immune cell, often posing obstacles to CD8⁺ T cells, while favoring immunosuppressive cells¹⁰³⁻¹⁰⁵. These data demonstrate a cell specific modulation operated by the TME metabolic composition and its role in remodeling the immune heterogeneity within solid tumors. Finally, factors - such as age, gender, nationality, diet, metabolism, microbiome alteration and lifestyle- are able to modulate the immune heterogeneity within tumors. This complex network is still far from being completely elucidated; thus, a higher comprehension of the TME landscape at single cell level in a large cohort of patients will be informative to develop a more precise diagnostic and prognostic score towards personalized medicine.

4. CD8⁺ T cells crosstalk with tumor immune compartment

As is the case with many solid tumor malignancies, CRC is a very heterogeneous disease comprised of multiple unique histologic subtypes that harbor distinct molecular signatures. In this scenario, it's conceivable that the immune cell populations will differ by CRC subtype, if not from case to case.

The presence of various immune cell populations has previously been suggested as a potential modifier of CD8⁺ T cell activity in tumors^{42,46}

a. CD4⁺ T cells

CD4⁺ T cells regulate anti-tumor responses by providing help to CTLs activation in the TME¹⁰⁶. However, CD4⁺ T cells in the TME are often skewed toward a Treg differentiation state and play a pro-tumoral role by suppressing CD8⁺ T cells activity. Tumor cells can promote CD4⁺ T cell differentiation into Treg by inducing dendritic cells to produce TGFβ,

which is fundamental for Treg differentiation and survival¹⁰⁷. Moreover, FOXP3⁺ Treg cells are recruited to the TME by different chemotactic molecules such as CCL17, CCL22, CCL5, CCL6, CCL28 and IL10, that can be produced by TAMs, MDSCs and cancer cells^{107,108}. The accumulation of FOXP3^{high} Treg cells in the TME suppresses the activity of CTLs either by contact-mediated mechanisms, or via IL2 depletion^{109,110} or through the release of suppressive soluble molecules like TGF β and IL35^{111–113}.

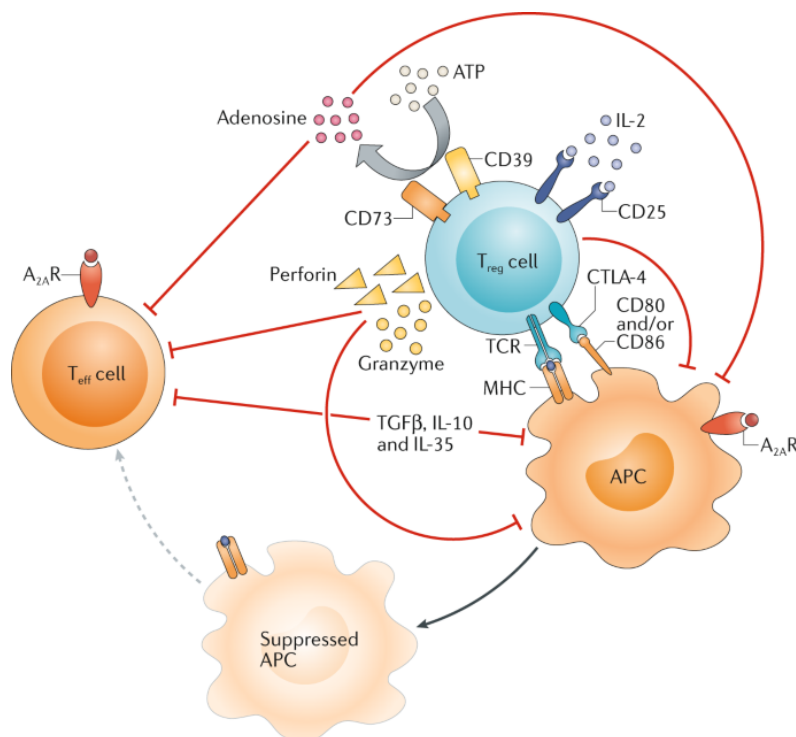


Figure 5. Mechanisms of immunosuppression operated by Treg.

Regulatory T (T_{reg}) cells constitutively express the IL2 receptor subunit- α (CD25) which binds with the high-affinity IL2, thus reducing the availability of this cytokine to effector T (T_{eff}) cells. T_{reg} cells also constitutively express cytotoxic T lymphocyte antigen 4 (CTLA-4), which binds to CD80 and CD86 on antigen-presenting cells (APCs), thereby transmitting suppressive signals and reducing their capacity to activate T_{eff} cells. Furthermore, CTLA-4 binds, with a higher affinity than CD28, the CD80 and CD86, thus competing with T_{eff} cells. T_{reg} cells are also producers of immunosuppressive cytokines, such as IL10, IL35 and transforming growth factor- β (TGF β), which can downregulate the activity of APCs and T_{eff} cells, moreover the release of granzymes and perforin that can directly kill other immune cells. Ultimately, the release of large amounts of ATP, which is converted by CD39 and CD73 to adenosine, an immunosuppressive signal for T_{eff} cells and APCs.¹¹⁴

Abundant Treg cell infiltration into tumors is associated with poor clinical outcomes in various types of cancers^{115,116}. However, the role of Treg cells is controversial in CRC, where FOXP3⁺ T cell infiltration has been associated also with better prognosis. In particular, CRCs infiltrated by FOXP3^{low} T cells showed significantly better prognosis than those with a predominant FOXP3^{hi} Treg cell infiltration^{28,115–120}.

Another particular subset of Treg cells identified as FOXP3⁻CD4⁺ T cells are the so-called Tr1 cells, found enriched in tumor and metastasis. These cells are endowed with suppressing

activity, and their presence in CRC and NSCLC TME is correlated with disease progression¹²¹.

In all, these studies findings suggest a complex heterogeneity in the intratumoral Treg compartment, composed by different subsets with tissue-specific functions and precise immunoregulatory mechanisms that can be exploited in immunotherapeutic approaches.

b. B cells

An important role in anti-tumor immune response is played by B cells present both in the tumor and in draining lymph nodes¹²². Indeed, several studies demonstrate that their presence and functionality correlate with better prognosis and improve response to immunotherapy in lung cancer¹²³, melanoma^{124,125}, pancreatic adenocarcinoma¹²⁶ sarcoma¹²⁷ and CRC¹²⁸. Plasma cells within the tumor are able to produce a large amount of antibodies driving antibody-dependent cellular cytotoxicity (ADCC) and phagocytosis, which in turn facilitate antigen presentation by dendritic cells to lymphocytes. These functions are important components in anti-cancer response, however their direct role in shaping T cells response is still under investigation.

B cells can present antigens to CD8⁺ and CD4⁺ T cells reinforcing their cytotoxic cancer specific response¹²⁹. Their APC function provides an alternative immunotherapeutic approach to enhance T cells response. Indeed, B cells are less responsive than DCs to inhibitory molecules present in the TME, such as IL10, TGF β and VEGF and are easily isolated from peripheral blood (PB), expanded and activated in vitro, for their in vivo application¹²². For several years B cells were considered in relation to the humoral immune response but recently a more complex scenario has highlighted their function in cancer response and kicked off the development of new strategies of cancer immunotherapy. In the TME, indeed, B cells are able to generate TLSs^{130,131}, peculiar lymphoid structures within solid tumors that favor maturation and isotype switching of tumor-specific B cells and the recall and clonal expansion of T cells^{132–134}.

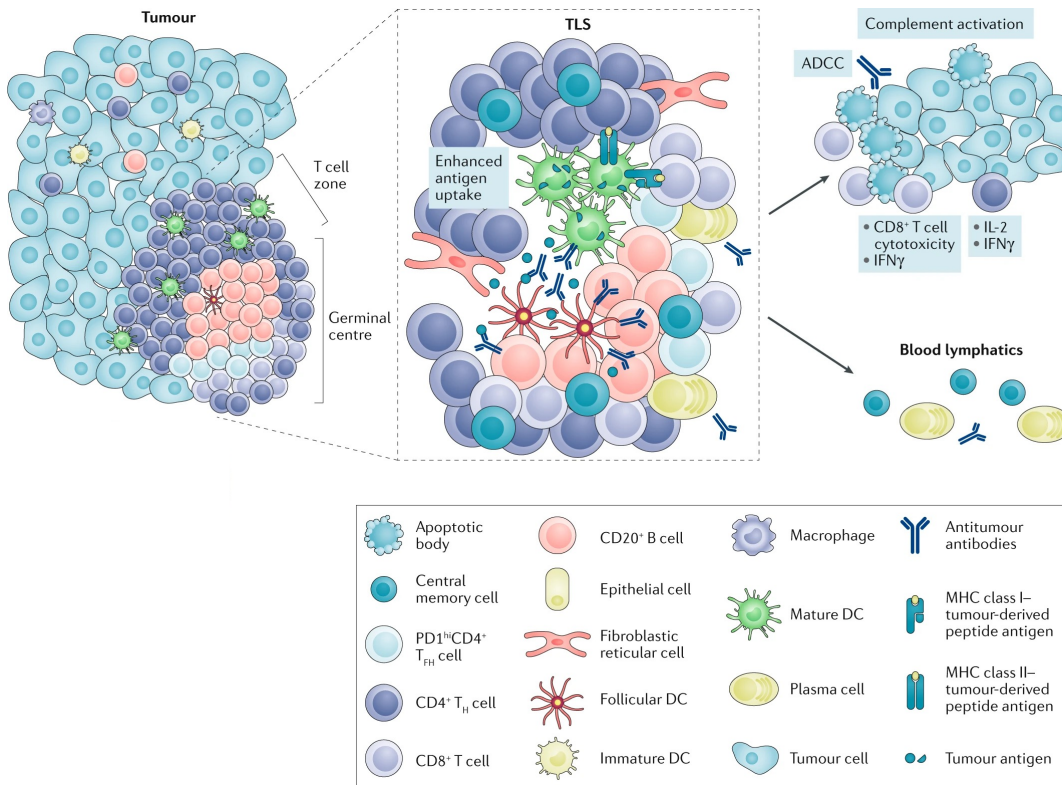


Figure 6. Tertiary Lymphoid structure (TLS) within tumors.

TLS within tumors present a CD3⁺ T cell rich zone containing dendritic cells (DCs), fibroblastic reticular cells (FRCs) and a CD20⁺ B cell zone with a germinal center, plasma cells, antibodies forming immune complexes with tumor antigens and follicular DCs (FDCs). CD8⁺ cytotoxic effector T cells and B cells generated within the TLSs can operate direct cancer cell killing, antibody-dependent cellular cytotoxicity (ADCC) mediated by macrophages and other phagocytic cells and local complement activation. Moreover the central memory T and B cells generated in TLSs circulate and protect against metastasis and tumor recurrence.¹³⁰

Recent studies demonstrated better prognosis in early-stage CRC with associated TLSs and an increase in B cells infiltrate and TLSs formation in responders to ICB immunotherapy compared with non-responders^{125,134}. This analysis supports a positive role of B cells and TLSs in anti-cancer response and paves the way for the application new targets of intervention in solid tumors.

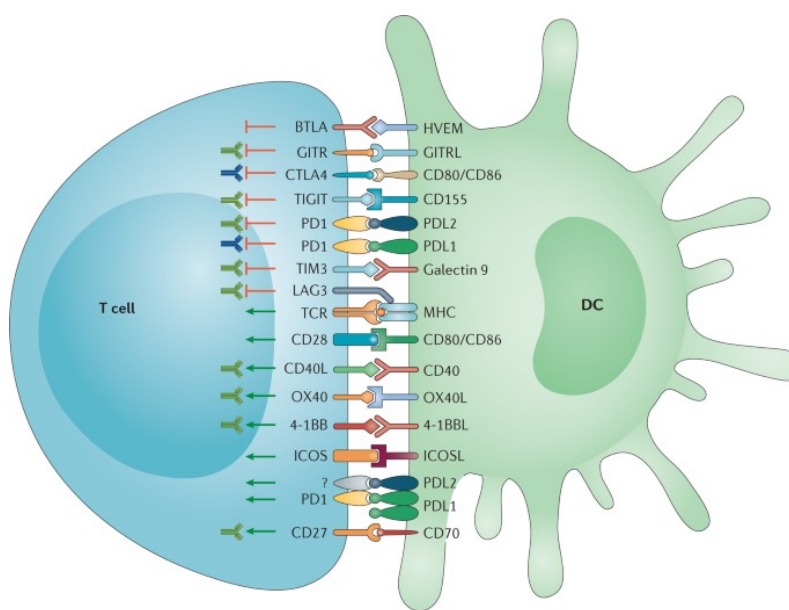
c. Dendritic cells

CD8⁺ T cells anti-tumor response starts with the recognition through T-cell receptor (TCR) of tumor antigens presented by MHC-I on the tumor cells and MHC-II on the surface of antigen-presenting cells (APCs), such as macrophages, DCs and B cells. The sensing operated by APCs leads to the activation of CD8⁺ T cells, which starts biochemical signals aiming to generate an effective and precise target-cell killing^{51,135}.

DCs are specialized APCs presenting antigens through MHC-II to naïve CD8⁺ T cells. However, CD103⁺ (DC2) have been recently identified as a DCs subset able to also promote proliferation of both naïve and differentiated effector CD8⁺ T cells in the tumor

microenvironment (TME), sustaining CTLs activity by the release of GM-CSF (Granulocyte-macrophage colony-stimulating factor) and FLT3L (Fms Related Receptor Tyrosine Kinase 3 Ligand)¹³⁶. DCs activity is directly dependent from the TME, where the presence of immunosuppressive soluble molecules can affect their differentiation and function^{137,138}. Among them, IL6 produced by tumor cells, TAMs and some type of neutrophils reduced the maturation and migration of DCs in certain type of solid tumors^{139,140}. IL10, released by cancer cells as well as immune cells, induced the conversion of immunogenic canonical DCs into tolerogenic DCs, leading to reduced T cell priming and induction of apoptosis in CD8⁺ T cells^{141,142}. VEGF and TGFβ have also been found to inhibit DCs maturation and to take part to the immunosuppressive milieu of the TME. Furthermore, DCs in the TME increase the expression of inhibitory molecules such as PDL1 and PDL2, galectin 9, CD80/CD86 and CD155, leading to further impairment of CD8⁺ T cells function and taking part as putative target of ICB therapy^{137,143}.

As major sentinels in the TME, DCs play a pivotal role in cancer immunotherapy. Seventeen clinical trials using DC based therapies have shown promising results alone or in combination with other therapies¹⁴⁴.



Nature Reviews | Immunology

Figure 7. Dendritic cells (DCs) molecules regulating CD8⁺ T cells activity. ¹⁴⁵

d. Macrophages

Macrophages are a subset of myeloid cells exhibiting APC functions. Two main classes of macrophages have been described: classically activated macrophages (M1) and alternatively activated macrophages (M2). The polarization towards M1, mostly driven by IFNγ, TNFα and lipopolysaccharide (LPS), is defined by the expression of CD68, CD86 and CD80,

accompanied by the secretion of TNF α , IL1 β , IL12, CXCL9, CXCL10 and NOS2 production. M1 macrophages play an important role as pro-inflammatory cells inducing a Th1 response¹⁴⁶. In contrast, the polarization towards M2, promoted by IL4 and IL13, is characterized by the expression of CD163, CD204 and CD206 and is mainly playing an immunosuppressive function¹⁴⁷. This last subset has been defined TAMs and often associated to tumor progression, metastasization and immunotherapy resistance^{148–150}. However, single cell technologies have shed light on the heterogeneity of M1 and M2 populations^{148,151} and recent clinical studies have demonstrated that macrophages are accompanied by different prognostic value since they play different roles in cancer progression depending on the specific tissue. Usually, M2-like macrophages enrichment is associated with worst prognosis in melanoma¹⁵², breast,¹⁵³ lung^{154,155} and gastric cancer¹⁵⁶. On the contrary, peculiar CD14⁺CD2⁺LY75⁺ macrophages have been associated with better survival in patients with melanoma¹⁵⁷ and, independently from the polarization state, better prognosis is correlated with macrophages infiltration in colorectal cancer¹⁵⁸. Additionally, TAMs influence the PDL1 and PD1 expression on tumor and CD8⁺ T cells, respectively. Indeed, TAMs-derived TNF α positively correlated with PDL1 expression in cancer cells in pancreatic cancer (PDAC)¹⁵⁹, as well as TAM-derived IL6 was able to induce an upregulation of PD1 on CD8 T cells and correlate with worst prognosis in lung cancer¹⁶⁰. As major sentinels in the TME, both DCs and macrophages play a pivotal role in cancer immunotherapy. Seventeen clinical trials using DC based therapies have shown promising results alone or in combination with other therapies¹⁴⁴. On the other side, more than 100 clinical trials have been developed using macrophage-targeting agents¹⁵², with the aim of reducing the number of TAMs and/or inducing a repolarization from M2 to M1 with anti-tumor activity.

e. Granulocytes

The interaction between T cells and granulocytes has been poorly investigated so far, especially in the context of cancer biology due to their short lifetime and technical challenges to analyze their phenotype *ex vivo*. Eosinophils, composing 1-5% of the total leukocytes in the blood, have been found enriched in many types of tumors, including CRC, melanoma, lung cancer, and recently they have been reported to play a role in enhancing of CD8⁺ T cells infiltration, thus reducing cancer progression^{161–164}. Interestingly the local tumor irradiation causes eosinophils infiltration, further supporting the cytotoxic T lymphocyte recruitment and better response to immunotherapy in non-small cell lung cancer (NSCLC) and nasopharyngeal carcinoma NPC patients¹⁶⁵. However, in another study, eosinophils

expressing CD16 were described as immunosuppressive since they inhibit T cell function by releasing the immunoregulatory protein galectin-10¹⁶⁶. Thus, further studies are needed to better understand their role on anti-tumor immunity.

Myeloid-derived suppressor cells (MDSCs) are pathologically activated cells with potent immunosuppressive activity. According to their origin from the granulocytic or monocytic myeloid cell lineages two major groups of MDSCs are described: the granulocytic/polymorphonuclear MDSCs (PMN-MDSCs) and monocytic MDSCs (M-MDSCs), respectively. However, their differentiation from neutrophils and monocytic cells is controversial. In particular, PMN-MDSCs are described as a differentiation state coming from immature neutrophils released from the bone marrow prematurely due to the emergency hematopoiesis taking place during infection, inflammation and cancer¹⁶⁷. MDSCs/immature neutrophils are detected in the circulation and within the TME of cancer patients and are recognized by GIEMSA staining.

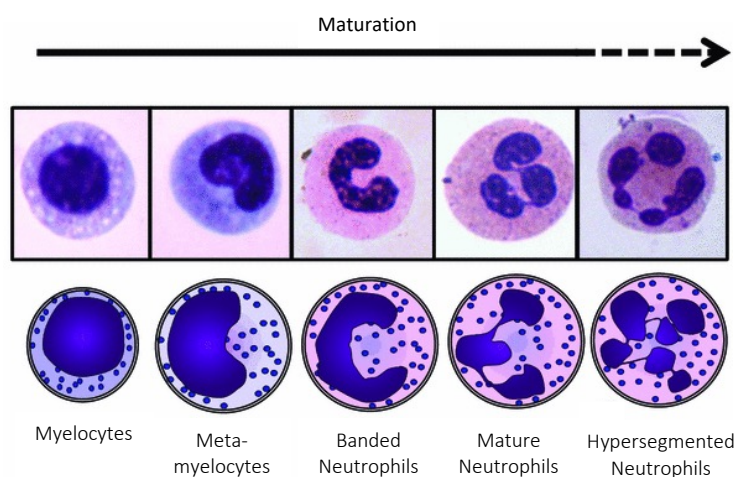


Figure 8. Neutrophils phenotype during maturation.

Schematic representations and images of the morphology of human neutrophils during different maturation stages. Myelocytes mature into metamyelocytes, banded neutrophils, and finally into mature segmented neutrophils. Neutrophils may also assume an hypersegmented nuclear shape, with more than 4 nuclear lobes in particular conditions.

However, there is no clear evidence of specific markers to address their identity by flow cytometry or differentially expressed genes while their definition is mostly related to their functional profile (arginase-I, ROS, NOS and IL10 production)¹⁶⁸. Thus, PMN-MDSCs could be classified as a precise differentiation state of neutrophils in pathological conditions, included cancer, with a peculiar immunosuppressive role.

f. Neutrophils

Neutrophils are one of the major effector cells of the innate immune system accounting for 50-70% of the total human leukocytes in the circulation and represent a first line defense in infection and acute inflammation. It is well known that they accumulate in the TME of solid tumors recruited by pro-inflammatory chemokines and cytokines.

A lot of work has been done to investigate the neutrophils phenotype in the TME, however the short lifetime of these cells hampers a deep phenotypical and functional characterization. Even if the application of genetically engineered mouse models has been fundamental to understanding neutrophils dynamic in tumor progression, the difference in lifetime and phenotype across species reduces the possibility to exploit mouse models for their functional characterization in relationship with human diseases. For these reasons, understanding their impact in cancer development required a huge effort in clinical studies.

The definition of neutrophils as phagocytic cells able to release granules' content (lytic enzymes) and Reactive Oxygen Species (ROS) has been changing in a more complex interpretation accompanied by their ability to interact and prime others immune components¹⁶⁹. They release soluble molecules, participating in the design of a cytokines fingerprint of the TME in defined time and space. Several studies employing scRNAseq analysis and MPFC have highlighted that neutrophils can assume multiple phenotype and function¹⁶⁹⁻¹⁷¹. In this context, neutrophils take part as new putative targets not only for prognostic purposes but most importantly for new therapeutic approaches.

i. Neutrophils in solid tumor

Neutrophils infiltrating the TME of solid tumor can exert a dual role in cancer progression with a combination of anti-tumoral and pro-tumoral effects^{169,170,172}. However, the data collected with the advent of high-throughput genomic technologies and the possibility to integrate different clinical studies collected established a negative correlation between the Tumor-Associated Neutrophils (TANs) and the probability of survival¹⁷³. Nevertheless, TANs, due to their ability to kill cancer cells, can directly participate in anti-cancer responses. They form immunological synapses with cancer cells through the Complement Receptor 3 (CR3), composed of CD11b and CD18 and kill cancer cells by the release of Nitric Oxide (NO)¹⁷⁴. Factors such as granulocyte colony-stimulating factor (G-CSF), CXC-chemokine ligand 8 (CXCL8), CXC-chemokine ligand 5 (CXCL5) and CC-chemokine ligand 2 (CCL2), lipopolysaccharide (LPS) and interferon β (IFN β) promote an oxidative burst and the release of hydrogen peroxide (H₂O₂) in neutrophils lead to cancer death¹⁷⁵.

Moreover, the expression of the immunoglobulin G (IgG) Fc receptors (Fc γ receptor (Fc γ R)) and the IgA Fc receptor (Fc α RI) on their surface mediates antibody-dependent cellular cytotoxicity (ADCC) to eliminate antibody-opsonized cancer cells by the ingestion of their plasma membrane in a process called trogoptosis¹⁷⁶.

One of the main actions played by neutrophils in primary immune response is the extrusion of DNA and histones dressed up with granules of proteolytic cytotoxic enzymes such as myeloperoxidase (MPO) and pro-inflammatory-associated proteins; this process give rise to Neutrophils Extracellular Trap (NET) formation. NET was firstly discovered in response to bacteria and operates a trap for pathogens by exposing them to cytotoxic factors.¹⁷⁷

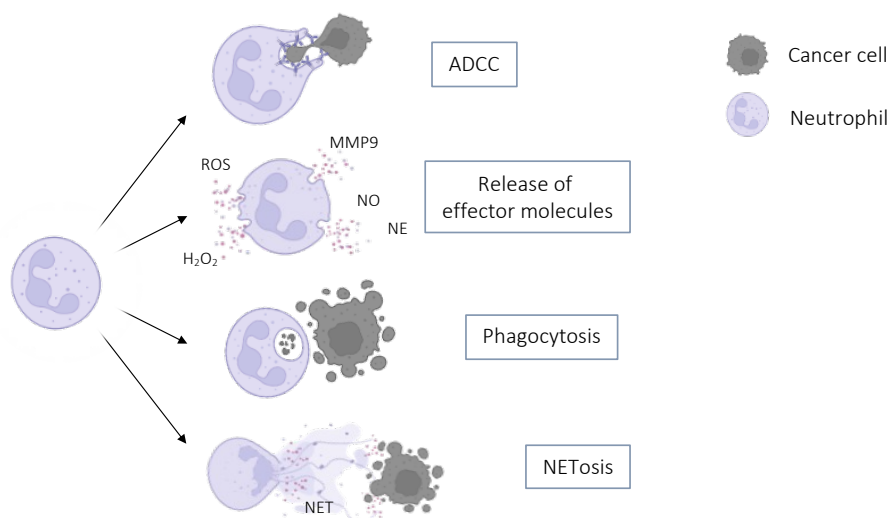


Figure 9. Neutrophils in anticancer response.

Neutrophils play different anti-tumor activity. Through the antibody dependent cytotoxicity (ADCC) can interact and kill cancer cells. They can release effector molecules such as reactive oxygen species (ROS) Nitric Oxide (NO), Hydrogen peroxide (H₂O₂), Neutrophils elastase (NE) and Myeloperoxidase (MMP9) and kill cancer cells by phagocytosis. Moreover, the Neutrophils Extracellular Trap (NET) mediate the direct interact with trap cancer cells and deliver effector molecules. (Created with BioRender.com)

NET has been reported to increase tumor growth and facilitate metastasization driven by CAF-derived Amyloid β in melanoma¹⁷⁸, G-CSF released by cancer cells in lung¹⁷⁹, TGF β in gastric cancer¹⁸⁰ and CCDC25 expression on the surface of cancer cells in CRC and breast cancer¹⁸¹. Moreover, NET has been linked to neo-angiogenesis VEGF-mediated, extracellular matrix (ECM) degradation by Matrix metalloproteinase 9 (MMP9) and neutrophil elastase (NE), and tumor cells extravasation (through IGF-1) favoring metastasis formation¹⁸². Moreover, transforming growth factor- β receptor (TGF β R) accumulated in the TME is able to induce in neutrophils reactive oxygen species (ROS) production and NO release further cooperating in tissue damage^{175,183}.

An increase of proteins related to degranulation have been shown to induce cell growth in both human and mouse models of lung cancer. The release of NET, prostaglandin E2 (PGE2) and hepatocyte growth factor (HGF) induces proliferation of pre-neoplastic and cancer cells^{174,184,185}.

Interestingly, a role of neutrophils in fuel cancer cells with lipids was recently described by Peishan et al., suggesting a neutrophils role as “energetic reservoir” and their intervention in the metabolic complexity within the tumor¹⁸⁶.

Several studies have demonstrated the direct contribution of TANs to promote tumor progression, but, it has also been demonstrated that the accumulation of neutrophils in distal tissue from the original tumor site generates a favorable niche to micro-metastasis colonization^{187,188}.

All these data suggest a more complex profile instead of the classical poor plastic vision of neutrophils and led to applied single cell technologies for their characterization in human to shed light on the phenotype of progenitor granulocytic cells within the bone marrow, dissecting the maturation process¹⁸⁹, and their heterogeneity in the circulation as well as within the TME. In this regard, Montaldo et. al demonstrated a clear modulation of neutrophils phenotype in different conditions, including cancer, completely overcoming the concept of neutrophils as a unique population after the release from the bone marrow¹⁷¹.

In this contest the crosstalk between neutrophils and CD8⁺ T cells is still controversial.

ii. Neutrophils-T cells interaction

Neutrophils are able to cooperate in cancer immunity toward a fine-tuned network of interaction with other immune cells. Their release of cytokines in the TME participates in the recall and activation, suppression or differentiation state of other immune cells. However, among the innate compartment, neutrophils represent one of the major T cell suppressor populations. In this complex scenario, the crosstalk between neutrophils and CD8⁺ T cells is still controversial.

Activated neutrophils in head-and-neck cancer or mammary carcinoma were able to inhibit T cell proliferation through ROS production and degranulation after direct contact. This resulted in change in morphology, mitochondrial dysfunction and adenosine triphosphate depletion in T cells and dump T cells proliferation, revealing the detrimental role of activated neutrophils on T cells¹⁹⁰. Same results were observed in neutrophils isolated from mice colon tumors. The depletion of neutrophils in CRC tumor-bearing mice leads to reduction of cancer mass together with higher T cell infiltration, supporting the immunosuppressive role of neutrophils. Neutrophils release MMP9 in the TME which activates the precursor form of

TGF β turning off CTLs response¹⁹¹. In a pioneering study, Eruslanov et al. demonstrated a feedback loop between neutrophils and CD8⁺ T cells. In early-stage human lung cancer CD66b⁺ CD15^{high} CXCR2⁺ CXCR4⁺ neutrophils have been demonstrated to be enriched and active within the TME and their ability to promote T cell proliferation *in vitro* and their cytotoxic activity has been proven. On the other side, T cells are able to increase the viability of neutrophils *in vitro*. Interestingly the crosstalk between neutrophils and T cells has been demonstrated to take place in a contact-dependent mechanism.

ROS and NO, released by activated neutrophils in the TME, negatively modulate the activity of others immune components, resulting in immunosuppression on the T cells compartment^{175,192}. Interestingly, the interaction between CXCR1 and CXCR2 and their ligands induce NET formation. NET, in turn, protects tumor cells from CTL and NK cytotoxicity generating a mechanical barrier and prevent the immunological synapsis formation¹⁹³. Moreover, NET was found to positively correlate with Treg cells, further suggesting its pro-tumoral role in hepatocellular carcinoma¹⁹⁴.

Although several studies suggest that tumor associated neutrophils suppress the anti-tumor activity of infiltrating T lymphocytes, data are still scattered and frequently controversial. The interaction between neutrophils and gamma delta ($\gamma\delta$ T) T cells showed both pro- and anti-tumorigenic properties, based on the TME composition. The release of IL10 and arginase by neutrophils and IL17 by $\gamma\delta$ T cells have been shown to induce immunosuppression of T cells cytotoxic activity leading to cancer progression in breast cancer¹⁹². Instead, NETosis, together with the ROS and NOS produced by neutrophils and GZMs and PRFs by $\gamma\delta$ T cells, have been found as key factors for tumor cells lysis¹⁹⁵. In lung cancer, the interferon- γ (IFN γ) and granulocyte-macrophage colony-stimulating factor (GM-CSF) promote the differentiation of immature neutrophils into APC-like cells and trigger CD4⁺ and CD8⁺ T cells activity¹⁹⁶. Moreover, their ability to acquire an APC-like phenotype has been also demonstrated in draining lymph nodes of head and neck cancer improving patients' prognosis¹⁹⁷.

The crosstalk between CTLs and neutrophils has been also demonstrated by the colocalization within the TME, noticing that their physical interaction is an important player in cancer immunity. Governa et al. demonstrate that neutrophils are able to induce a central memory phenotype in CD8⁺ T cells *in vitro*, with an increase in CD69 expression and IFN γ release, through the interaction of CD11b and CD54/ICAM1 on neutrophils¹⁹⁸. Further studies are necessary to clarify the role played by neutrophils in the complexity of the TME and their intervention in cancer progression.

5. Multiomics approaches to dissect tumor heterogeneity

Several studies have managed to deeply immune-profile at single cell level different type of cancers. The application of different technologies such as scRNAseq, MPFC, cytometry by time of flight (Cytof) and multiplex immunofluorescence (mIF) not only have identified new immune populations completely renewing the idea of heterogeneity in the TME but allow to perform a single cell analysis even starting from limited amount of sample, crucial for application in human studies.

The first tools used for transcriptomic analysis in immunological studies were based on microarrays targeted RNA. This technique allows the identification of a specific selected transcript even with a very low expression of it and starting from a low amount of material¹⁹⁹. Nowadays, the targeted RNA transcriptomics has been developed and with the application of BD Rhapsody Express system it is possible to detect target RNA analysis at single cell level.

For several years an incredible number of studies took advantage from the bulk-RNA sequencing. However, this tool has difficult application in immunological characterization of complex sample, like tumors, where it is impossible understand the ownership of a specific differentially expressed genes (DEG) identified²⁰⁰. To overcome this limitation, an enrichment of the population of interest by FACS-sorting or magnetic isolation is necessary but challenge due to the small amount of material and the low abundance of the immune populations within the TME. The advent scRNAseq has completely renewed the cancer immunology. The possibility to analyze the transcriptional profile at single cell level has given rise in the last decade to an incredible amount of new data about cell differentiation and function, with the discovery of immune subpopulations and mechanistic information. These results have paved the way for the dissection of the huge tumor immune heterogeneity and most importantly for a fast and scientific relevant translation in clinical applications.

The antigen specificity of the lymphocytes within the TME is another important feature to be elucidated in order to predict the response to the therapy and the patient prognosis. Both with bulk analysis and single cell technologies we can obtain the clonotype of T and B cells using specific oligonucleotides. Despite the cost of the single cell analysis, it allows to obtain matched information about the clonotype and the complete transcriptional profile of the cells.²⁰¹

A second branch of interest for immunological studies is dissecting the epigenetic profile of the immune cells. scATACseq (single cell Assay for Transposase-Accessible Chromatin using sequencing)^{202,203} is the prominent techniques in the field, however scChIP-seq (single cell chromatin immunoprecipitation sequencing)²⁰⁴, scHi-C-seq (single cell high-throughput

chromosome sequencing)^{205,206} and several other techniques are emerging on the scene to dissect the epigenetic regulation of immune cells in differentiation processes, in adaptation within different tissue and pathological condition, included cancer.

On the other side, the proteomic analysis is fundamental to complete the immune-profiling and get functional information. Continuous improvement in flow cytometry is now allowing to analyze up to 40 antigens simultaneously with the advantage to get quantitative information. Together with scRNAseq, MPFC is the main applied technique to generate immune-profiling in patients derived samples and has generated important results not only to understand biological processes but, most importantly, to discover new therapeutic targets.²⁰⁷ Nevertheless, in the last decade, the development of CyTOF allows the detection of up to 45 proteins simultaneously, which has represented an important achievement for functional immunological studies²⁰⁸. Indeed, the use of heavy metal isotopes avoids the background associated with fluorescent antibodies used for flowcytometry and limits the high rates of autofluorescence.

Finally, technologies like mIF (multiplexed immunofluorescence imaging) for proteins detection and RNAScope (RNA in situ hybridization) for the in situ analysis of the transcriptome, top up the lack of localization information and resolution by integrating proteomics and transcriptomics profiling with the localization in the tissue²⁰⁹.

The continuous development of these technologies generates an incredible amount of data at single cells level in complex samples leading to the development of new tools of analysis. Thus, new and sophisticated bioinformatics algorithms have been developed to generate computational analysis able to explore the complexity of the sample, discover new populations together and get information regarding the relationships, which associate and differentiate each other's. t-distributed Stochastic Neighbor Embedding ((t-SNE)²¹⁰ and Uniform Manifold Approximation and Projection (UMAP)²¹¹ are techniques of dimensional reduction and are fundamental for the visualization of complex samples. However, to dissect the heterogeneity of the samples it is necessary to define specific populations characterized by a common proteomic/transcriptional profile (clusters). To reach this aim additional machine learning techniques compute the similarity toward neighborhood events and, after the construction of a network of connections, algorithms detect the density of neighborhood events with a peculiar profile and define clusters.

Focusing our attention on the analysis of MPFC, after a well-defined workflow of preprocessing²¹², repository available algorithms are applied to generate exploratory analysis of the samples. It is important to highlight that the number of clusters could be fixed by the researcher (FlowSOM)²¹³ or detected by the algorithm in an unbiased way (Phenograph)²¹⁴. The PhenoGraph algorithm allows to identify multiple and unexpected clusters

independently from the number of events associated by a common profile but only based on the level of similarity between two group of cells. A fundamental point to take into account when performing this kind of analysis is to avoid that large clusters obscure the presence of rare populations, which is important feature to utilize this approach for the detection of new cell type in heterogeneous human derived sample such as cancer specimens. New algorithms, such as PhenoGraph for MPFC, are optimized to maintain a good separation of small populations even if the number of clusters is unbiased. To validate the ability of the algorithms to detect real cell populations is good practice to identify the same cell phenotype using the manual gating strategy. This procedure is always recommended after the identification of a new population by computational analysis to confirm and refine the profile of the novel cells.

The combination of multiple techniques is a potent tool to dissect immune heterogeneity within and across small samples derived from cancer patients.

In this study, we combined several techniques to dissect the composition of the TME, mainly focusing on the crosstalk between neutrophils and CD8⁺ T cells and its impact on anti-tumor response and clinical outcome.

Methods

1. Ethics approval for the research

The European Institute of Oncology (IEO) Institutional Review Board (protocol n. R1083/19-IEO 1149) approved the use of patients derived sample collected from patients diagnosed with CRC. All the patients enrolled in the study were non-metastatic and treatment-naïve at the time of surgical resection. The collection of peripheral blood from healthy donors has been approved by the IEO's Ethical Committee (registered as IEO 1781) and all the donors provided written informed consent in accordance with the Declaration of Helsinki.

Mice were housed and bred in a specific-pathogen-free animal facility and treated in accordance with the European Union Guideline on Animal Experiments. Animal handling and experimental protocols were reviewed and approved by the Institutional Animal Care and Use Committee of The Jackson Laboratory under the protocol number AUS#17027.

For mouse experiments, we used C57BL/ 6J male mice of 10 weeks in each experiment. The number of biological replicates was indicated in the respective figure legends.²¹⁵

2. Cell lines

Caco-2 were obtained from American Type Culture Collection (ATCC). HT-29 MTX cells were a gentle gift from Dr. Monteleone (University of Rome Tor Vergata, Italy). Caco-2 were cultured in flasks in Eagle's minimal essential medium (EMEM, Merck) supplemented with FBS, HEPES, sodium pyruvate, non-essential amino acids, L-Glutamine. HT-29 MTX were cultured in DMEM supplemented with FBS and HEPES. For co-culture experiments, Caco-2 and HT-29 MMTX were cultured in Caco-2 medium. Human Microvascular Endothelial Cells (HMEC-1) were obtained from Center for Disease Control and Prevention (CDC) of Atlanta. HMEC-1 were cultured in collagen-coated flasks in MCBBD 131 medium supplemented with FBS, HEPES, Hydrocortisone and human epidermal growth factor (EGF). MC38 cell line was a gift from Dr. Chih-Hao Chang lab at The Jackson Laboratory. MC38 cells were maintained in DMEM supplemented with 10% fetal bovine serum (FBS). Cells were cultured in a humidified environment at 37 °C in 5% CO₂.²¹⁵

3. Tissue dissociation and cells isolation

Primary tumors (T) and normal adjacent tissue (NAT, collected at 10cm from the tumor site) were collected just after surgery. One fraction was collected for histological assays, and one was reduced into single-cell suspension.

Firstly, a mechanical dissociation was performed by cutting the sample using tweezers and scalpel in 1 ml of ice-cold PBS. The dissociated tissue was transferred into a 15ml Falcon tube on ice where liquid and solid parts of the samples were separated by 10 minutes sedimentation at 1 g. The interstitial fluid (InF), the liquid part of the tissue, was collected and used freshly or stored at -80°C. While the solid part of the tissue was enzymatically digested with 20µg/ml DNase (Sigma-Aldrich) and 2mg/ml collagenase (Merck) for 30 minutes at 37°C to obtain a single cell suspension. The single cell suspension was then filtered through 100µm and 70µm cell strainers and washed in Hank's Balanced Salt Solution (HBSS) without Ca²⁺ and Mg²⁺. Cells were either stained for MPFC or FACS-sorting, further processed for scRNAseq or frozen in liquid nitrogen according to standard procedures for future used.

For the isolation of peripheral blood mononuclear cells (PBMCs), a density-gradient separation from peripheral blood (PB) was performed. PB was diluted in 1:1 ratio with PBS and gently layered on top of Ficoll solution in a 1:1 ratio. After centrifugation at 300g for 30 min at room temperature (RT), PBMCs were collected, washed, counted and stained for MPFC or employed for CD8⁺ T cells isolation. Aliquots of PBMCs were cryopreserved in

freezing media composed by FBS supplemented with 10% dimethyl sulfoxide (DMSO). CD8⁺ T cells were isolated from PBMCs by negative magnetic separation using the Miltenyi CD8⁺ T Cell Isolation Kit Human following the manufacturer's instruction.

Human polymorphonuclear leukocytes (PMNs) enriched pellet was diluted with 20 ml of PBS and a 3% dextran solution in HBSS was added in a 1:1 ratio. After 30 min at 1g at RT the supernatant was collected and washed, and red blood cell lysis was performed according to manufacturer's instruction (Red Blood Cell Lysis Solution, Mylteni).

Bone marrow (BM) derived mouse neutrophils were purified through positive selection. Briefly mice legs were collected, and the bone isolated then cut at the extremities. The BM was extracted by flushing into the cavity of the bone. After washing Ly6G⁺ cells were enriched by the anti-Ly6G magnetic beads (Miltenyi Biotech) according to the manufacturer instructions.

Mouse CD8⁺ T cells were isolated from spleen and lymph nodes. After mechanically dissociation and filtering to obtain a single cell suspension, cells were washed and treated with ACK to remove the erythrocytes. After counting CD8⁺ T cells are enriched by negative magnetic separation using the Miltenyi CD8⁺ T Cell Isolation Kit Mouse following the manufacturer instructions.

Mice tumors were collected and cut using tweezers and scalpel. The single cell suspension was obtained by enzymatic digestion with 1,5 mg/ml collagenase, 0,75 mg/ml hyaluronidase and 0,1mg/ml Dnase I in RPMI 10% FBS for 1h at 37°C. Cell suspension was filtered through 100µm and 70µm cell strainers, washed, counted, and stained for MPFC or FACS-sorting.

Sorting/isolation efficiency and yield of isolated human and mouse immune populations were checked by FACS, and we obtained a purity around 90 ±10%).

4. Multiparametric flow cytometry (MPFC) and sorting

High-dimensional flow cytometry was performed on tumor (T), normal adjacent tissue (NAT) and peripheral blood (PB) with conjugated antibodies shown in the following table.

Marker	Fluorophore	Manufacturer	Cat. #	Dilution
CCR7	BV421	BD	562555	1:100
CD10	APCR700	BD	659120	1:100
CD11b	BV786	BD	740965	1:100
CD11C	APC R700	BD	566610	1:100
CD127	APCR700	BD	565185	1:100
CD14	BV421	BD	565283	1:100
CD15	APC	BD	551376	1:100
CD16	BV650	BD	563692	1:100
CD19	BV650	BD	563226	1:100
CD206	APC	BD	550889	1:100
CD25	PE-CF594	BD	562403	1:100
CD3	BB700	BD	566575	1:100
CD33	BV421	BD	562854	1:100
CD39	PECF594	BD	563678	1:100
CD4	BV605	BD	562658	1:100
CD45	APCH7	BD	560178	1:100
CD45Ra	FITC	BD	555488	1:100
CD66b	PE	BD	561650	1:100
CD68	BV421	BD	564943	1:100
CD69	APCCY7	BD	560912	1:100
CD69	APC	BD	555533	1:100
CD8	BV605	BD	564116	1:100
CD8	BV786	BD	563823	1:500
CD80	PE	BD	557227	1:100
CTLA4	BV421	BD	562743	1:100
CXCR2	BV421	BD	744195	1:100
CXCR2	FITC	BioLegend	320704	1:100
CXCR4	PECY7	BD	560669	1:100
GRZK	PE	Santa Cruz Biotechnology	sc-56125	1:100
HLA-DR	BV605	BD	562845	1:100
LAG3	PE	BD	565616	1:100
Fixable Viability Stain 510		BD	564406	1:100
PD1	BV650	BD	564104	1:100
TCR γ/δ	PE-CF594	BD	562511	1:100
TIM3	BB515	BD	565568	1:100
TCRgd	PerCP-Cy5.5	BioLegend	331224	1:10
NKG2A	FITC	Miltenyi	130-113-568	1:100
CD39	APC-H7	BioLegend	328226	1:50
TIGIT	APC	BioLegend	372706	1:50
CD25	BV786	BD	741035	1:600
CCR7	BV711	BD	566602	1:20
OX40	BV650	BD	563658	1:20
CD161	BV605	Biolegend	339916	1:10
CD27	BV570	BioLegend	302825	1:20
CD11b	BV510	Biolegend	301334	1:10
PD1	BV480	BD	566112	1:20
CD103	BV421	BioLegend	350214	1:100
CD8	BUV805	BD	564912	1:200
CD28	BUV737	BD	564438	1:10
HLADR	BUV661	BD	565073	1:100
CD4	BUV615	BD	624297	1:400
CD45RA	BUV563	BD	565702	1:100
CD3	BUV496	BD	564809	1:20
CD69	BUV395	BD	564364	1:100
CD45	PE-Cy7	Biolegend	3.04016E+11	1:2500
CD56	PE-CY5.5	eBioscience	35-0567-42	1:20
CD127	PE-CY5	eBioscience	15-1278-42	1:20
CX3CR1	PECF594	Biolegend	341624	1:50
GZMB	APC-R700	BD	560213	1:600
GZMK	PE	Santa Cruz	sc-56125	1:200

Table 2. List of antibodies applied for the multiparametric flow cytometry analysis.

Adapted from Tiberti et al.

Single-cell suspensions were stained fresh or after thawing in pre-warmed RPMI with 10% FBS. Cells were washed in staining buffer (PBS with 2%FBS and 2mM EDTA) and incubated for 30 min at 4°C with surface antibody cocktail in staining buffer, washed in staining buffer, fixed and permeabilized using Fixation/Permeabilization Solution Kit (BD). When necessary, cells are stained intracellularly for 2h at 4°C with antibody cocktail in permeabilization solution. To acquire samples FACSymphony A5 or FACSCelesta BLYG equipped with FACSDiva version 8.0.1 were used. Compensation Beads (Ultracomp, Thermofisher) were used for single-stained controls for electronic compensation.

CD8⁺ T cell subsets and neutrophils populations were sorted to high purity using FACSARIA III (BD Bioscience) with the application of single staining controls on the same tissue and fluorescence minus one (FMO) control for the fundamental markers of the sorted populations. CD8⁺ T cells were simulated 3 h with PMA (20 ng/ml), ionomycin (1ug/ml) and GolgiPlug protein-transport inhibitor (brefeldin A, 1:1000) to evaluate *ex vivo* cytokines production.

Software FlowJo v10 (TreeStar) was utilized to analyze and visualize all the FCS files generated.

5. MPFC data analysis

The large amount of data obtained from CRC patients derived T, NAT and PB required computational analysis to reduce the complexity of the samples and dissect the heterogeneity of the infiltrate. The Phenograph algorithm²¹⁴ was applied to compute the similarity toward neighborhood events.

Briefly after compensation and isolation of singlet, LD negative, CD4⁻, CD3⁺, CD8⁺ T cells, CD8 analysis was performed on 3000 events per sample and all concatenated by the “cytof_exprsMerge function”. In the first iteration of the algorithm, K value (the number of nearest neighbors identified), was set to 100. FlowJo version 10 (FlowJo) was utilized to generate and visualize the dimensional reduction by Uniform Manifold Approximation and Projection (UMAP) and t-distributed stochastic neighbor embedding (tSNE). The under-represented clusters (<0.5%) were discarded from the analysis.

The balloon plots generated a further meta-clustering classification by the interpolation of the MFI and the frequency of each marker per cluster and was performed using the ggplots2 R package.

Euclidean distance and Ward-linkage methods via cytofkit package were applied to generate hierarchical meta-clustering of Phenograph generated clusters based on age, gender and stage of disease.

6. Immunohistochemistry (IHC), Immunofluorescence (IF), and GIEMSA staining

Slides (5 μm) from formalin-fixed paraffin embedded (FFPE) samples were stained after deparaffinization by heating 30 min at 55°C and rehydration in consequent steps of 5 min within in order: Xylene (3 times), ETOH 100% (2 times), EtOH 95%, EtOH 70%, EtOH 50% 5 min and ddH₂O. Heat-induced antigen retrieval (citrate buffer pH 6 or 9, Thermofisher) was performed with the application of the microwave. For IHC 3% H₂O₂ incubation was used to block endogenous peroxidase activity. Slides were incubated ON at 4 °C with mouse anti-human CD66b antibody (BioLegend, 305102, 1:100 for both IHC and IF), anti-human CD8 (Invitrogen, 53-0008-82, 1:100), rabbit anti-human GZMK (Invitrogen, LS-C119554-50, 1:100), rabbit anti-human E-Cadherin (Abcam, Ab1416, 1:100), rat anti-human Ki67 (eBioscience, SolA15, 1:200), rabbit anti-human EPCAM (Abcam, Ab32394, 1:400), mouse anti-human SDF-1 (R&D, MAB350, 1:100), anti-human αSMA (Abcam, Ab8211, 1:200) in a blocking solution composed of 3% BSA, 5% goat serum (Invitrogen, 10000 C) and 0.1% Triton in PBS. After 30 min of incubation with HRP-secondary antibody and Aminoethyl Carbazole (AEC) + High Sensitivity Substrate Chromogen (Dako) for IHC or fluorophore-conjugated antibodies (Invitrogen, goat anti-mouse 488; Invitrogen, goat anti-rabbit 647; Invitrogen, goat anti-rabbit 488; Invitrogen, goat anti-mouse 555; 1:500; Invitrogen, goat anti-rat 555, all 1:500 for 1h at RT) for IF, slides were mounted and acquired by using Aperio for IHC or SP8 confocal microscope (Leica) for IF, respectively. GIEMSA staining was performed on neutrophils freshly isolated from PB or FACS-sorted from tumors after cytopsin on the surface of glass slides at 300 RPM 4 min following manufacturing instruction for the staining with methylene blue, azure B and eosin (Hemacolor, Sigma).

7. Imaging analysis

For quantification of GZMK signal on human colorectal cancers, sections were labeled with DAPI, anti-GZMK, anti-CD66b and Alexa Fluor 488-conjugated anti-CD8 primary antibodies and images captured with a Nikon CSU-W1 spinning disk (Nikon Europe BV) using a 40 \times /1.15 NA water immersion objective lens (pixel size 0.1625 \times 0.1625 μm^2). For the tumor area identification, previews of tissue sections on the DAPI channel were acquired with a 10 \times /0.3 NA dry objective lens. Inside the tumor areas, 3 to 4 regions were randomly chosen for the acquisition with a 40 \times /1.15 NA water immersion objective lens. Each region was made of 12 adjacent tiles covering a total area >4mm² per tissue section.

The quantification of the GZMK signal in CD8⁺ cells was done with a custom-made Fiji macro103. Briefly, images were pre-processed with denoising and background subtraction, and nuclei were segmented on the DAPI channel with the plugin StarDist104, using the built-in model Versatile (fluorescent nuclei) and the intensity parameters, including “mean intensity” and “raw integrated density”, of CD8, GZMK and CD66b fluorescence were quantified in a band of thickness 1µm around each nucleus.

CD8⁺ cells were identified from the database by setting criteria on the intensity parameters of the specific fluorescence. Particularly, a cell was considered as positive for CD8 fluorescence channel if its “raw integrated density” was above a threshold value, set by the comparison in images of the “raw integrated density” values of cells expressing CD8 fluorescence and the “raw integrated density” of cells expressing only autofluorescence signal. The same procedure described above was used for the detection of CD66b positive cells. Differences between two groups were calculated by unpaired, two-tailed Student’s t test. The analysis of GZMK fluorescence in CD8⁺ cells lying in the proximity of a neutrophil (CD66b⁺) was performed as follows: the distance between a CD8⁺ cell and its nearest neutrophil was computed per each field of view. Only distances below 10 µm were considered to select pairs of CD8⁺ cell-neutrophil that were close to each other. The mean intensity of GZMK fluorescence in CD8⁺ cells close to neutrophils was compared to the GZMK mean intensity of cells close to neutrophils that were not positive for CD8.

In order to evaluate the expression of GZMK of CD8⁺ cells in relation to their distance from a neutrophil, we performed the computation of lymphocytes and neutrophils distances in Tumor Area. The distances of CD8⁺ cells from each neutrophil were calculated in each acquired image using an R script and these distances were filtered with a min function in order to consider the «nearest» neutrophil per each CD8⁺ cell. For the analysis, we considered only distances <10µm (Touching) and between 10 and 20 µm (Near).

For the quantification of SDF-1 in cells positive for αSMA, human colorectal cancers sections labeled with DAPI, anti-SDF-1, anti-αSMA, and anti-EPCAM primary antibodies, and captured with a Nikon Eclipse Ti widefield microscope (Nikon Europe BV) using a 20×/0.75 NA dry objective lens (pixel size 0.32 × 0.32 µm²). For the tumor area’s identification, previews of tissue sections were acquired with a 4×/0.2 NA dry objective lens. Inside the tumor areas, regions were randomly chosen for the acquisition with 20×/0.75 NA dry objective lens for a total acquired area >35 mm² per tissue section.

The quantification of SDF-1 signal in αSMA⁺ cells was done with Qupath v. 0.2.3105 through a custom-made script. Briefly, cell nuclei were detected on DAPI channel with the StarDist extension and a cell expansion of 1 µm was applied in order to measure fluorescence in the cytoplasmic/membrane cell’s area. For the nuclei segmentation with StarDist, a

custom model was trained and tested using the StarDist (2D) network in ZeroCostDL4Mic106: a training dataset was generated by the manual annotation of nuclei in QuPath and labeled images were exported for the deep-learning training; the model's training and quality control assessment were performed with the StarDist (2D) notebook. For the detection of pixels positive for α SMA staining, a pixel classifier was created with the QuPath's function Create thresholder and the quantification of the positive area inside each segmented cell was added as a measurement parameter in the detection's results table. Other two-pixel classifiers in the red and far-red channels were similarly created to be used in the statistical analysis step. The expression of SDF-1 was quantified as the mean intensity of the corresponding fluorescence signal in the band around the nucleus.

Cells with an area $> 3 \mu\text{m}^2$ (estimated as the 10% of the area of a band created around a nucleus with area size $46 \mu\text{m}^2$) of pixels classified as positive for α SMA were considered as α SMA⁺. Cells overlapping with red blood cells were discarded from the analysis.²¹⁵

8. *In vitro* CD8⁺ T Cells and Neutrophils co-culture and treatment with Interstitial fluid (InF)

After isolation, CD8⁺ T cells were stimulated with plate-bound anti-human CD3 (2mg/mL) and anti-human CD28 (2mg/mL) for 6h. After activation, CD8⁺ T cells and freshly isolated neutrophils were co-cultured at different ratio in complete RPMI-1640 media after washing of CD8⁺ T cells to remove the anti-human CD3 and anti-human CD28 antibodies in order to avoid Anti-body-dependent cellular cytotoxicity (ADCC) of neutrophils on CD8⁺ T cells and analyzed at different timepoints.

To evaluate the effect of T and NAT interstitial fluid (InF), both CD8⁺ T cells and neutrophils were cultured in 96well plates and treated with InF in a ratio of 1:3 with the cell media for 24 and 2 hours, respectively. In the control, the 1/3 of the media is substituted with PBS. After incubation time, cells were stained for MPFC and analyzed.

9. *In vitro* GZMK and SDF-1 treatment

HT-29 and CACO2 cells were cultured in transwells in 1:9 ratio (CACO2:HT-29) for 16 days and the media was changed every two days. After 16 days of culture, trans-epithelial electrical resistance (TEER) was measured to assess the epithelial formation. Cells were treated with rHu-GZMK (Enzo Life Sciences) 10 μ M for 24h with or without the GZMK inhibitor (PRO-328 100nM, Prospec).

For treatment of neutrophils, freshly PMNs from PB of HD were treated with SDF-1 100 ng/ml (R&D biosystems) and analyzed at different time points and with different assays as indicated in the results and relative figures.

10. Neutrophils migration assay

Custom-made microfluidic device in Polydimethylsiloxane (PDMS) was used to perform a migration assay of neutrophils isolated from PB of HD. It was composed by three parallel channels separated by two lines of pillars. A collagen matrix solution (composed by a mix of PBS 10x, NaOH 1N, 8.04 mg/ml rat tail Collagen type I and RPMI culture medium) was injected in the central channel of the microfluidic chip, incubated at 37°C and hydrated by injecting culture medium into the lateral channels.

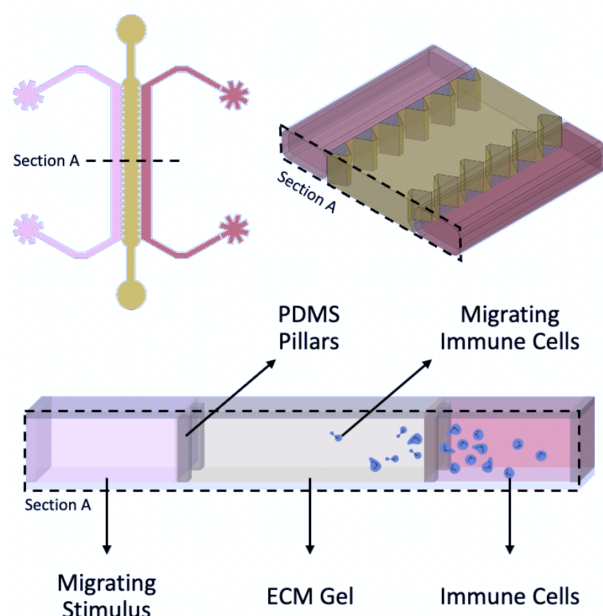


Figure 10. Schematic overview of neutrophils migration-on-Chip.

Microfluidic chip with an immune cells channel (700 μ m wide, 1.1 cm long and 150 μ m high) and a chemoattractant channel (700 μ m wide, 1.1cm long and 150 μ m high) separated by extracellular matrix (ECM) (1300 μ m wide, 1.1 cm long and 150 μ m high). Trapezoidal micropillars (bases 270 and 60 μ m, height 190 μ m, spacing 120 μ m, pillar height 150 μ m) confine ECM in the central region were used for motility assay. In time-lapse experiments, migrating neutrophils invading the ECM channel, were counted.

The right channel of the device was injected with purified human neutrophils (3x10⁶/ml) from healthy donor labeled with calcein-AM (1:1000, Invitrogen), Hoechst 33342 (1:10,000, Euroclone) and DRAQ7 (1:1000, Vinci-Biochem). In order to have neutrophils lying at the interface between lateral channel and collagen gel the chips were incubated at 37°C for 20 min on an angled surface. Invasion of neutrophils in the collagen gel was evaluated through time lapse experiments performed using Nikon Eclipse Ti (3 fields for chip, 1 image every 2.30 min for 4 h at 10x magnification) following addition of chemoattractant solutions or

culture medium to the left channel. Interstitial fluid from patient's tissues, purified CXCL6 (400 ng/ml), SDF-1 (100ng/ml) and IL8 (100 ng/ml) (R&D biosystems) were added to the system and the number of migrating cells was analyzed using imagej version 2.0.

11. Neutrophils gelatinase assay

DQ gelatin (molecular Probes, 100ug/ml final concentration) was used to measure gelatinase activity from a triplicate of HD-derived PB isolated neutrophils with or without SDF-1 treatment (100 ng/ml). Neutrophils were incubated with DQ gelatin and every 15 min the fluorescent output was measured at room temperature on GloMax Discover microplate reader (Ex~495nm, Em~515nm) Promega Instrument) and corrected for background. Internal calibration curve was generated using *Clostridium histolyticum collagenase* (0.15 U/ml).²¹⁵

12. Neutrophils adhesion assay

To label the cells, freshly neutrophils isolated from PB of HD were stained with Calcein-AM (1:1000, Invitrogen) and Hoechst 33342 (1:10,000, Euroclone) for 20 min at 37°C. Stained cells were incubated in RPMI media with or without SDF-I (100 ng/ml) for 1 h at 37°C in a 96-well on a monolayer of HMEC1. Before to proceed with the acquisition of the images, two washes with PBS were performed to remove non-adherent cells. The images of three fields for each well collected at the EVOS microscope (EVOS FL Cell Imaging System) at 4x magnification were analyzed. Calcein positive neutrophils were counted to calculate the number of adherent neutrophils using ImageJ version 2.0.0.

13. *In vivo* animal experiments

C57BL/6J were subcutaneously injected with 1×10^6 MC38 cells per mouse. When the tumor reaches the volume of $<1\text{cm}^3$ and $>1\text{cm}^3$ mice were euthanized to evaluate CD8⁺ T cells and neutrophils frequency and phenotype during progression.

The neutrophils enrichment in mice were obtained by intraperitoneal injection (i.p.) of G-CSF (2.5µg/mouse) daily from the day 16 after tumor injection as previously described¹⁸⁶. Mice were euthanized for analysis at day 22.

The depletion of neutrophils *in vivo* was obtained by i.p. of anti-Ly6G (clone 1A8, Bio X Cell) and anti-rat mouse IgG2a, Kappa immunoglobulin (clone MAR 18.5, Bio X Cell) or isotype controls (for anti-Ly6G and for anti-rat mouse IgG2a). Mice were treated with anti-

Ly6G or isotype daily (day 0-20) via i.p., (25 µg/mouse) for day 0–6, and 50 µg/mouse for day 7–18; while anti-rat mouse IgG2a or isotype was administrated every other day, i.p., (50 µg/mouse), i.p. for the combo injection days, injection of anti-rat IgG2a first, and 2 h later, do the injection of anti-Ly6G¹⁸⁶. Mice were euthanized for analysis at day 20.

The treatment with SDF-1 inhibitor (ADM3100) was performed by i.p. of ADM3100 (1 mg/kg) at day 5, 7, 9, 11 after tumor injection. Mice were euthanized for analysis at day 13. All mouse experiments were conducted in agreement with requirements permitted by our ethical committee.

The day of analysis, primary tumors were collected and dissociated to a single cell suspension as previously described and used for the analysis.

14. Bead-based multiplexed ELISA

Multiplexed ELISA on InF from matched T and NAT fresh tissues were performed on a Luminex 200 platform (Luminex Inc.,) using custom kits of pre-mixed antibody-coated beads (R&D System Inc., MN). The custom designed panel included the following analytes: CCL11_eotaxin, CCL13_MCP4, CCL17_TARC, CCL2_MCP1, CCL22_MDC, CCL26_EO-TAXIN3, CCL5_RANTES, CCL8_MCP2, CD25_IL2Ra, CX3CL1_FRAC-TALKINE, CXCL1_GROa, CXCL10_IP10, CXCL11_ITAC1, CXCL13_BLC_BCA1, CXCL4_PF4, CXCL5_ENA78, CXCL6_GCP2, EGF, IFN γ , GMCSF, HGF, IL10, IL1ra_IL1F3, IL7, IL8_CXCL8, TRAIL, VEGFA, IL1b_IL1F2, IL5, IL6, IL17F, IL22, IL23, TNF α , LXSAHM-01, CCL3_MIP1a, CCL4_MIP1b, FGFbasic_FGF2, GCSF, IL1a_IL1F1, IL2, IL4, IL12 p70, IL13, IL15, IL17/ IL17A, CXCL12_SDF1, TGF β 1, TGF β 3. The assay was performed based on manufacturer recommendations. Briefly, 50µl of samples together with kit standards were added to each well in duplicate and incubated with the diluted Microparticle Cocktail at 4 °C, on a shaker at 850 rpm overnight (ON). Unbound soluble molecules were removed by washing the plate, then the Biotin-Antibody Cocktail specific to the analytes of interest was added to each well for 1h at RT. After washing, into the wells the Streptavidin-Phycoerythrin conjugated was added and incubate 30 min at RT. After the final washing steps, the microparticles are resuspended in the kit buffer for reading on a Luminex 200 platform. Upon centering and scaling using the scale function in R (SD from mean pg/mL), the outputs (pg/mL) were statistically analyzed and visualized in R. To generate the heatmap of expression the Complex-Heatmap package was applied. Soluble molecule concentrations were associated with the CD15^{high} neutrophils frequency by Spearman correlation and visualized using the corrplot package.

15. Single cell RNA sequencing (scRNAseq)

T and NAT single cells suspension was counted and resuspended in PBS without Ca_2^+ and Mg_2^+ with 0.04% BSA. Approximately 2,000 cells/ μl from each sample were used for the analysis. Briefly, using a Chromium Single Cell 3' v2 Reagent Kit (10x Genomics) every sample were loaded into one channel of Single Cell Chip A. Cells are captured and lysate and complementary DNA was synthesized and amplified over 14 cycles according to the manufacturer's protocol (10x Genomics). From 50ng amplified cDNA the library was prepared and sequenced with the NovaSeq 6000 System (Illumina). An average sequencing depth of at least 50,000 reads per cell was obtained for each sample.

The cells are captured into droplets through the formation of a water-in-oil emulsion through microfluidic devices. Cells are captured lysed with a lysis buffer and specifically barcoded during the reverse transcription. Barcoded cDNAs are synthesized with specific index from thousands of cells in parallel. After reverse transcription cDNAs from different cells are pooled by breaking the droplets and amplified. and then sequencing libraries are prepared. The pooling of cDNA increases the throughput because thousands of cells can be sequenced in a single library resulting in a faster protocol and lower cost.

16. RNA sequencing

The RNA sequencing (RNAseq) of CD8^+ T cells after coculture was performed after the isolation of 1×10^6 CD8^+ T cells with Miltenyi CD8^+ T Cell Isolation Kit Human. For transwell epithelial model of intestine treated with rHu-GZMK, cells were detached and wash with PBS before to proceed with RNA extraction. The RNA was extracted by the RNA easy mini kit (quiagen). The RNA concentrations after extraction were determined using Thermo Scientific NanoDrop 2000 spectrophotometer and the quality assessed by 2100 Bioanalyzer Instrument.

17. RNA data analysis²¹⁹

RNA data were analysed as reported in Tiberti et al., 2022. Briefly, single cells data analysis was performed on samples from 11 patients (for each one NAT and T were sequenced). The results were aligned using Cellranger count v. 3.1 on human genome hg38 and only droplets with a minimum number of unique molecular identifiers (UMI) were considered as "cells" by the Cellranger program.

Based on total cells in each patient and the distribution of each patient's cells within groups identified by UMAP, we excluded patients 3 patients for further analyses. Thus, 52316 cells were processed.²¹⁵ Clustering analysis of the single cell data were performed using Seurat v. 3R package²¹⁶. UMAP was generated from the first principal components of the PCA based on the expression of the most variable genes and normalized to identify cell populations and/or sub-populations. The different clusters were identified using nearest neighbor clustering (SNN) with the function "FindClusters" of the Seurat package. For the Pseudotime analysis was applied Monocle v. 3²¹⁷.

18. Survival analysis methods²¹⁹

RNA data were analysed as reported in Tiberti et al., 2022. To investigate the interplay of immune cytolytic activity and neutrophils infiltration on overall (OS) and disease-free survival (DFS), we interrogated the colon adenocarcinoma cohort (COAD) of The Cancer Genome Atlas (TCGA), and we performed a Kaplan–Meier analysis. The cytolytic activity index was quantified calculating geometric mean of granzymes and perforin expression and samples were split according to the Maximally Selected Ranks Statistics cutoff. Neutrophils and GZMK^{high} cell subtype relative abundance was obtained by running CIBERSORTx112 with a validated leukocyte gene signature matrix (LM22) on RNAseq data of COAD samples. Samples were divided into two groups according to the presence or absence of CD8⁺ T cells cells expressing "high" or "low" values of GZMK. The GZMK^{high} cells identified were used to build a gene signature able to discriminate the two cell sub-populations. The survival tables obtained from TCGA-COAD and TCGA-LUAD were used to ran Kaplan-Meier analysis, by using "survival" and "survminer" packages.

We used Cox Proportional-Hazards Model for investigating the association between the risk of relapse of CRC patients and predictor variables. Cox regression model was chosen because it works for both quantitative predictor variables and for categorical variables and allows to assess simultaneously the effect of several risk factors on survival time (multivariate analysis). The analysis was performed on 209 CRC from TCGA-COAD public dataset looking at infiltration of CD8 GZMK-high cells, sex, age and stage of the tumor.

19. Statistics and Data visualization.

The statistics analyses were performed using Prism version 8.4.2 (GraphPad) or R software version 4.0.2. Significance p value was set at $P < 0.05$, unless otherwise specified and the tests used for each specific analysis are indicated in the figure legend.

Results

1. Immune-profile in non-metastatic CRC patients

Although CRC is considered a “hot” tumor where infiltrating CD8⁺ T cells are an independent positive prognostic factor, the tumor infiltrate is highly heterogeneous.

In this scenario, it’s of pivotal importance to decode the interplay between different cell compartments at the tumor site and their impact on the clinical outcome.

Here, we combined multiparametric flow cytometry (MPFC), multiplex enzyme-linked immunosorbent assay (ELISA), single cell RNA sequencing (scRNAseq) and confocal microscopy imaging together with *in vitro* and *in vivo* functional studies, to characterize the heterogeneity of the immune infiltrate within and across CRC patients. We profiled peripheral blood (PB), tumor (T) and normal adjacent tissue (NAT >10 cm from tumor tissue) from a cohort of 46 treatment-naïve early-stage CRC patients (8th ed. AJCC stages I, II and III) undergoing surgical resection. (Figure 11)

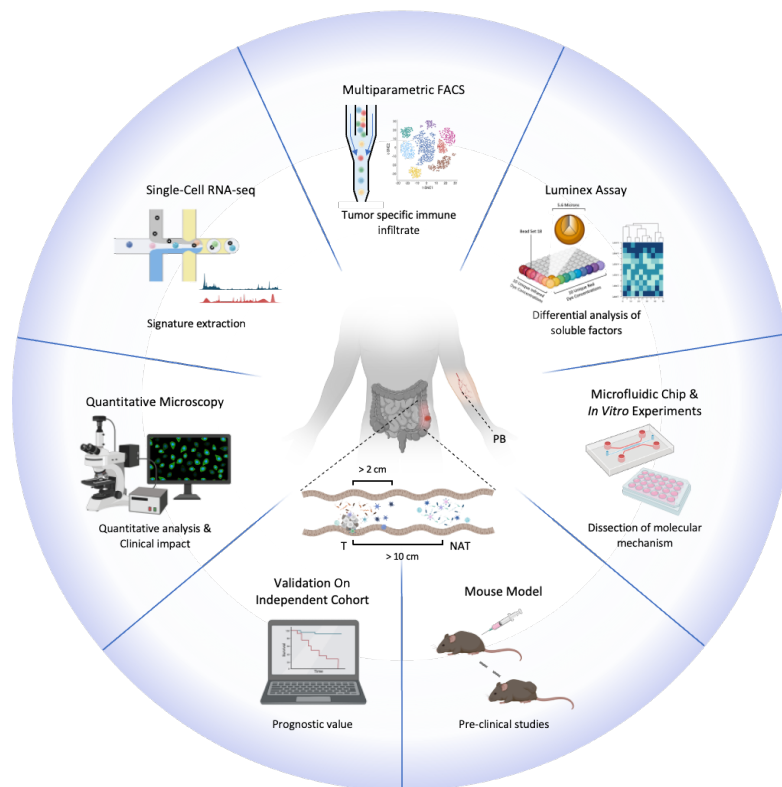


Figure 11. Study design.

Analysis of Tumor tissue (T), Normal Adjacent Tissue (NAT), and Peripheral Blood (PB) of non-metastatic CRC patients (n = 46) with multiomics techniques. (Created with BioRender.com)

Details for all the patients involved in the study -age, gender, stage at first diagnosis, Body Mass Index (BMI), site of primary tumor, tumor type, relapse and MSI/MSS classification- are summarized in Table 3.

Study Cohort		
	Count	Frequency (%)
Total of patients	46	100
Relapse (2 years)	4	8.7
MSI	6	13
Age		
<50	2	4.4
50-70	23	50
>70	21	45.6
Gender		
F	21	45.6
MSI	25	54.4
Stage firs diagnosis		
I	12	26.1
II	16	34.8
III	18	39.1
BMI		
Normal	19	41.3
Overweight	15	32.6
Obese	7	15.2
NA	5	10.9
Site of primary tumor		
Left	20	43.5
Right	24	52.2
Medium Transverse Colon	2	4.3
Tumor type		
Adenocarcinoma	43	93.5
Mucinous adenocarcinoma	3	5.5

Table 3. Characteristics of CRC patients.

Indication of Age, Gender, Stage at first diagnosis, Body Mass Index (BMI), Site of primary tumor, and Tumor type are shown for the cohort of this study.

Adapted from Tiberti et al.

2. CRC TME is mainly infiltrated by CD8⁺ effector memory T (T_{EM}) cells

CD8⁺ T cells infiltration is considered as a positive prognostic factor in many solid tumors, including CRC^{21,22,32}. However, independently of the grade of T cell infiltration, over a third of early CRC patients' relapse. Interrogating a TCGA database of non-metastatic CRC patients with a cytolytic CD8⁺ T cell transcriptional signature failed to significantly stratify CRC patients (Figure 12). This evidence suggests the CD8⁺ anti-tumor immune response is somehow "leaky" and mechanisms behind immune evasion in CRC patients need to be further elucidated.

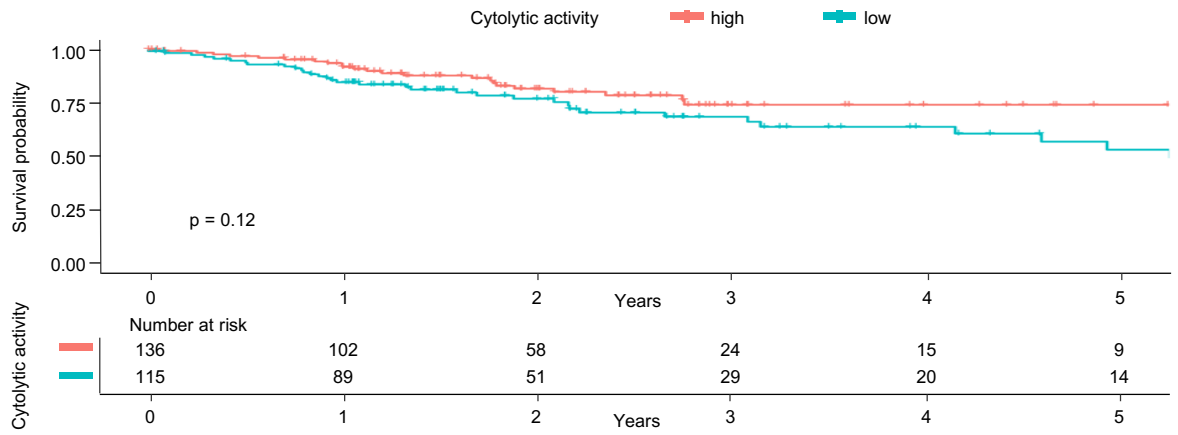


Figure 12. Cytolytic activity is not able to predict Overall survival (OS) in early-stage colorectal cancer (CRC) patients.

Kaplan-Meier analysis of the association of cytolitic activity with disease free survival (DFS) on the TCGA-COAD cohort (n=284). High infiltration of cytotoxic cells is indicated in red, low infiltration in turquoise. The table shows the ‘number at risk’ subjects.

Adapted from Tiberti et al.

In our cohort, CD3⁺ T cells were enriched in T compared to NAT across all CRC patients (Figure 13 panel A); while B cells (identified as CD45⁺, CD3⁻, CD19⁺) were underrepresented (Figure 13 panel B). In the T, the composition of CD3⁺ T cells was mainly characterized by conventional CD4⁺ T helper (Th) cells (52% ± 10) and CD8⁺ T cells (28.5% ± 9), followed by Treg (10% ± 4.5), and Tγδ (3.5% ± 2.5) (Figure 13 panel C).

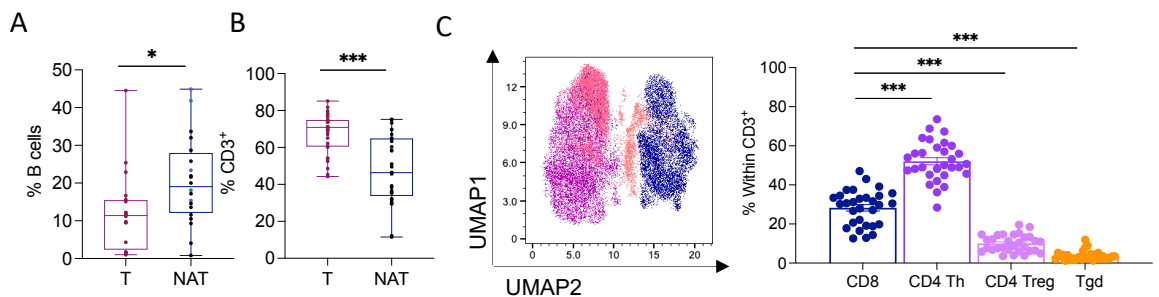


Figure 13. T lymphocytes are the main component of CRC infiltrate.

Quantification of B cells (n=19) within CD45⁺ cells in Tumor (T) and normal adjacent tissue (NAT). Box and whisker plot indicates Min to Max value. *, P < 0.05; paired t test. **B.** CD3⁺ T Lymphocytes frequency within CD45⁺ in T compared with NAT (n=29). Box and whisker plot indicates Min to Max value. ***, P < 0.001; paired Wilcoxon test. **C.** UMAP representation of concatenated CD3⁺ T cells from T sample with bar plot quantification. Cytotoxic CD8⁺ T cells (blue), Th CD4⁺ (purple), Treg CD4⁺ (pink) and Tγδ cells (orange) distribution (n=29). Dot plot indicates Min to Max value. ***, P < 0.001; paired t test.

Adapted from Tiberti et al.

To gain further insights into the diversity occurring specifically in the CD8⁺ T cell compartment, we applied high dimensional flow cytometry and designed a multiparametric panel that includes memory and effector differentiation markers (CD45RA, CCR7, CD27, CD28, CD127, CX3CR1, CD161), activation markers (OX40, CD25, HLA-DR), inhibitory receptors (PD1 and TIGIT), tissue residency and tumor reactivity markers (CD69, CD103

and CD39) and effector molecules (GZMB and GZMK). The list of all the analyzed markers is included in Table 4.

Marker	Fluorophore	Dilution
TCRgd	PerCP-Cy5.5	1:10
NKG2A	FITC	1:100
CD39	APC-H7	1:50
TIGIT	APC	1:50
CD25	BV786	1:600
CCR7	BV711	1:20
OX40	BV650	1:20
CD161	BV605	1:10
CD27	BV570	1:20
CD11b	BV510	1:10
PD1	BV480	1:20
CD103	BV421	1:100
CD8	BUV805	1:200
CD28	BUV737	1:10
HLADR	BUV661	1:100
CD4	BUV615	1:400
CD45RA	BUV563	1:100
CD3	BUV496	1:20
CD69	BUV395	1:100
CD45	PE-Cy7	1:2500
CD56	PE-CY5.5	1:20
CD127	PE-CY5	1:20
CX3CR1	PECF594	1:50
GZMB	APC-R700	1:600
GZMK	PE	1:200

Table 4. Multiparametric flow cytometry panel.

List of the markers with the corresponding Fluorophore and dilution.

Based on the expression of CCR7 and CD45Ra, we were able to discriminate between Naïve cells (T_N ; CCR7⁺, CD45RA⁺), central memory cells (T_{CM} ; CCR7⁺, CD45RA⁻), effector memory cells (T_{EM} ; CCR7⁻, CD45RA⁻) and effector cells re-expressing CD45RA (T_{EMRA} ; CCR7⁻, CD45RA⁺). In accordance with previous studies²², the majority of intratumoral CD8⁺ T cells were composed by T_{EM} cells (74.3%± 16.5) (Figure 14 panel A-B). Moreover, based on the differential expression of CD27 and CD28, we further characterized the T_{EM} cell population in EM₁ (CD27⁺, CD28⁺), EM₂ (CD27⁺, CD28⁻), EM₃ (CD27⁻, CD28⁻) and EM₄ (CD27⁻, CD28⁺)²¹⁸, showing that EM₃ and EM₄ T cells, representing effector-like and memory-like phenotypes, respectively, were the most represented CD8⁺ T cells subtypes in T (Figure14 panel C-D).

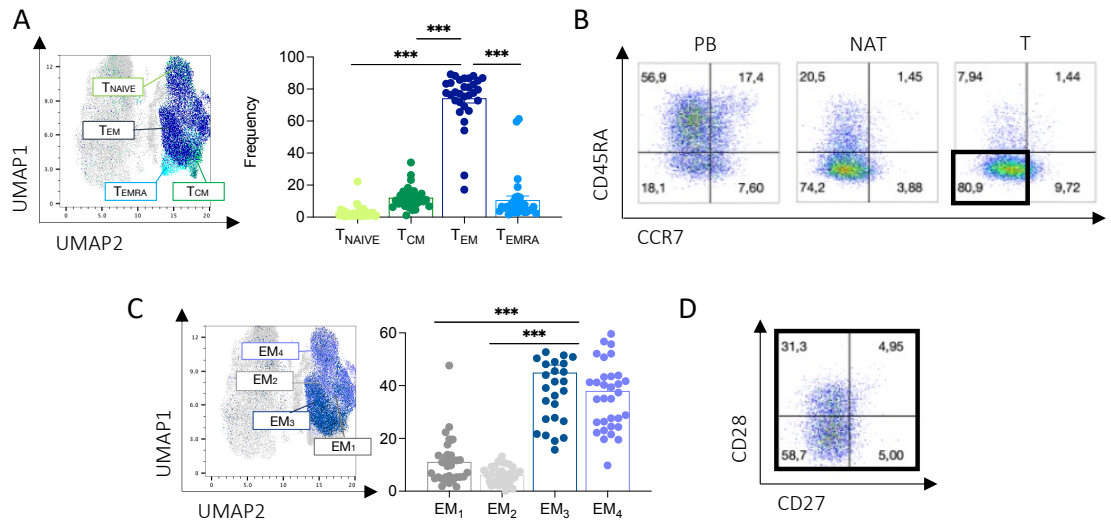


Figure 14. CD8⁺ T cells within colorectal cancer (CRC) tumor are mainly effector memory cells (T_{EM}). A-C. UMAP Representation of concatenated CD3⁺ T cells from tumor (T) sample with bar plot quantification. A. Naïve T cells (T_{NAIVE}, light green), central memory T cells (T_{CM}, dark green), effector memory T cells (T_{EM}, dark blue), effector memory cells re-expressing CD45RA (T_{EMRA}, light blue) distribution (n=31). Bars indicate mean ± s.e.m. ***, P < 0.001; paired t test. B. Representative dot plot of CD45RA and CCR7 expression within CD8⁺ T cells in peripheral blood (PB), normal adjacent tissue (NAT) and T. C. Effector memory T cells subtypes (EM₁₋₄) (n=31). Bars indicate mean ± s.e.m. ***, P < 0.001; paired t test. D. Representative dot plot of CD28 and CD27 expression within CD8⁺ T_{EM} within the T.

Adapted from Tiberti et al.

Interestingly, only a minority of intratumoral CD8⁺ T cells were T_{EMRA}, a phenotype associated with a terminally differentiated phenotype. In accordance, when we analyzed the expression of PD1, LAG3, TIM3 and CTLA4 only low frequencies of CD8⁺ T cells (~1.5%) co-express more than one exhaustion marker, a trait associated with an exhausted phenotype (Figure 15 panel A). Indeed, within the PD1⁺ population, CD8⁺ T cells were still expressing markers (i.e. CD69, CD25 and GZMB) indicative of an “activated” and “functional” phenotype (Figure 15 panel B).

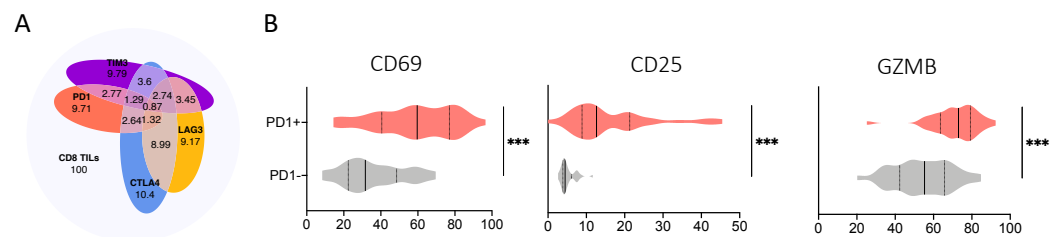


Figure 15. CD8⁺ T cells within colorectal cancer (CRC) are not exhausted.

A. Venn diagram of exhaustion markers frequencies within CD8⁺ in the tumor (T, n=34). B. Frequency of CD69⁺, CD25⁺ and GZMB⁺ within PD1⁺ and PD1⁻ cells in T (n=34). Violin plot indicates Min to Max value. ***, P < 0.001; paired t test.

These data prompted us to speculate that CRC relapse could be explained by other mechanisms rather than the canonical T cell exhaustion.

3. The TME of CRC is infiltrated by two main CD8⁺ T cell populations identified by differential expression of CD39 and GZMK

To dissect the heterogeneity of CD8⁺ T cells in the three different compartments analyzed, we adopted the PhenoGraph algorithm. Overall, tSNE revealed that the CD8⁺ T cell profile was substantially distinct at single-cell levels in the PB, NAT and T compartments (Figure 16 panel A). Accordingly, unbiased hierarchical clustering also separated PB, NAT and T samples, independently from other factors like patient's age, gender or tumor stage (Figure 16 panel B).

We were able to identify a total of 20 clusters (CL 9 and 16 were excluded because the number of cells was underrepresented; <0.5%) based on the interpolation between the mean fluorescence intensity (MFI) of the fluorophores analyzed and the frequency of the positive population detected for each marker (Figure 16 panel C).

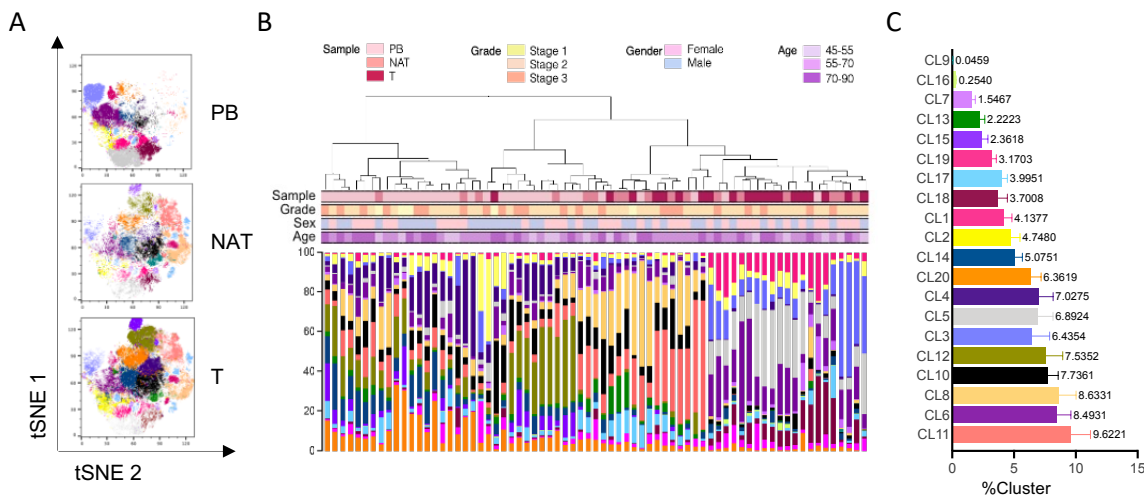


Figure 16. Clustering analysis reveals high heterogeneity among CD8⁺ T cells in early-stage colorectal cancer (CRC) patients within different compartments.

A. tSNE representation of clusters identified by the PhenoGraph algorithm of concatenated CD8⁺ T cells (3,000 cells/sample) from peripheral blood (PB, n = 22), normal adjacent tissue (NAT, n=17) and tumor (T, n=34). **B.** Hierarchically meta-clustering of CRC patients derived samples based on PhenoGraph identified clusters using Ward's minimum variance method. For all the sample is explicated, in order Sample type, Grade, Sex, Age. **C.** Mean frequencies of the 20 clusters of CD8⁺ T cells identified by the unsupervised clustering analysis (n=34). Bars indicate mean ± s.e.m.

Adapted from Tiberti et al.

Multiple clusters that were characterized by lack of expression of residency markers (CD69, CD103) were mostly enriched in PB compared to NAT and T. Specifically, CL3 is annotated as T_N (naïve cells) and characterized by high levels of CD45RA, CCR7 and CD127 expression and lack of expression of activation markers (such as CD25, CD69, PD1, CD39). CL1, 5 and 18 were annotated as T_{EMRA} due to high CD45RA and low CCR7 expression, general lack of expression of memory/activation markers along with high level of the

cytolytic molecule GZMB. CL6 is annotated as T_{CM} (central memory) and characterized by expression of several memory markers (CCR7, CD127, CD27, CD28) but absence of activation and cytotoxic markers such as GZMB and GZMK. Two other clusters (CL8 and CL11) were instead enriched in T and NAT compared to PB, indicating that they were colon-specific CD8⁺ T cell subsets and were annotated as T_{RM} (tissue-resident memory T cells) since they displayed high expression of markers of memory (CD127 and CD28) and residency (CD69 and CD103). These two colon-specific T_{RM} subsets expressed intermediate levels of CD161 and are enriched mainly in NAT. A different cluster is CL19 represented by CD161^{high} mucosal associated invariant T cells (MAIT)²¹⁹, cells equally represented in PB, NAT and T. Importantly, 4 different clusters, namely CL4, CL12, CL14 and CL20, were specifically and significantly enriched in T compared with PB. CL 4, 14 and 20 formed a meta-cluster of T_{EM} cells characterized by CD45RA⁻, CCR7^{int}, CD28^{high}, CD27^{low} expression pattern with a peculiar high expression of GZMK. These cells showed variable expression levels of activation markers and GZMB, low levels of PD1 and lack of tumor reactivity and residency (assessed by CD39 and CD69 - CD103 expression, respectively⁶⁹. Conversely, CL12 identified T cells with a phenotype reminiscent of tumor reactive T cells (Treact)^{67,75,220–222}, displaying increased expression of markers of residency (CD69 and CD103) and tumor-reactivity (CD39). Importantly CL4 and CL12 are significantly enriched in T compared with NAT while CL14 and 20 are equally distributed between T and NAT (Figure 17 panel A-B, Figure 18).

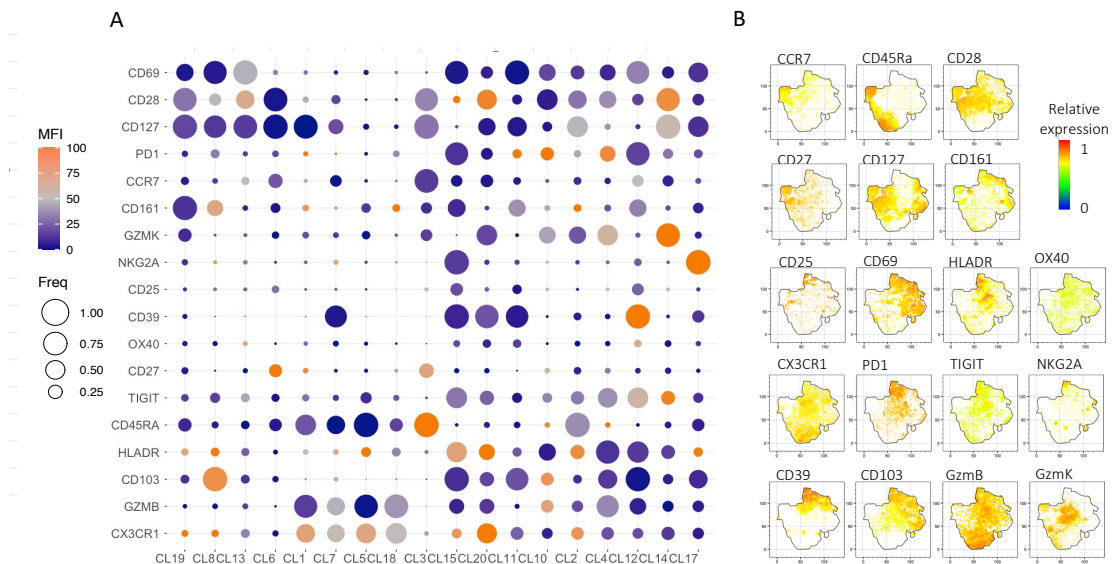


Figure 17. CD8⁺ T cells phenotype is described by 18 clusters.

A. Balloon plot of the average expression levels and frequencies of 18 selected markers within the 18 clusters analyzed (n=34). **B.** tSNE representation of Mean fluorescence expression (rMFI) of positive events for the marker indicated.

Adapted from Tiberti et al.

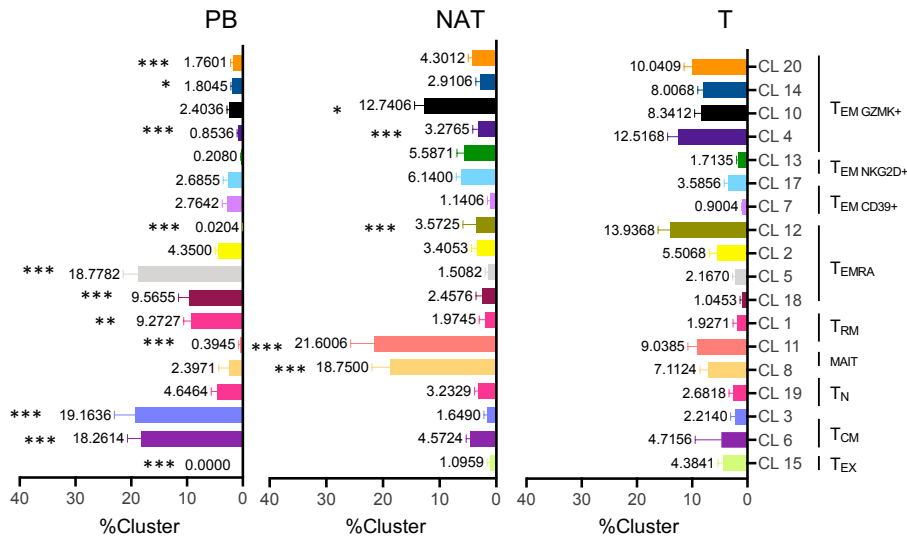


Figure 18. CD8⁺ T cells clusters are differentially distributed across tissues.

Cluster representation in different tissues: PB, NAT, T. Bars indicate mean \pm s.e.m. *, $P < 0.05$; **, $P < 0.01$; ***, $P < 0.001$; two-way Anova. Clusters are annotated as effector memory T cells (T_{EM}) GZMK⁺, NKG2D⁺, CD39⁺, Effector Memory CD45RA⁺ (T_{EMRA}), Tissue resident memory T cells (T_{RM}), mucosal associated invariant T (MAIT), Naïve T cells (T_N), central memory T cells (T_{CM}) and exhausted T cells (T_{EX}). Adapted from Tiberti et al.

We decided to focus our attention on CL4 and CL12 because they were significantly enriched in T compared with both NAT and PB. These two clusters are composed by T_{EM} mainly distinguished by the expression of CD39 and GZMK. While CL12 expresses high levels of CD39 and low GZMK, CL4 expresses low levels of CD39 and high levels of GZMK (Figure 19 panel A-B).

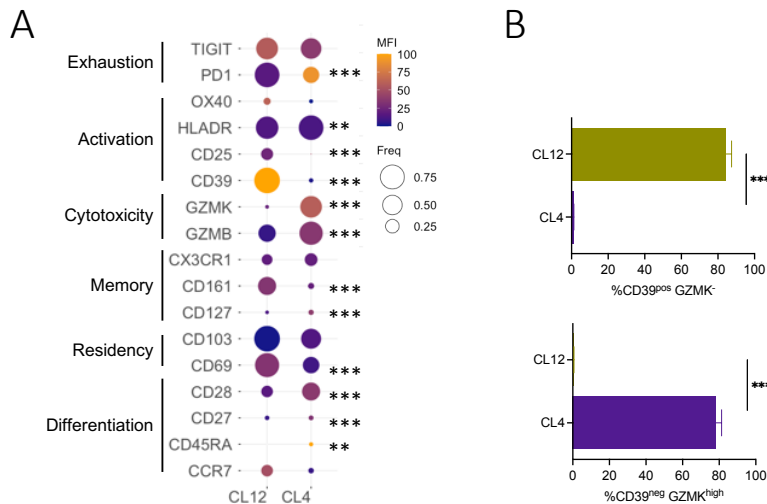


Figure 19. Colorectal cancer (CRC) is mainly infiltrate by two clusters of CD8⁺ T_{EM} characterized for the differential expression of CD39 and GZMK.

A. Balloon plot of the average expression levels and frequencies of markers of differentiation, residency, memory, cytotoxicity, tumor reactivity, activation and exhaustion in clusters identified as enriched in tumor (T, n=34). **, $P < 0.01$; ***, $P < 0.001$; two-way Anova. **B.** Bar plot of CD39^{pos} GZMK⁻ and CD39^{neg} GZMK^{high} frequency within Cluster 4 (CL4) and Cluster 12 (CL12), respectively (n=34). Bars indicate mean \pm s.e.m. ***, $P < 0.001$; paired t test.

Adapted from Tiberti et al.

We confirm the above finding by adopting a classic manual gating strategy. The majority of intra-tumoral T_{EM} were CD39⁻ with a strong expression of GZMK (Figure 20 panel A-B).

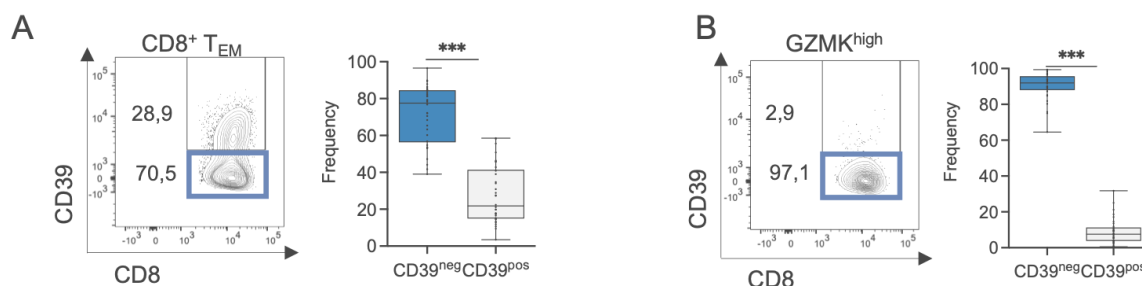


Figure 20. Colorectal cancer (CRC) is mainly infiltrate by CD39⁻ GZMK^{high} CD8⁺ effector memory T cells (T_{EM}).

A. Representative contour plot and relative quantification of CD39^{neg} and CD39^{pos} frequency within CD8⁺ T_{EM} (n=34). Box and whisker plot indicates Min to Max value. ***, P < 0.001; paired Wilcoxon test. **B.** Representative contour plot and relative quantification of CD39^{neg} and CD39^{pos} frequency within GZMK^{high} CD8⁺ T_{EM}.

Adapted from Tiberti et al.

Of note, the expression of CD69 and CD103, as tissue resident markers, by the CD39⁻ T_{EM} population excluded that these cells were derived from blood contamination (Figure 21 panel A-B). Despite the low level of CD39, GZMK^{high} cells enriched in TME present a peculiar activation profile with high expression of activation markers (CX3CR1, HLA-DR, and CD28) and GZMB and low expression of exhaustion markers (PD1 and TIGIT) (Figure 21 panel C).

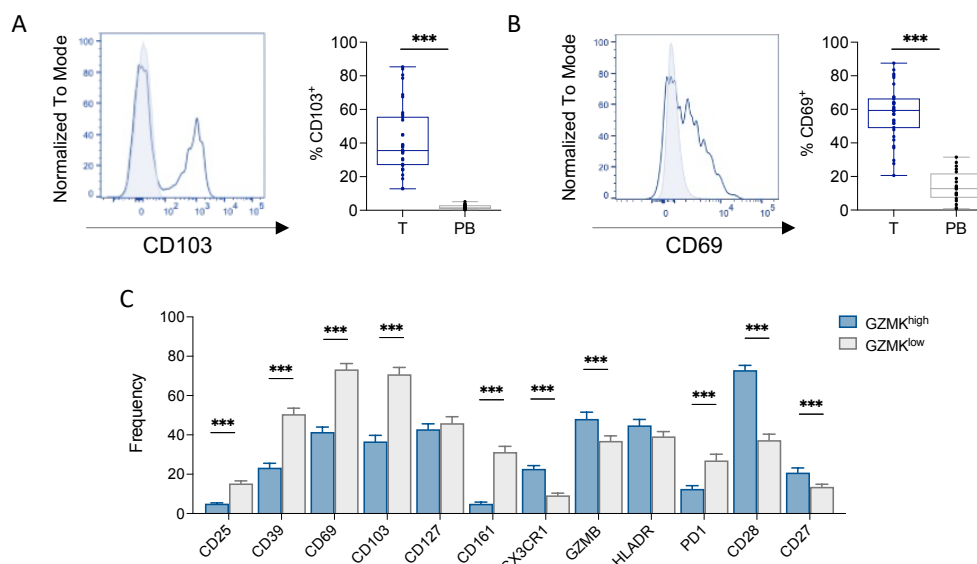


Figure 21. CD39⁻ GZMK^{high} CD8⁺ T_{EM} are resident activated cells.

A-B. Representative histogram and quantification of CD103 (A) and CD69 (B) frequency within CD39^{neg} CD8⁺ T_{EM} within tumors (T, n=34) and peripheral blood (PB, n=18). Box and whisker plot indicates Min to Max value. ***, P < 0.001; paired t test. **C.** CD25, CD39, CD103, CD127, CD161, CX3CR1, GZMB, HLA-DR, PD1, TIGIT, CD28, CD27 frequencies within GZMK^{high} and GZMK^{low} CD8⁺ T_{EM}. Bars indicate mean ± s.e.m. ***, P < 0.001; paired Wilcoxon test.

Adapted from Tiberti et al.

We next FACS-sorted CD39⁻ and CD39⁺ CD8⁺ T_{EM} cells from the CRC tumors and confirmed that CD39⁻ CD8⁺ T cells produced significantly higher levels of GZMK (Figure 22 panel A), while retained the ability to produce IFN γ , TNF α and GZMB compared to their CD39⁺ counterparts (Figure 22 panel B). These results confirmed an active state of these cells excluding a differentiation toward an exhausted phenotype. This overall “activated” profile differentiated them from the recently described “exhausted-like” GZMK⁺ CD8⁺ T cells^{45,62,223}.

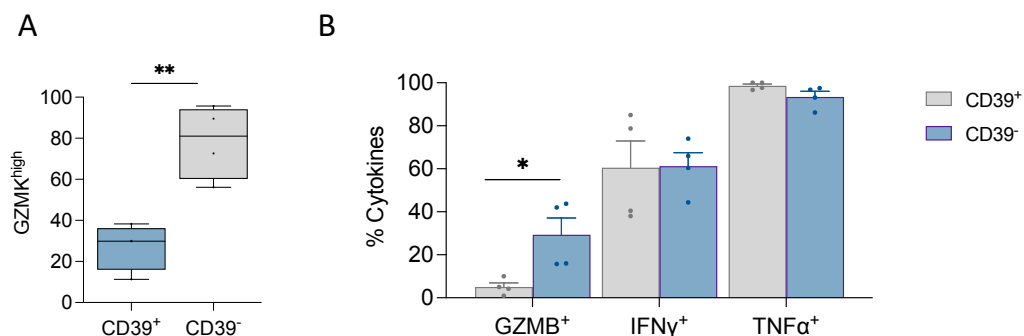


Figure 22. CD39⁻ CD8⁺ T_{EM} have a high cytotoxic activity.

A. GZMK^{high} frequency within FACS sorted CD39⁻ and CD39⁺ CD8⁺ T_{EM} from tumor (T) tissue (n=4). Box and whisker plot indicates Min to Max value. **, P < 0.01; paired t test. **B.** Frequency of GZMB, IFN γ and TNF α cells within sorted CD39⁻ and CD39⁺ CD8⁺ T_{EM} from T (n=4). Bars indicate mean \pm s.e.m. *, P < 0.05; paired t test.

Adapted from Tiberti et al.

In conclusion, we reported that the TME of resectable CRC patients was highly infiltrated by a unique GZMK^{high} CD8⁺ T_{EM} cell population, characterized by a low CD39 expression.

4. GZMK expression correlates with a distinct transcriptional program in CD8⁺ T_{EM}

To better characterize infiltrating GZMK^{high} CD8⁺ T_{EM} cells and assess their prognostic value, paired T and NAT tissues from 8 HN patients were analyzed by scRNAseq. We were able to collect a total of 52316 cells. The mean number of reads per cell were 94183 (min:37500; max:235694) with a median number of genes detected per cell of 3779 (min:1433; max:5392). The scRNAseq was performed on the total live cells obtained after the digestion of the sample to allow the simultaneous characterization of cancer cells and immune cells associated with the tumor. All the CD45⁺ cells have been detected and reflects the proportion detected by flow cytometry. However, the number of cells per population is low, impairing our capability to analyze the neutrophil population even if we were able to detect their representation in the tissue. (Figure 23)

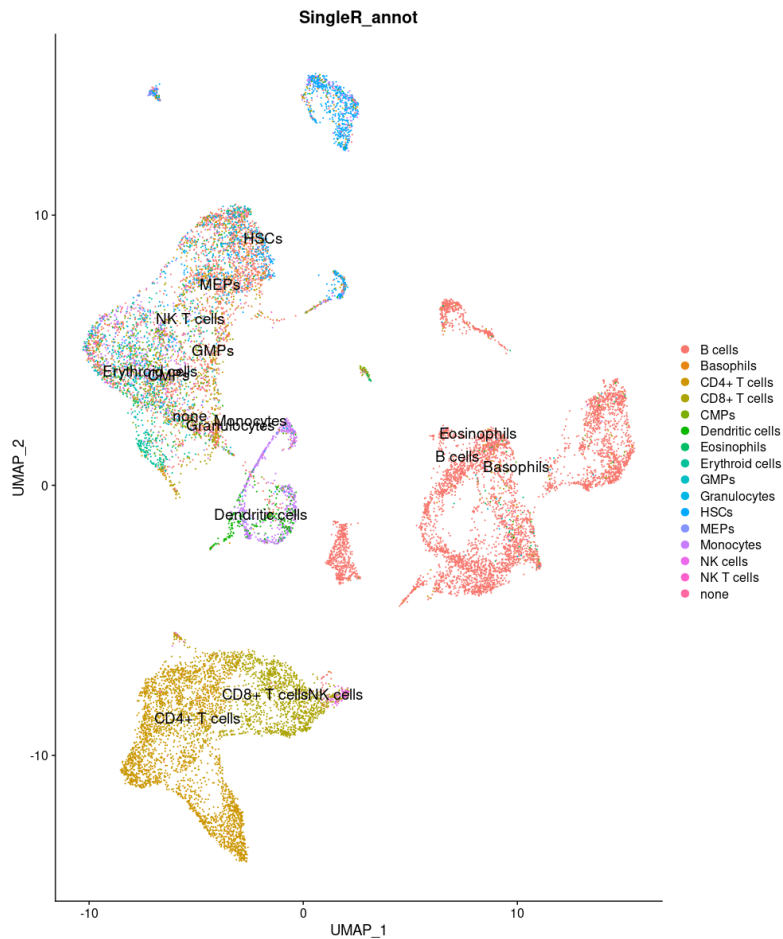


Figure 23. Single cell RNA sequencing (scRNAseq) analysis confirm the high abundance of T cells within the tumor (T).

Uniform manifold approximation and projection (UMAP) projection of all the cells analyzed by scRNAseq. Colors represent different cell types.

We focus our analysis on the 8523 cells composing the T/NK clusters and we generated a new UMAP in which we were able to distinguish seven T cell subtypes (Cluster 5 has been excluded because underrepresented) (Figure 24 panel A). The cluster 1 was enriched in the expression of CD4 while clusters 3 and 4 were enriched in CD8⁺ T cells and in line with our FACS data GZMK expressing cells were mostly included in CD8⁺ clusters 3 and 4 (Figure 24 panel B-C), confirming results from our phenotypic analysis.

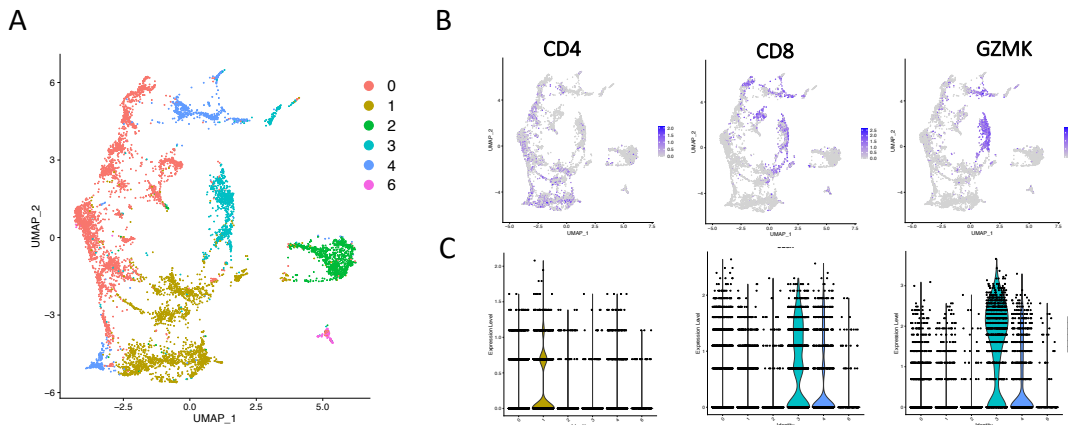


Figure 24. GZMK is mainly expressed by the CD8⁺ T cells cluster.

A. UMAP projection of cells from the T/NK cluster in of 8 patients. Colors represent the Shared Nearest Neighbor (SNN) identified meta clusters. **B.** Expression level of indicated T cell markers is shown. **C.** Violin plots showing the expression of indicated T cells selected genes for each cluster.

Adapted from Tiberti et al.

We focused our attention on the two clusters enriched in CD8⁺ T cells and we were able to identify eleven sub-clusters which we manually annotated with curated gene-sets based on literature⁶⁶. Most of the cells are represented by CD8⁺ T cells while a small fraction of CD4⁺ T_{EM} and FOXP3 expressing Treg, CD40LG positive mucosal associated invariant T (MAIT), Tγδ Co-expressing of TRDC and TRGC1 and NK cells distinguished for the expression of AKR1C3, CXC3R1, FCER1G, NKG7 and PRF1 were detected. In the CD8⁺ compartment we were able to identify naïve-like T cells (Naive_like) detected for the expression of IL7R, CCR7 and SELL and T exhausted cells (T_{EX}) defined for the expression of CTLA-4, PDCD-1, CXCL13, HAVCR2, ENTPD1 and LAYN. As expected, and in line with previous data, the main population detected is composed by CD8⁺ T_{EM} cells characterized by high expression of GZMK. In line with previous results CD8⁺ T_{EM} cells represent a different T cells population in respect to CD8⁺ T_{EX}. (Figure 25)

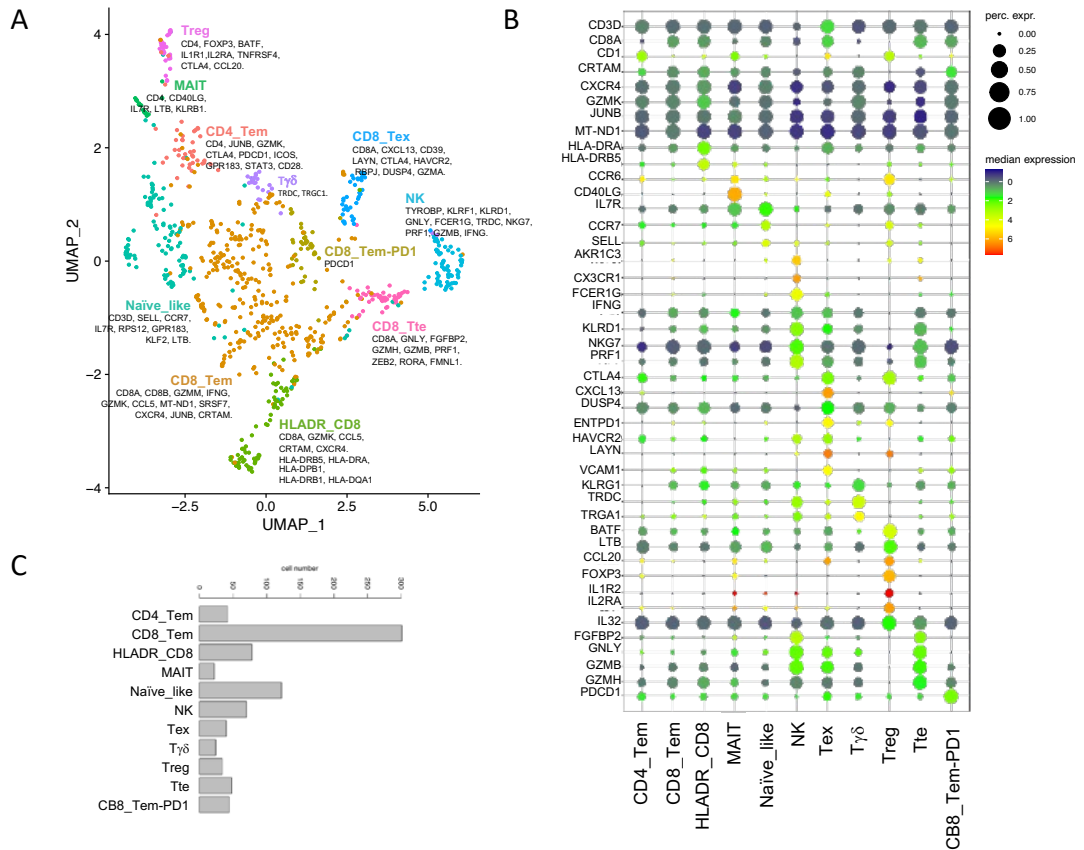


Figure 25. CD8⁺ T are mainly effector memory cells T_{EM} expressing GZMK.

A. Uniform manifold approximation and projection (UMAP) of CD8⁺ T cells selected clusters. Colors represent different T cell subtypes. Key genes used for manual annotation are indicated. **B.** Balloon plot showing the expression of selected markers for each manually annotated T cell subtype indicated in A. The size of the bubble represents the fraction of cells with at least one Unique Molecular Identifier (UMI) for a specific gene, while the color indicates the median of the scaled normalized expression. **C.** Bar plot represents the number of cells in each subtype.

Adapted from Tiberti et al.

In addition, we excluded all the cells with a signature specific of non CD8 subtypes and we performed a pseudotime analysis to understand the relationship within the populations previously identified. Despite the low number of cells, it has been possible recapitulate at least in part the clusters obtained in the previous UMAP (Figure 26 panel A) and CD8_Tem cells were closer to Naive-like T cells suggesting a different differentiation trajectory as compared with both terminally differentiated effectors cells (Tte) as well as Tex cells (Figure 26 panel B).

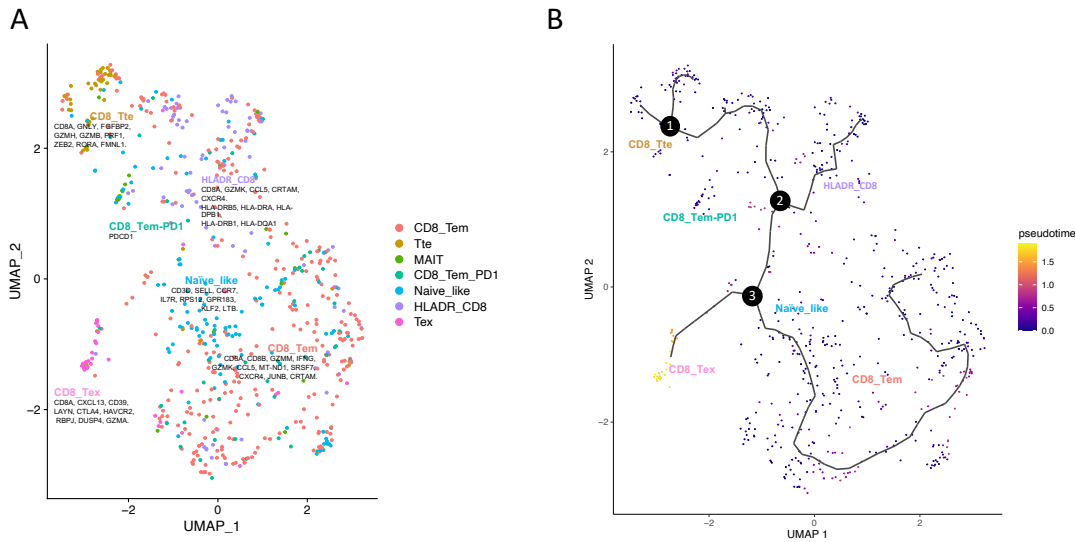


Figure 26. Pseudotime analysis describes CD8⁺ effector memory (T_{EM}) T cells in between naïve and terminally differentiated/exhausted cells.

A. Uniform manifold approximation and projection (UMAP) of CD8⁺ T cells specific clusters. Colors represent different T cell subtypes. Key genes used for manual annotation are indicated. **B.** Monocle pseudotime analysis of the CD8⁺ T cell subtypes identified in figure 25 and reported in panel A. The pseudotime line connects the indicated T cell subtypes.

CD8_Tem expressing high levels of GZMK, presented lower cytotoxic potential compare with Tte and NK cells (padj= 0.005) and were not impaired in proliferation. Moreover, CD8_Tem had low expression of lymphocyte activation and migration signatures and high cell-cell adhesion signatures. (Figure 27)

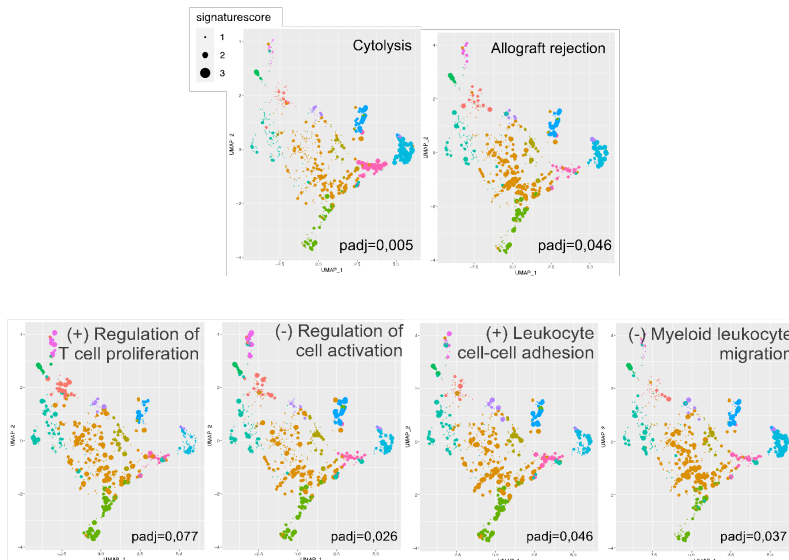


Figure 27. CD8⁺ effector memory (T_{EM}) cells are characterized by cytolytic and alloreactive signatures.
A. Uniform manifold approximation and projection (UMAP) of CD8⁺ T cells cluster showing the expression of Cytolysis and Allograft-rejection signatures and regulation of T cell proliferation and activation, Leukocyte cell-cell adhesion and Myeloid leukocytes migration.
 Adapted from Tiberti et al.

The GZMK^{pos} cells in the Tem cluster expressed the same amount of TNF α of GZMK^{neg}, in line with FACS data and confirming their cytotoxic potential and their identity from Tex cells. (Figure 28)

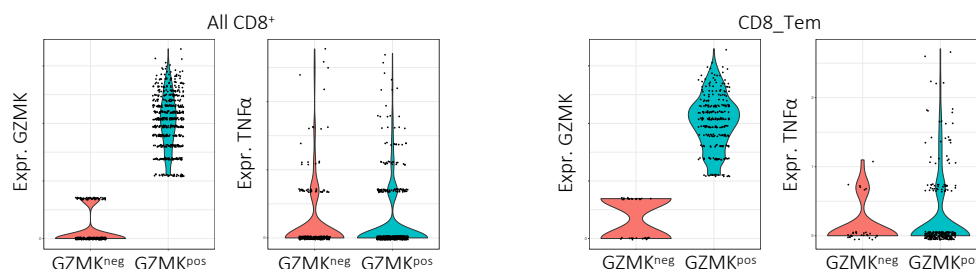


Figure 28. GZMK CD8⁺ effector memory (T_{EM}) cells express also TNF α .

A. GZMK and TNF α quantification within GZMK^{neg} and GZMK^{pos} cells within all CD8⁺ T cells identified by single cell RNA sequencing (scRNAseq). **B.** GZMK and TNF α quantification within GZMK^{neg} and GZMK^{pos} cells within CD8_{Tem} cells.

Adapted from Tiberti et al.

Analyzing the transcription factors (TF) within CD8_{Tem}'s differentially expressed genes (DEGs), we found three annotated TF with an important role in CD8⁺ T cells differentiation. The first one is RORA, downregulated in the Tem cluster, which is well known to be associated with effector function and cytotoxicity activity rather than memory differentiation patterns²²⁴. This downregulation is flanked by the upregulation of AP1⁶², inducer of cytotoxic differentiation in CD8⁺ T cells and recently associated with deficiency in the suppression of CD8⁺ T cells response leading to excessive cytotoxic function and tissue damage²²⁵. (Figure 29)

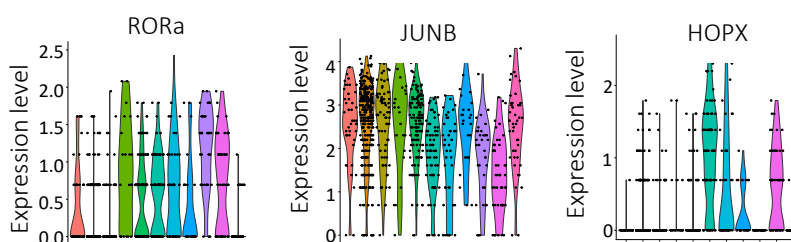


Figure 29. Peculiar transcription factors (TF) are drivers for the cytotoxic phenotype of GZMK CD8⁺ effector memory (T_{EM}) cells.

Violin plots of RORa, HUNB and HOPX expression level within different T cells subtypes. In order: CD4_Tem, CD8_Tem, CD8_Tem-PD1, HLADR_CD8, MAIT, Naïve_like, NK, CD8_Tex, Tgd, CD8_Tte, Treg.

Adapted from Tiberti et al.

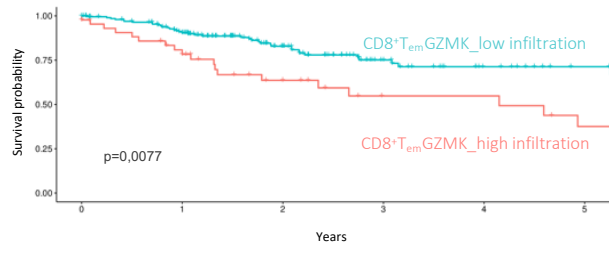
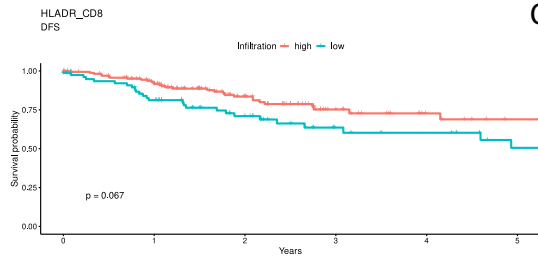
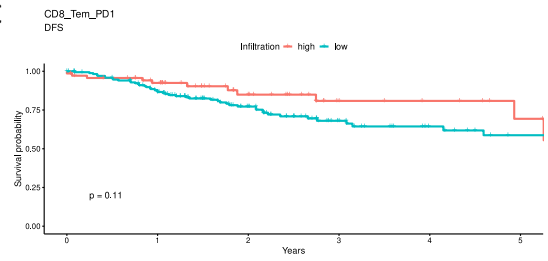
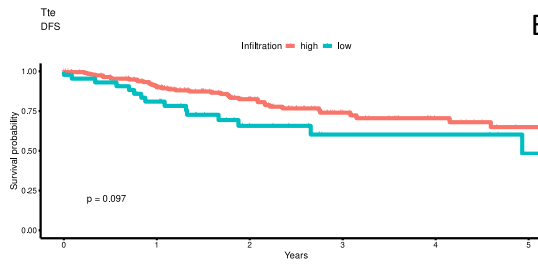
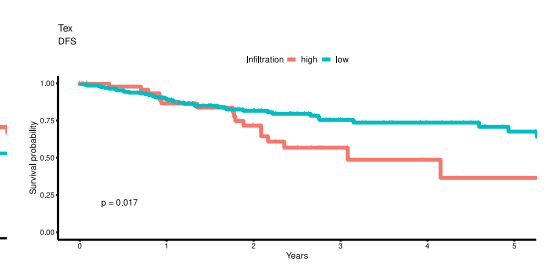
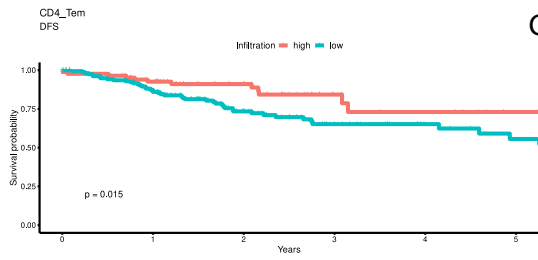
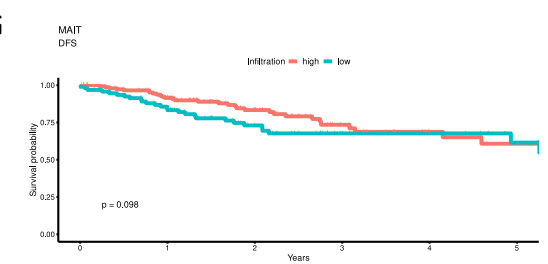
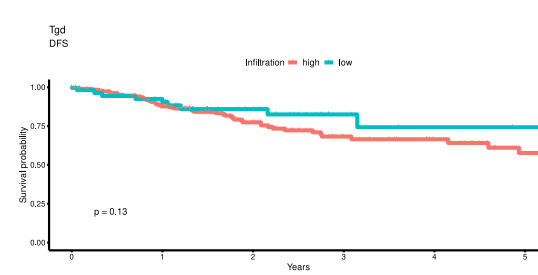
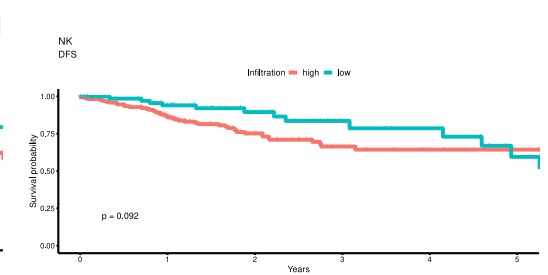
In conclusion we identified GZMK^{high} CD8⁺ T_{EM} cells as the main population within T cells infiltrate, and their transcriptional and functional profile corroborated the MPFC analysis. These cells present high cytotoxic function and alloreactive signature suggesting their potential role in cancer progression.

5. The transcriptional signature of GZMK⁺ CD8⁺ T_{EM} predicts prognosis in CRC patients

We wondered if the GZMK^{high} CD8⁺ T_{EM} cells identified may predict the risk of encountering secondary events in CRC patients and, potentially, in other types of cancer.

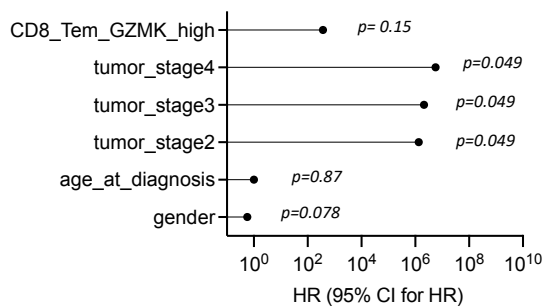
To address this question, we used the CD8_Tem genes set obtained by scRNAseq and tested as a predictor clinical outcome in CRC. By querying publicly available CRC datasets on TCGA we found a significant correlation with genes upregulated in CD8_Tem and worst prognosis in patients with early-stage CRC (Figure 30 panel A). Instead, none of the transcriptional profile of other tested lymphocyte resulted into an efficient stratification, neither peculiar populations of CD8 (CD8_HLADR, CD8_PD1, Tte, Tex) nor other type of lymphocytes (CD4_Tem, MAIT, Treg, NK) (Figure 30 panel B-I).

To investigate the association between the risk of relapse of CRC patients and the most common predictor variables, we applied a Cox Proportional-Hazards Model. Firstly, we performed the univariate analysis separately looking at infiltration of CD8 GZMK-high cells, sex, age and stage of the tumor for 209 CRC cases from TCGA-COAD cohort. From this analysis it emerges that both sex and stage are associated with the risk of relapse with males having a higher risk of relapse compared to women and stage I showing a lower risk compared to higher stages of the tumor (stage II, III, IV), while the association with age is not significant. The CD8 GZMK-high cells infiltration is correlated with high Hazard Ratio (HR) even if do not reach the statistical significance and is consistent to what observed in the Kaplan-Meier plot, with higher infiltration of these cells being associated with a higher chance of relapse (HR = 570). (Figure 30 panel J) Then, we combined these predictors into a multivariate model and observed a similar trend. Sex and stage were still associated with risk of relapse, while we observed a decrease in the significance after adjusting for other confounders. Finally, the infiltration of CD8 GZMK-high cells the same trend as in the univariate analysis even after adjusting for other confounders (HR = 370), still failing to be significant. (Figure 30 panel K)

A**B****C****D****E****F****G****H****I**

J

Univariate Analysis



K

Multivariate Analysis

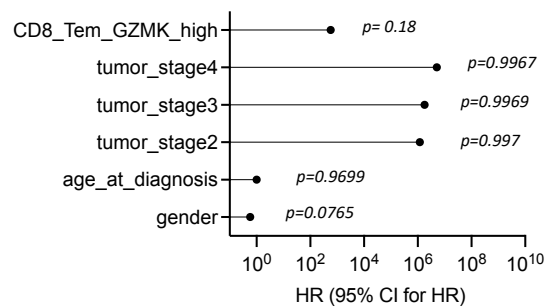


Figure 30. CD8⁺ effector memory (T_{EM}) expressing GZMK predict Overall survival (OS) in early-stage colorectal cancer (CRC) patients.

A-I. Kaplan-Meyer analysis of the association of different cell type abundance with disease free survival (DFS) on the TCGA-COAD cohort (n=284). In A CD8_Tem, in B HLADR_CD8, in C CD8_Tem_PD1, in D Tte, in E Tex, in F CD4_Tem, in G MAIT, in H Tgd, in I NK. High infiltration is indicated in red, low infiltration in turquoise. **J-K.** Cox Proportional-Hazards univariate (J) and multivariate (K) analysis (n=209).

Adapted from Tiberti et al.

Of note, GZMK⁺ CD8_Tem signature was able to predict clinical outcome also in the lung adenocarcinoma (LUAD) in the TCGA dataset, extending its prognostic value to other type of tumor beyond CRC (Figure 31).

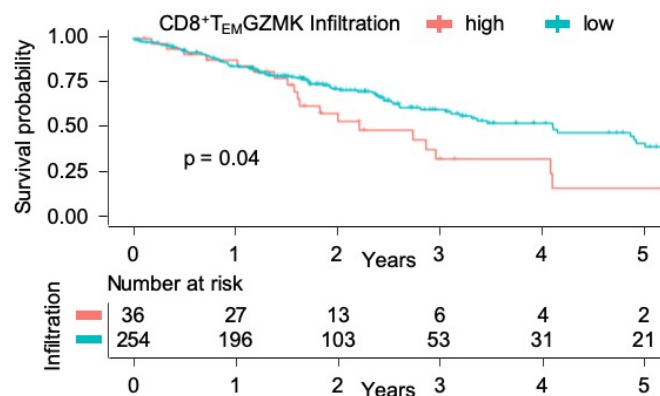


Figure 31. CD8⁺ effector memory (T_{EM}) expressing GZMK predict Overall survival (OS) in lung adenocarcinoma patients.

Kaplan-Meyer analysis of the association of CD8_Tem cell subtype' abundance with overall survival (OS) on the TCGA-LUAD cohort (n= 295). High infiltration is indicated in red, low infiltration in turquoise. The table shows the 'number at risk' subjects.

Adapted from Tiberti et al.

In summary, the transcriptional and functional profile of tumor-infiltrating immune cells led to an effective stratification of the patients and can predict the risk of encountering secondary events in CRC patients and, potentially, in other types of cancer.

6. GZMK produced by infiltrating CD8+TEM is associated with early relapse in CRC

In our cohort of patients, 4 out of 46 patients experienced early-relapse. We thus profiled the tumor of these relapsed patients, and we found an increase in GZMK production in CD8⁺ T cells (Figure 32 panel A) and in particular an increase in the CD39⁻ GZMK^{high} T_{EM} CD8⁺ T cells population (Figure 32 panel B) as well as in CL4 (Figure 32 panel C).

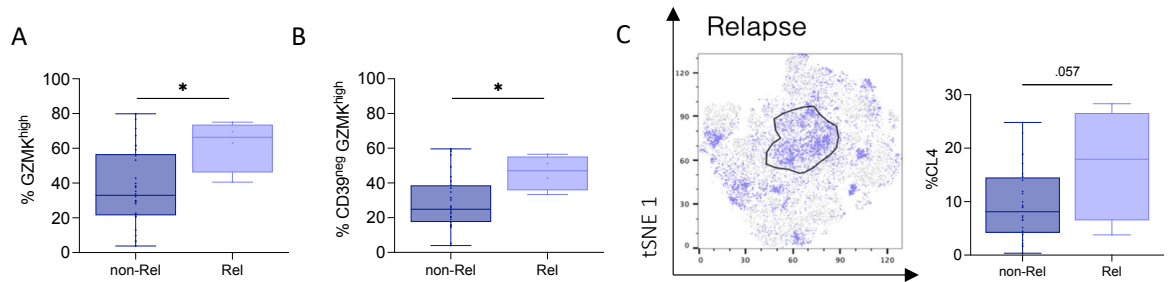


Figure 32. CD39⁻ GZMK^{high} CD8⁺ T_{EM} are accumulated within tumor (T) of colorectal cancer (CRC) patients which experienced early-relapse.

A. GZMK^{high} frequency within non-relapsed (non-Rel, n=27) and relapsed (Rel, n=4) patients' tumor (T). Box and whisker plot indicates Min to Max value. *, P < 0.05; unpaired t test. **B.** GZMK^{high} frequency within non-Rel (n=27) and Rel (n=4) T. Box and whisker plot indicates Min to Max value. *, P < 0.05; unpaired t test. **C.** tSNE visualization of tumor CD8⁺ T cells of early-relapsed patients (n=4, Rel in light blue). **D.** CL4 frequency within non-Rel (n=27) and Rel (n=4) T. Box and whisker plot indicates Min to Max value. *, P < 0.05; unpaired t test.

Adapted from Tiberti et al.

Overall, our data support a model where GZMK^{high} CD8⁺ T cell promote relapse in CRC patients.

Of note, as already demonstrated by the manual gating strategy, the T_{EM} CD39⁻ GZMK^{high} population present also high levels of GZMB in line with a super cytotoxic potential (Figure 33 panel A-B). Interestingly, while the GZMK production is peculiar to relapse patients compared with blood, we don't observe the increase in GZMB production in our cohort of patients in CD8⁺ TILs compared with PB. Indeed, the GZMB production in T_{EM} in CRC patients is still high in the circulation, supporting a main role of GZMK in CRC progression.

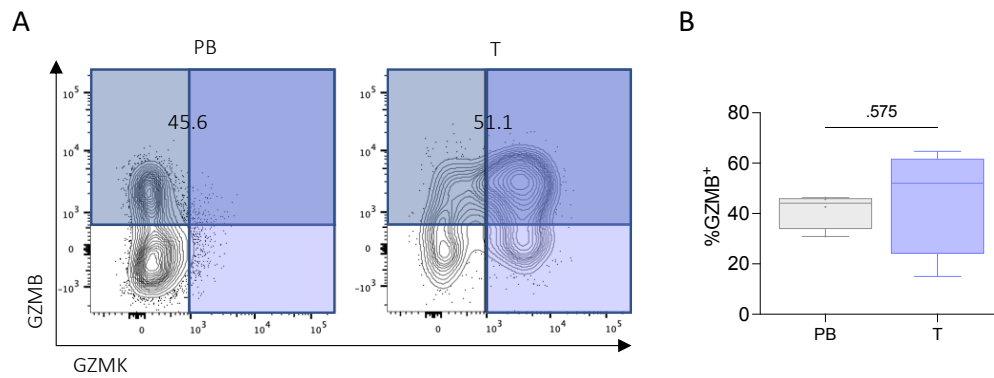


Figure 33. GZMB is not subject to remodeling within the tumor.

A. Representative contour plots of GZMB and GZMK expression in peripheral blood (PB) and tumor (T) of early-relapsed (Rel) patients. **B.** Box plot of GZMB⁺ cells frequency in PB and T of Rel patients (n=4). Box and whisker plot indicates Min to Max value. paired t test.

Adapted from Tiberti et al.

7. CRC tumors are highly infiltrated by neutrophils

Among the infiltrating immune cell populations analyzed, in T compared to NAT, we reported no significant differences in DC (defined as CD45⁺, CD3⁻, CD19⁻, CD11c⁺), lower proportion of conventional NK cells (defined as CD3⁻, CD56⁺) and an enrichment in macrophages (defined as CD45⁺, HLADR⁺, CD14⁺) - albeit they were present at low frequencies - as well as in neutrophils (identified as CD45⁺, CD56⁻, CD11b⁺, HLA-DR⁻, CD66b⁺ cells with an intermediate to low expression of CD33)^{226,227}(Figure 34 panel A). Neutrophils were significantly enriched in T compared to NAT both in terms of frequencies as assessed by FACS (10± 20% of the total CD45⁺ cells in T versus 2± 10% in NAT) (Figure 34 panel B-C) and density as assessed by IHC for CD66b (Figure 34 panel D).

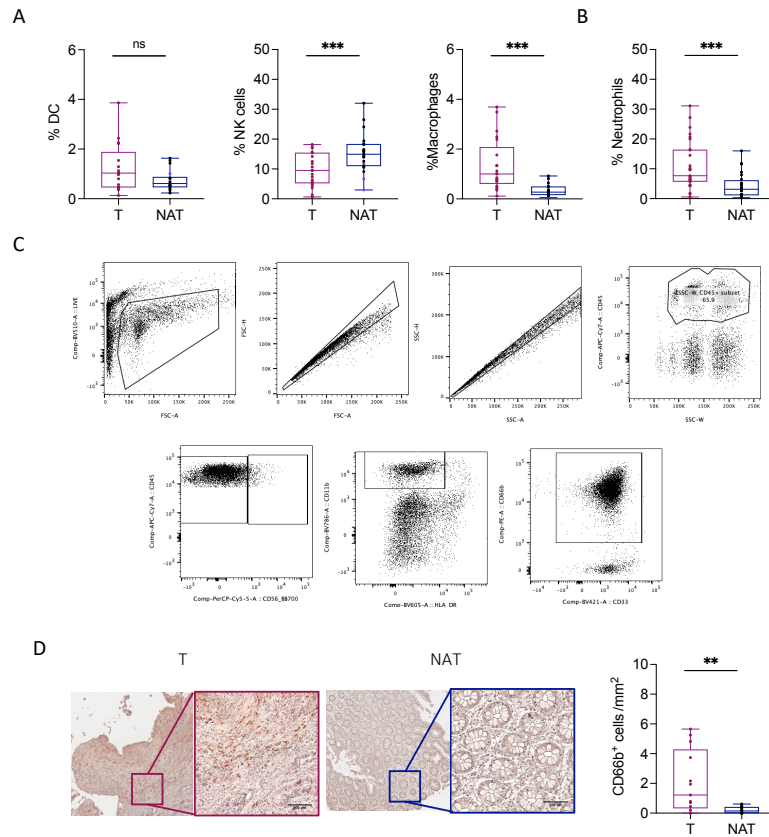


Figure 34. Neutrophils are strongly enriched within colorectal cancer (CRC).

A. Quantification of dendritic cells (DC) (n=20), macrophages (n=27) and NK cells (n=22) within CD45⁺ cells in Tumor (T) and normal adjacent tissue (NAT). Box and whisker plot indicates Min to Max value. ***, P < 0.001; paired t test. **B.** Frequency of tumor infiltrating neutrophils defined as CD45⁺ CD11b⁺ HLADR⁻, CD56, CD66b⁺ within CD45⁺ immune compartment in T compared with NAT samples in CRC patients (n=27). Box and whisker plot indicates Min to Max values. ***, P < 0.001; paired t test. **C.** Flow cytometric gating strategy for the identification of CD15^{high} tumor infiltrating neutrophils. **D.** Representative immunohistochemistry images and quantification of CD66b⁺ cells in paired T and NAT tissues (n=13). Scale bar 100µm. Box and whisker plot indicates Min to Max value. **, P < 0.01; paired t test.

Adapted from Tiberti et al.

Due to the lack of an effective definition of the role of neutrophils in CRC progression and their debated function in shaping T cell functionality, we decided to focus our attention on their characterization.

8. CRC patients can be stratified based on the abundance of CD15^{high} neutrophils in the TME

We next evaluated the expression of CD15 on neutrophils, also known as Lewis x or Lex, which is a marker for neutrophils differentiation and activation and has been shown to modulate neutrophils function within TME^{168,169}. Interestingly, in our cohort of CRC patients, we identified two subgroups of patients based on the abundance of neutrophils expressing high level of CD15: patients with low CD15^{high} neutrophils (LN, frequency <50% with 31,1% incidence in our cohort) and patients with high CD15^{high} neutrophils (HN,

frequency >50% with 68,9% incidence in our cohort) (Figure 35 panel A-D). The cut-off used for the classification of tumors as LN or HN (50%) has been extrapolated from the distribution of frequencies across patients of CD15^{high} neutrophils (Figure 35 panel F) - identified based on CD15 MFI (Figure 35 panel E)- and matches the minimum value between the two picks highlighted in the bimodal distribution. Of note, the differential abundance of CD15^{high} neutrophils is maintained not only in the CD45⁺, CD56⁻, CD11b⁺, HLA-DR⁻, CD66b⁺ population but also in the total infiltrate (CD45⁺) (Figure 35 panel C), confirming not only a change in neutrophils phenotype in this group of patients but also their enrichment in the TME. The expression of CD15 was specifically modulated within the TME. Indeed, CD15^{high} neutrophils were found at similar frequencies in both PB and NAT of LN and HN patients (Figure 35 panel G), suggesting a tumor-specific downregulation of CD15 by neutrophils infiltrating LN tumors.

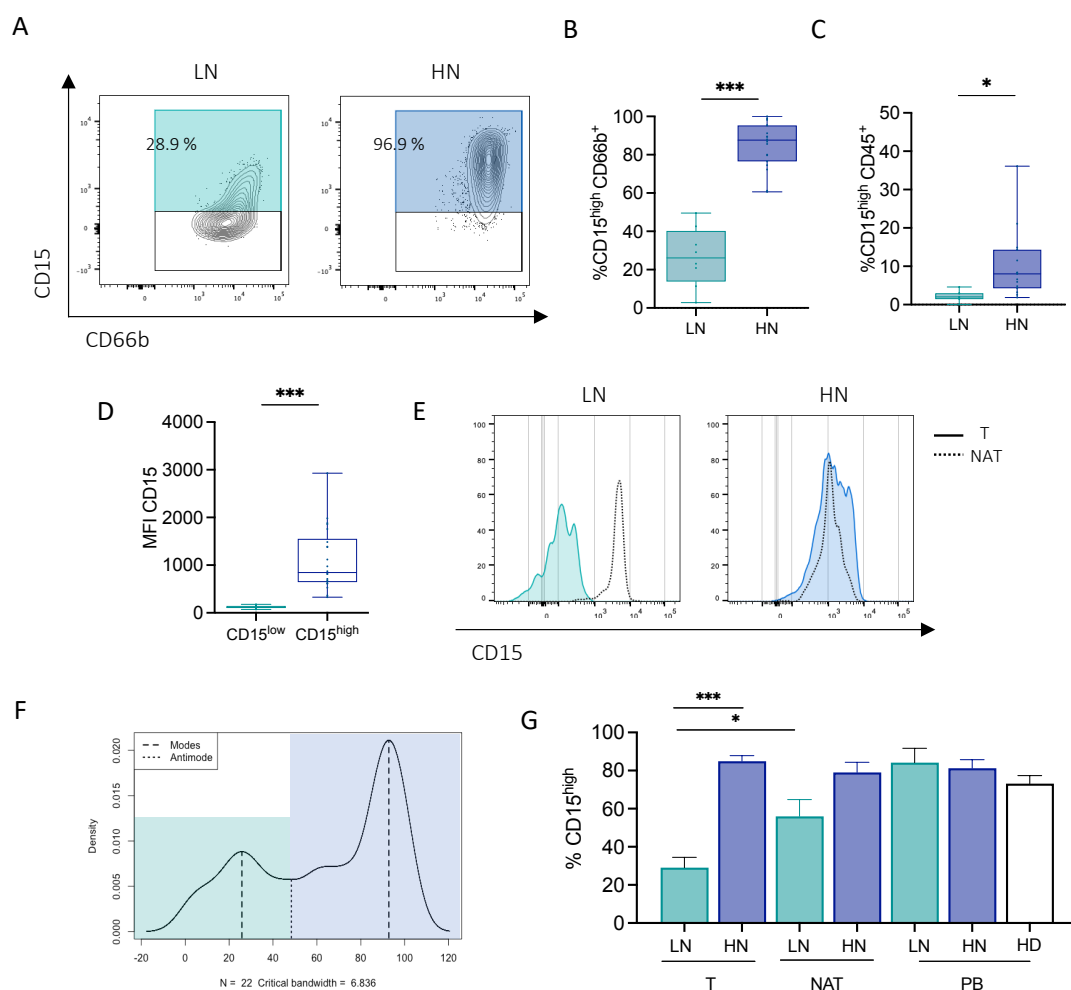


Figure 35. Neutrophils' CD15 expression is modulated within the tumor microenvironment (TME).

A. Representatives contour plots of CD15 expression in low (LN) and high neutrophils (HN) patients. **B.** Box plot of CD15^{high} cells frequency in LN and HN patients within CD66b⁺ neutrophils (n=8 LN and n=19 HN). Box and whisker plot indicates Min to Max value. ***, P < 0.001; unpaired t test. **C.** Box plot of CD15^{high} cells frequency in LN and HN patients within CD45⁺ cells (n=8 LN and n=19 HN). Box and whisker plot indicates Min to Max value. *, P < 0.05; unpaired t test. **D.** Quantification of CD15 MFI within CD15^{low} and

CD15^{high} neutrophils (n=22). Box and whisker plot indicates Min to Max value. ***, P < 0.001; paired t test. **E.** Representative histogram of CD15 expression on neutrophils in tumor (T) and normal adjacent tissue (NAT) within LN and HN patients. **F.** Density plot of CD15^{high} neutrophils within the CRC cohort (n=27). Black lines represent the mode and anti-mode of the distribution. **G.** Quantification of CD15^{high} neutrophils within T, NAT, and Peripheral Blood (PB) of LN (n=9) and HN (n=17) patients and PB of healthy donors (HD) (n=15). Bars indicate mean ± s.e.m. *, P < 0.05; ***, P < 0.001; paired and unpaired t test.

Adapted from Tiberti et al.

Since CD15 is a distinguishing marker for human neutrophil¹⁶⁹, to demonstrate that CD15^{low} cells were neutrophils, we FACS-sorted CD15^{high} and CD15^{low} from PB and T and examined their morphology by GIEMSA staining, which confirmed a multi-lobed nuclei and granular cytoplasm typical of neutrophils. (Figure 36)

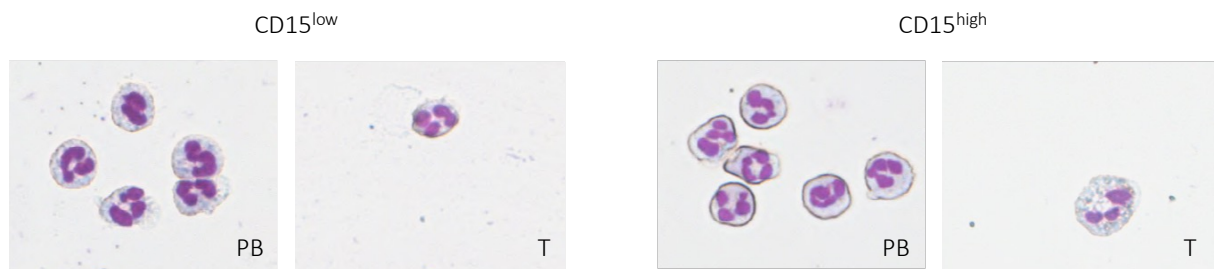


Figure 36. Neutrophils can lose CD15 expression.

Representatives Giemsa staining of CD15^{low} and CD15^{high} neutrophils sorted from peripheral blood (PB) and tumor (T), respectively.

Adapted from Tiberti et al.

9. CD15^{high} neutrophils accumulating in HN tumors hold a N2-like pro-tumoral phenotype

To better define the maturation/activation status of CD15^{high} and CD15^{low} neutrophils, we first analyzed the expression of CD10, a marker discriminating between mature and immature, as well as immunosuppressive from immunostimulatory neutrophil populations²²⁸. Both CD15^{high} and CD15^{low} neutrophils expressed CD10, with the CD15^{high} neutrophils displaying higher levels of CD10 compared with their CD15^{low} counterpart. (Figure 37 panel A) Thus, we speculate that intra-tumoral CD15^{high} neutrophils were mature neutrophils with a plausible tumor-promoting activity. Accordingly, CD15^{high} compared to the CD15^{low} neutrophil compartment displayed significantly higher CXCR2⁺CXCR4⁺ double positive cells (Figure 37 panel B), typical of N2-like tumor-promoting neutrophils¹⁶⁹. Likewise, HN tumors were significantly enriched in CXCR2⁺CXCR4⁺ neutrophils (Figure 38 panel C). Of note, the frequencies of aged neutrophils (defined as CXCR4⁺CXCR2⁻)¹⁶⁹ were comparable between CD15^{high} and CD15^{low} neutrophils as well as in HN and LN tumors (Figure 37 panel D-E). On the other hand, the expression of CXCR2 and CXCR4

was not modulated in PB, NAT nor PT, confirming the unique role of the TME in recruiting and modulating the phenotype of infiltrating neutrophils (Figure 37 panel F).

To further support the pro-tumorigenic role of CD15^{high} neutrophil population, we analyzed the production of Reactive Oxygen Species (ROS) from neutrophils, in view of its pro-tumorigenic attribute^{183,229}. We observed that neutrophils from HN tumors produce higher levels of ROS compared with LN patients. (Figure 37 panel G)

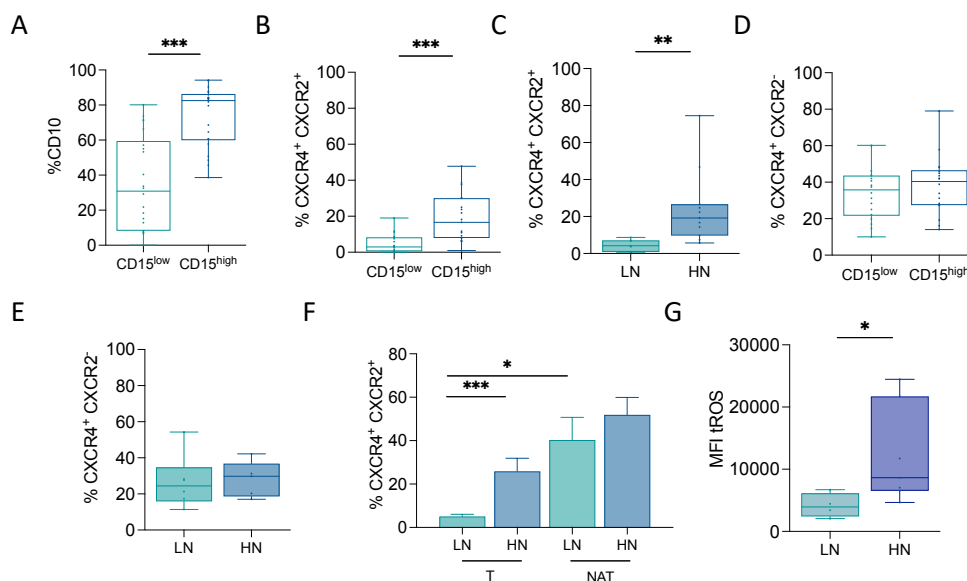


Figure 37. CD15^{high} neutrophils present an N2-like phenotype.

A. Frequency of CD10⁺ cells within CD15^{low} and CD15^{high} neutrophils (n=28). Box and whisker indicate Min to Max value. ***, P < 0.001; unpaired t test. **B.** Box plot of CXCR4⁺ CXCR2⁺ frequency within CD15^{low} and CD15^{high} neutrophils (total n=19). Box and whisker plot indicate Min to Max value. ***, P < 0.001; paired Wilcoxon test. **C.** Box plot of CXCR4⁺ CXCR2⁺ frequency within low (LN) and high neutrophils (HN) patients (n=7 LN and n=11 HN). Box and whisker plot indicates Min to Max value. ***, P < 0.001; Mann-Whitney test. **D.** Frequency of CXCR4⁺ CXCR2⁻ within CD15^{low} and CD15^{high} neutrophils (n=18). Box and whisker plot indicates Min to Max value. paired t test. **E.** Frequency of CXCR4⁺ CXCR2⁻ within LN (n=6) and H (n=6) patients. Box and whisker plot indicates Min to Max value. Unpaired t test. **F.** Quantification of CXCR4⁺ CXCR2⁺ neutrophils within tumor (T) and normal adjacent (NAT) of LN (n=7) and HN (n=10) patients. Bars indicate mean ± s.e.m. *, P < 0.05; ***, P < 0.001; paired and unpaired t test. **G.** Bar plot representation of total ROS (tROS) MFI within neutrophils of LN and HN patients' tumor (n=11). Box and whisker plot indicates Min to Max value. *, P < 0.01; unpaired t test.

Adapted from Tiberti et al.

Overall, these data revealed that CRC patients can be stratified based on the abundance of a CD15^{high} neutrophil population, which might have tumor promoting functions.

10. CD15^{high} neutrophils are retained in the TME of HN CRC tumors

During an inflammatory response, “aged” neutrophils fail to return to the bone marrow and instead rapidly migrate to the site of inflammation²³⁰. Thus, we wonder if the identified CD15^{high} neutrophils were “aged” neutrophils. However, CXCR4⁺CXCR2⁻ “aged”

neutrophils were similarly represented between HN and LN patients (Figure 37 panel E), suggesting that limited recirculation of “aged” neutrophils is not the main mechanism driving CD15^{high} neutrophils accumulation in HN patients. Neutrophil homeostasis in peripheral tissues is also regulated by macrophage-dependent clearance^{230–236}. Indeed, the frequencies of macrophages within the TME anti-correlate with the abundance of CD15^{high} neutrophils and was significantly lower in HN compared to LN (Figure 38), suggesting that lower clearance by macrophages in HN tumors might contribute to higher abundance of neutrophils.

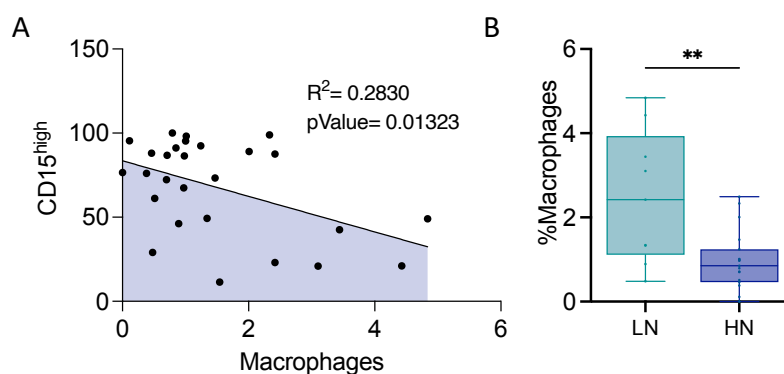


Figure 38. A different clearance characterized high (HN) and low (LN) neutrophils patients.

A. Pearson correlation between CD15^{high} neutrophils and macrophages (n=28) **B.** Frequency of macrophages within LN (n=9) and HN (n=19) patients. Box and whisker plot indicates Min to Max value. **, P < 0.01; unpaired t test.

Adapted from Tiberti et al.

Finally, other important players responsible for neutrophil recirculation are soluble molecules released in the TME by cancer cells, normal cells closely associated to the tumoral tissue and rewired to cooperate in cancer progression and different components of the immune compartment. Thus, we hypothesized that the presence of a differential distribution of soluble factors between LN and HN patients might impact on neutrophil dynamics. Thus, we exposed neutrophils freshly isolated from PB of healthy donors (HD) to interstitial fluid (InF) collected from LN and HN patients. We first noticed that, upon exposure to HN InF, neutrophils retain higher CD15 expression, confirming an active role of the TME in modulating neutrophil functions (Figure 39 panel A).

Moreover, when we performed a time lapse experiment using a 3D collagen matrix on a custom-made microfluidic device, surprisingly, we registered a lower motility of neutrophils exposed to HN InF compared to those exposed to LN InF. This result suggested that the higher intra-tumoral abundance of CD15^{high} neutrophils could be likely ascribed to their increased retention rather than augmented recruitment into the TME. (Figure 39 panel B)

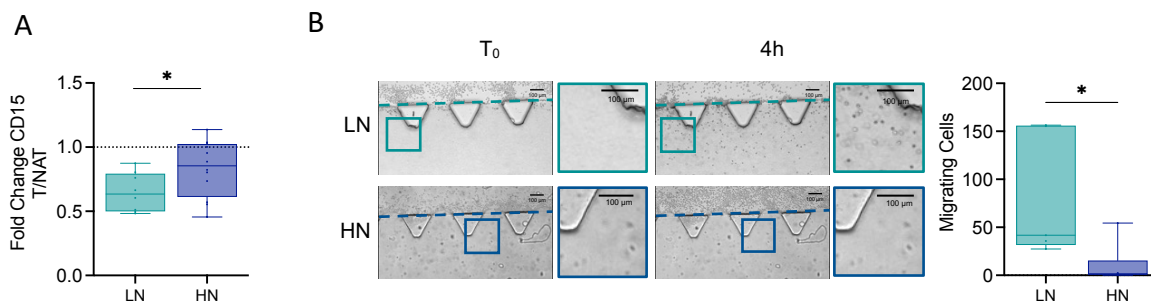


Figure 39. Soluble components of the tumor microenvironment (TME) favor neutrophils retention into the tumor of high neutrophils (HN) patients.

A. Fold change of CD15 expression within neutrophils from healthy donors treated with interstitial fluid (InF) from low (LN, n=8) or high (HN, n=12) neutrophils patients. Box and whisker plot indicates Min to Max value. *, $P < 0.05$; unpaired t test.

B. Representative brightfield images and quantification of neutrophils motility assay on the microfluidic device. Interstitial Fluid (InF) of T from HN and LN patients was tested on healthy donors (HD) derived neutrophils. Bar plot of number of migrating neutrophils on chip upon stimulation with IF from HN (N=6) and LN (N=5) patients. Scale bar 100 μ m. *, $P < 0.05$; Mann-Whitney test. Box and whisker plot indicate Min to Max value.

Adapted from Tiberti et al.

Therefore, we employed Luminex platform to screen a custom panel of 49 inflammatory soluble factors in the InF of T and NAT from CRC patients. Among the 33 molecules that gave consistent measurable results, we did not find any significant association with demographics or tumor grade. Nevertheless, a subset of these factors was significantly correlated with CD15 expression in neutrophils. In particular, CD15^{high} neutrophils were positively correlated with IL17E/IL25^{237–239}, which has been shown to be an important driver of inflammation in gut²³⁹. Indeed, it promotes expression of IL4, IL5 and IL13, which cause epithelial cell hyperplasia and hypertrophy in the gastrointestinal tract and production of CXCL1, CXCL10 and CXCL1, which are chemokines important for neutrophils recruitment²³⁷. As a matter of fact, CXCL1, CXCL10, IL4 and IL13 were positively correlated with CD15^{high} neutrophils.

Moreover, HN tumors harbor higher levels of several soluble factors playing a key role in polarizing neutrophils toward a pro-tumorigenic N2-like phenotype. For instance, CD15 expression was significantly correlated with EGF, G-CSF, IL10 and TGF β 3, which have been all associated with pro-tumoral functions^{175,240–245}. (Figure 40)

All these data supported a specific role for HN TME in driving neutrophil polarization toward N2-like functional state and favoring their retention at the tumor site.

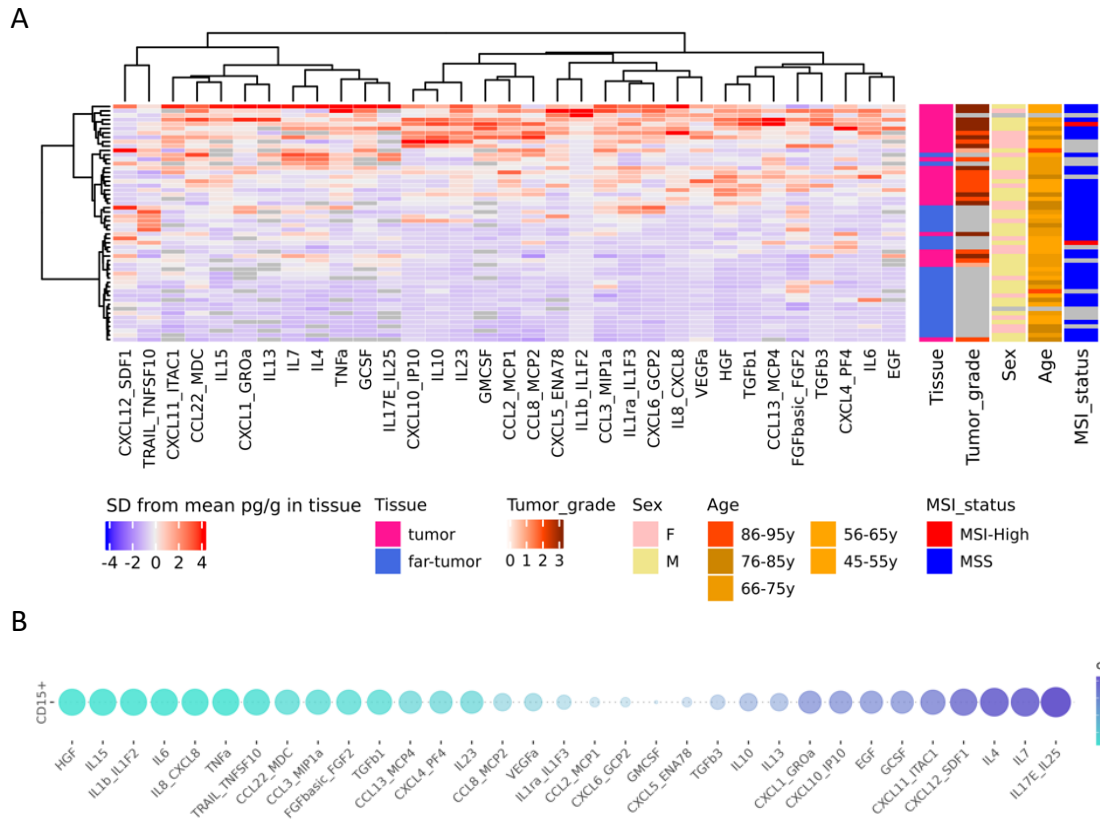


Figure 40. High neutrophils (HN) patients present a peculiar pro-tumoral milieu.

A. Heatmap showing the abundance of soluble molecules derived from InF of tumor (T) and normal adjacent tissue (NAT) (n=54). Soluble molecules are clustered by Ward's minimum variance method and samples by Euclidean distance. Tissue type, tumor grade, sex, age and Microsatellite Instability (MSI) status are indicated for all the samples. **B.** Spearman correlation between soluble molecules in T InF and CD15^{high} neutrophils (n=5).

Adapted from Tiberti et al.

11. Stromal cell-derived factor 1 (SDF-1) reshape the functional state of infiltrating neutrophils, promoting their differentiation and retention within the TME

Among all the detected factors, the C-X-C motif chemokine 12, also known as stromal cell-derived factor 1 (SDF-1), was of particular interest due to its role in promoting neutrophil trafficking and retention at inflammatory site through its binding to CXCR4^{246,247}. Indeed, the expression of CXCR4, in concert with CXCR2, was found to be highly expressed on CD15^{high} neutrophils compared to their CD15^{low} counterpart, as well as in HN compared to LN tumors (Figure 40 panel B-C). Accordingly, imaging analysis confirmed the accumulation of SDF-1 in HN tumors, as assessed by a larger number of α SMA⁺ cancer-associated fibroblasts (CAFs) expressing high levels of SDF-1 (Figure 41).

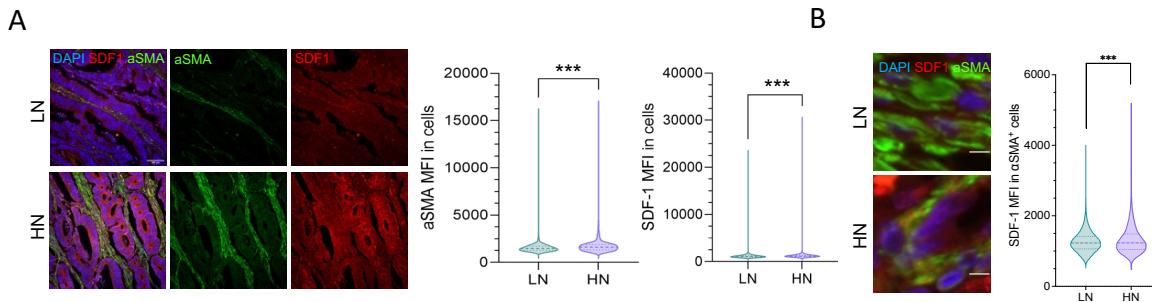


Figure 41. Cancer-associated fibroblasts (CAFs) produce stromal cell-derived factor 1 (SDF-1) in high neutrophils (HN) patients.

A-B. Representative confocal microscopy images and quantification of SDF-1 and SDF-1 in A and SDF-1 within α SMA⁺ cells in B on FFPE tumor tissues from low neutrophils patients (LN, n=4) and HN (n=5). DAPI in blue, α SMA in green, SDF-1 in red. Scale bar 100 μ m. ***, P < 0.001; unpaired t test. Violin plots indicate Min to Max value.

Adapted from Tiberti et al.

To fully understand the role of SDF-1 in shaping neutrophils profile, we treated HD derived neutrophils with SDF-1. SDF-1, compared to untreated controls, induced higher frequency of CXCR2⁺CXCR4⁺ double positive cells (Figure 42 panel A), elevated level of tROS (Figure 42 panel B) and increased gelatinolytic activity (Figure 42 panel C) compared to untreated controls, partially reproducing the *in vivo* observed phenotype. Moreover, upon SDF-1 treatment, we detected an increase in CD62L expression (Figure 42 panel D) in line with the hypothesis that SDF-1 induced a more active status²⁴⁸.

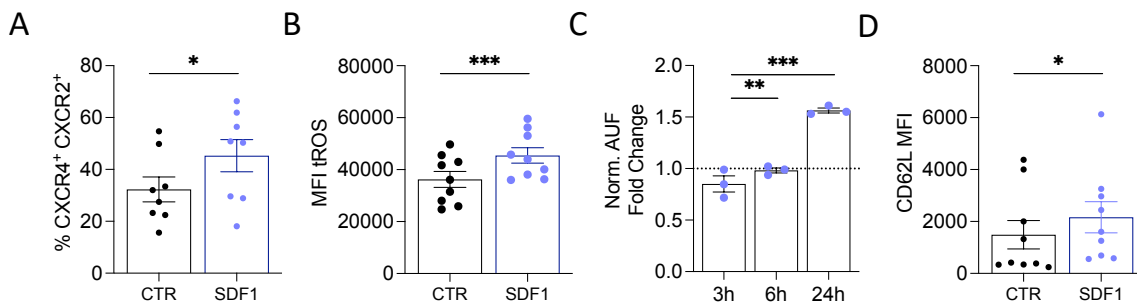


Figure 42. Stromal cell-derived factor 1 (SDF-1) induces an N2-like phenotype in neutrophils.

A. Frequency of CXCR4⁺CXCR2⁺ cells in healthy donors (HD) derived neutrophils treated with SDF-1 versus control medium (CTR, n=8). Bars indicate mean \pm s.e.m. *, P < 0.05; paired t test. **B.** Geometric mean of total ROS (tROS) MFI within HD fresh-isolated neutrophils treated with SDF-1 versus CTR (n=9). Bars indicate mean \pm s.e.m. ***, P < 0.001; paired t test. **C.** Gelatinase activity assay on HD freshly isolated neutrophils treated with SDF-1 for 2h, 6h and 24h (n=3). Bar plot representation of fold change over untreated control. Bars indicate mean \pm s.e.m. **, P < 0.01; ***, P < 0.001; paired t test. **D.** CD62L MFI in neutrophils isolated from HD peripheral blood (PB) treated with SDF-1 or CTR (n=9). Bars indicate mean \pm s.e.m. *, P < 0.05; paired t test.

Adapted from Tiberti et al.

Moreover, SDF-1 improved neutrophil adhesion to micro-endothelial cells (Figure 43 panel A) and maintained cell stillness (Figure 43 panel B), supporting a role for SDF-1 in promoting neutrophil retention in HN tumors. On the contrary, cytokines - like CXCL6, IL8 - that anti-correlated with CD15 expression and were predominant in LN tumors, showed a pro-migratory effect (Figure 43 panel B).

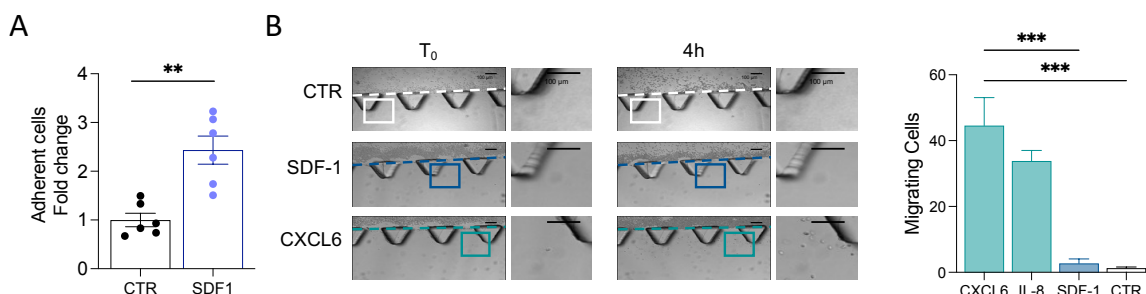


Figure 43. Stromal cell-derived factor 1 (SDF-1) induces neutrophils retention within the tumor.

A. Quantification of adherent neutrophils on endothelial cells after 2 hours treatment with SDF-1 versus control medium (CTR, n=6). Bars indicate mean ± s.e.m. **, P < 0.01; paired t test. **B.** Representative images and quantification of migrating neutrophils on microfluidic device upon stimulation with CXCL6 (400 ng/mL) (n=10), IL8 (100 ng/ml) (n=2), SDF-1 (100 ng/ml) (n=4) or culture medium for 4h (CTR, n=8). Scale bar 100µm. Bars indicate mean ± s.e.m. ***, P < 0.001; unpaired t test.

Adapted from Tiberti et al.

All together, these data indicate that, in HN tumors, elevated levels of SDF-1 induce changes in the functional state of neutrophils, favoring CD15^{high} neutrophil retention and accumulation.

12. CD15^{high} neutrophils abundance directly correlates with GZMK expression of CD8⁺ T cells

Multiple reports suggest that tumor-associated neutrophils (TANs) represent a significant fraction of the inflammatory cells in the TME of many types of cancers, and they have been shown to influence effector T cell functions in animal models and humans^{169,249–251}. However, evidence on how TANs affect anti-tumor CD8⁺ T cell response are still sparse and often contrasting. Likewise, the stratification of non-metastatic CRC patients in the TCGA database was not effective when combining neutrophils to the cytolytic CD8⁺ T cell transcriptional signature (Figure 44). Thus, how neutrophils regulate CD8⁺ T cell activity is still an open question.

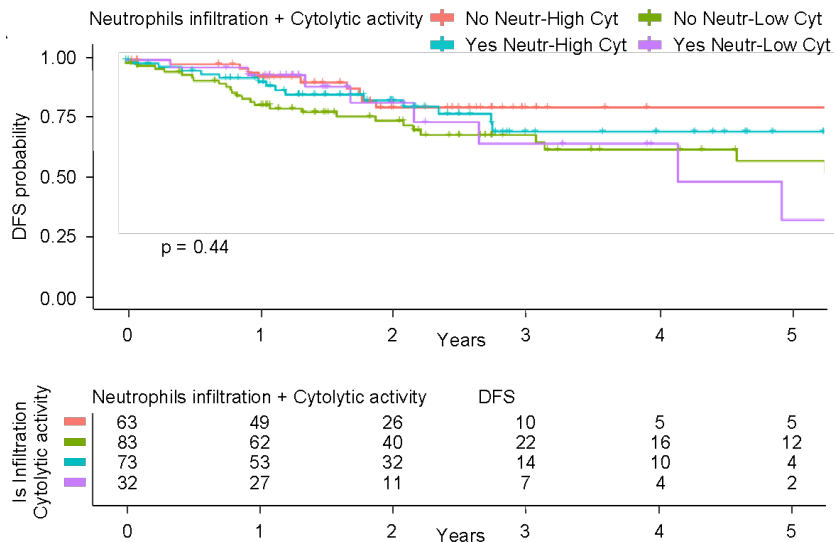


Figure 44. Neutrophils and CD8⁺ T cells infiltrate do not predict the overall survival per se.

Association of cytolitic activity and neutrophils' signature interplay on disease free survival (DFS) in a Kaplan-Meier analysis on the TCGA-COAD cohort. Based on the presence or absence of neutrophils and high or low level of cytolitic activity signatures samples were divided into four groups: no neutrophils infiltration + high cytolitic activity in red, no neutrophils infiltration + low cytolitic activity in green, neutrophils infiltration + high cytolitic activity in turquoise, neutrophils infiltration + low cytolitic activity in violet. Under the survival curves is shown the 'number at risk' table.

Adapted from Tiberti et al.

Here, we sought to determine if intratumoral TAN-CD8⁺ T cell crosstalk could be detected in CRC and if this might impact CD8⁺ T cell differentiation toward a GZMK^{high}CD39^{neg} T_{EM} phenotype. Therefore, we assessed the association of CD15^{high} TANs with specific CD8⁺ T cell subsets inside the TME. Pearson correlation analysis revealed that frequencies of intratumoral CD15^{high} were positively correlated with the frequencies of GZMK^{high} CD8⁺ T_{EM} cells (Figure 45 panel A). In line with an increased frequencies of CXCR2⁺CXCR4⁺ neutrophils in HN TME and within CD15^{high} cells, GZMK^{high} CD8⁺ T_{EM} cells were also positively correlated with CXCR2, CXCR4 and CXCR2⁺CXCR4⁺ neutrophils (Figure 45 panel B-D). These correlations suggested us a possible specific crosstalk between intratumoral neutrophils and GZMK^{high} CD8⁺ T_{EM} cells.

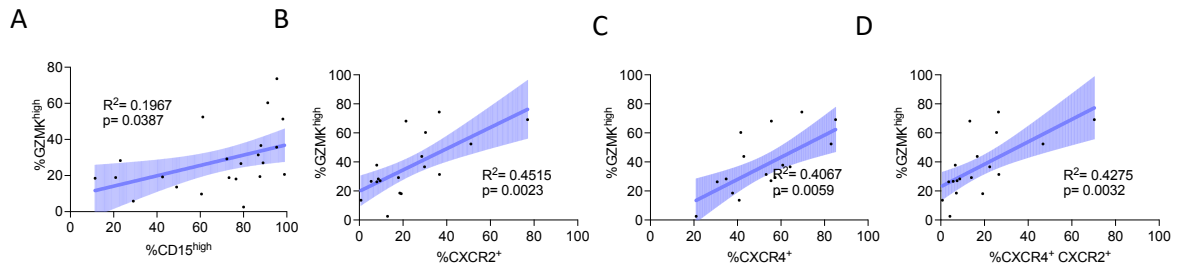


Figure 45. CD15^{high} neutrophils correlate with GZMK expression in CD8⁺ T_{EM}.

A-B. Pearson correlation between GZMK^{high} CD8⁺ T_{EM} within the tumor (T) and CD15^{high} (A, n=22), CXCR2⁺ (B, n=20), CXCR4⁺ (C, n=20) and CXCR4⁺ CXCR2⁺ neutrophils (D, n=20).

Adapted from Tiberti et al.

The correlation with GZMK^{high} CD8⁺ T cells was extremely specific, since no other correlation was found between CD15^{high} neutrophils and any other differentiation (Figure 46 panel A-B), exhaustion or activation marker of CD8⁺ T cells (Figure 46 panel C).

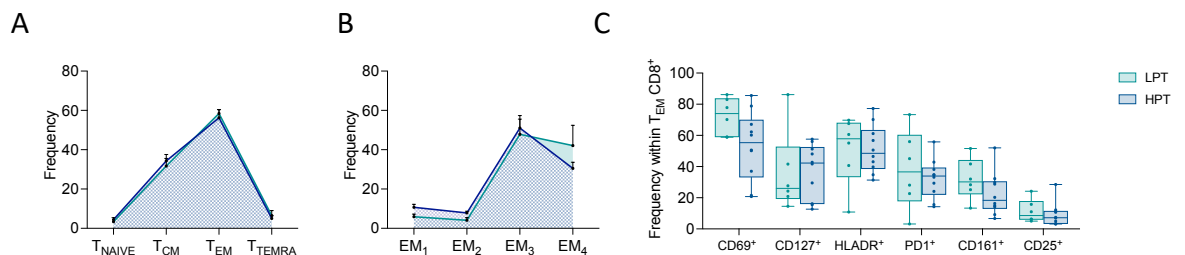


Figure 46. CD15^{high} neutrophils have no effect on phenotypic markers on CD8⁺ T_{EM}.

A. Frequency of Naïve (T_{NAIVE}), Central Memory (T_{CM}), Effector Memory (T_{EM}) and Effector Memory CD45RA⁺ (T_{TEMRA}) within CD8⁺ T_{EM} in tumor of low (LN, n=6) and high (HN, n=10) neutrophils patients. Lines graph indicates mean ± s.e.m. unpaired t test. **B.** Frequency of EM₁, EM₂, EM₃, EM₄ CD8⁺ T cells in LN (n=6) and HN (n=10) patients. Lines graph indicates mean ± s.e.m. unpaired t test. **C.** Frequency of CD69⁺, CD127⁺, HLADR⁺, PD1⁺, CD161⁺, CD25⁺ cells within CD8⁺ T_{EM} cells in LN (n=6) and HN (n=10) patients. Box and whisker plot indicates Min to Max value. unpaired t test.

Adapted from Tiberti et al.

Looking at other T cell compartments, we found a low expression of GZMK by conventional CD4⁺ T cells and no correlation between the frequency of GZMK^{high} CD4⁺ T cells and CD15^{high} neutrophils (Figure 47 panel A) neither a differential abundance between the HN and LN patients was detected (Figure 47 panel B). Interestingly, T $\gamma\delta$ cells also showed high production of GZMK and correlated with CD15^{high} neutrophils (Figure 47 panel C-D).

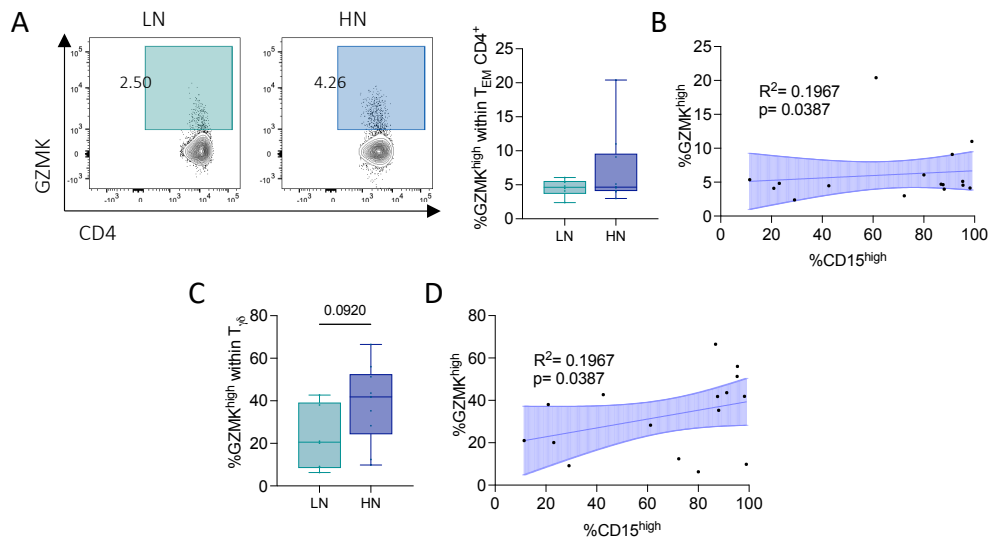


Figure 47. CD15^{high} neutrophils induce GZMK expression within T γ δ while CD4⁺ T_{EM} are not affected.
A. Contour plot and quantification in LN (n=6) and HN (n=10) patients of GZMK^{high} frequency within CD4⁺ T_{EM}. Box and whisker plot indicates Min to Max value. unpaired t test. **B.** Pearson correlation between frequency of GZMK^{high} CD4⁺ T_{EM} and CD15^{high} neutrophils (n=15). **C.** Contour plot and quantification in LN (n=6) and HN (n=10) patients of GZMK^{high} frequency within T γ δ . Box and whisker plot indicates Min to Max value. unpaired t test. **D.** Pearson correlation between frequency of GZMK^{high} T γ δ and CD15^{high} neutrophils (n=15).

Adapted from Tiberti et al.

The differential abundance of GZMK within CD8⁺ T cells in HN patients compared with LN was independently confirmed by FACS (Figure 48 panel A) and quantitative confocal imaging, which both highlighted that the expression of GZMK within CD8⁺ T cells is higher in HN patients compared with LN (Figure 48 panel B).

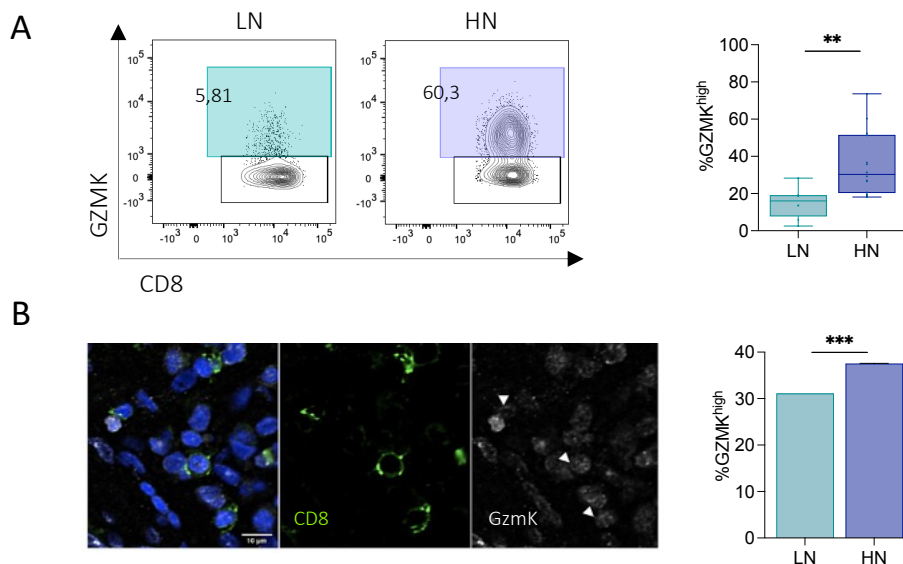


Figure 48. High neutrophils (HN) patients accumulate GZMK^{high} CD8⁺ T_{EM}.
A. Representative contour plot and quantification of GZMK^{high} CD8⁺ T_{EM} cells in low neutrophils (LN, n=7) and HN (n=14) patients. Box and whisker plots indicate Min to Max value. **, P < 0.01; unpaired t test. **B.** Representative image and quantification of GZMK Mean Fluorescence Intensity (MFI) in CD8⁺ T cells in LN (n=8) and HN (n=9) tumors. Scale bar 10 μ m. Bars indicate mean \pm s.e.m. ***, P < 0.001; unpaired t test.

Adapted from Tiberti et al.

In line with the negative correlation between macrophages and the frequency of CD15^{high} neutrophils, we found a negative correlation between macrophages and GZMK^{high} CD8⁺ T_{EM} cells (Figure 49 panel A), while no relation was detected between GZMK^{high} CD8⁺ T_{EM} and others innate components such as DC (Figure 49 panel B) and NK cells (Figure 49 panel C) quantified by flow cytometry. Notably, the negative correlation between Treg cells (identified as CD25⁺, CD127⁻)²⁵² and GZMK^{high} CD8⁺ T_{EM} (Figure 49 panel D) deserves further investigation; also in light of the recently identified immunosuppressive CD4⁺ EOMES⁺ Tr1-like subset also characterized by the expression of GZMK¹²¹.

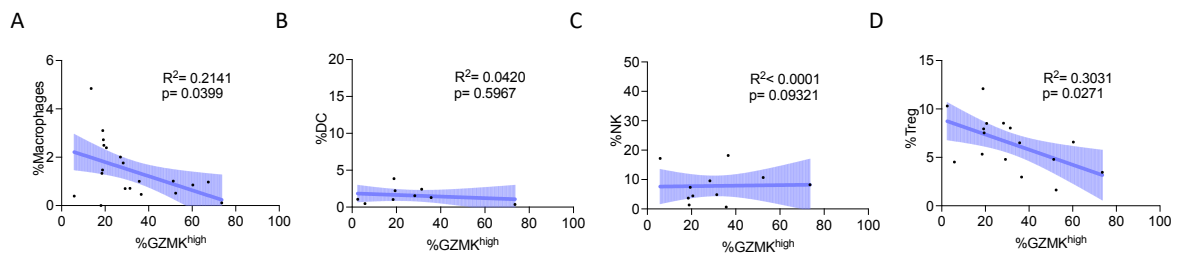


Figure 49. GZMK expression within CD8⁺ T_{EM} is negatively correlated with macrophages and Treg abundance in colorectal cancer (CRC).

Pearson correlation between GZMK^{high} CD8⁺ T_{EM} and macrophages in **A** (n=20), DC in **B** (n=9), NK in **C** (n=11) and Treg in **D** (n=16) within CD45⁺.

Adapted from Tiberti et al.

In agreement with previous reports^{62,224,225}, GZMK⁺CD8⁺ T cells were detected - albeit at low frequencies - in the peripheral blood of HD and CRC patients as well as in NAT at the same extent. However, intratumor CD8⁺ T_{EM} cells expressing higher levels of GZMK were specifically and significantly accumulated only in HN T compared to their corresponding NAT, which supports the idea that the GZMK⁺ immune signature we found is tumor-specific. (Figure 50)

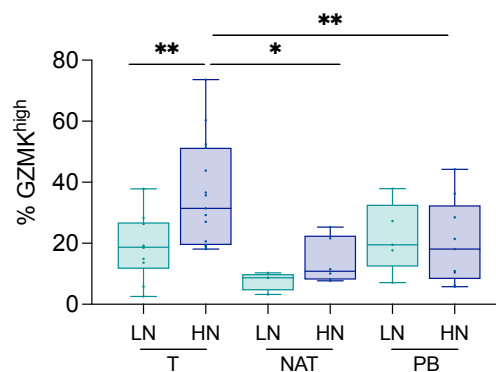


Figure 50. GZMK expression is specifically upregulated in CD8⁺ T_{EM} within tumors (T).

A. Quantification of GZMK^{high} CD8⁺ T_{EM} cells within low (LN, n=7) and high (HN, n=8) neutrophils patients in T, normal adjacent tissue (NAT) and peripheral blood (PB). Box and whisker plot indicates Min to Max value *, P < 0.05; **, P < 0.01; paired and unpaired t test.

Adapted from Tiberti et al.

All these data suggested us a specific cross talk between neutrophils and CD8⁺ T cells able to modulate the phenotype of these cells in the TME.

13. Neutrophil/CD8⁺ T cell interaction influences tumor control in an *in vivo* mouse model of CRC

Next, we employed the *in vivo* syngeneic MC38 mouse model of colon cancer to validate, on an immune-competent system, the correlation between the abundance of neutrophils and GZMK^{high}CD8⁺ T cells observed on patients, proof that the interaction is conserved across species and address causality.

We subcutaneously injected 1*10⁶ MC38 cells and tumors were collected when they reached ~ 500 mm³ (< 1 cm³) or ~ 1000 mm³ (> 1 cm³). In accordance with the idea that GZMK^{high} CD8⁺ T cells can have an impact on anti-tumor immunity, we found that tumor progression positively correlated with intratumoral frequencies of GZMK^{high} CD8⁺ T cells (Figure 51 panel A) and CD11b⁺, Ly6g⁺, CXCR2⁺ neutrophils (Figure 51 panel B), validating results observed in CRC patients. Interestingly CXCR2 is expressed during neutrophils maturation at the promyelocyte stage in mice and lost during aging. Thus, the more neutrophils in the TME present a mature phenotype and increase their functionality, the more they express CXCR2²⁵³.

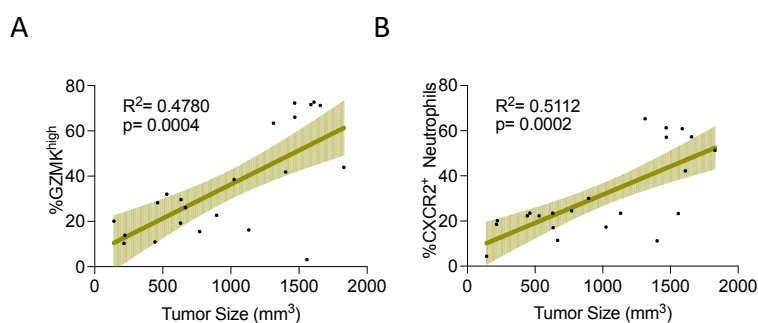


Figure 51. GZMK expression correlates with tumor growth in *in vivo* syngeneic MC38 mouse model of colon cancer.

A. Quantification of Pearson correlation between GZMK^{high} CD8⁺ T cells within tumor (T) of MC38 tumor bearing mice and tumor size (n=22). **B.** Pearson correlation between CXCR2⁺, Ly6G⁺ neutrophils within T of MC38 tumor bearing mice and tumor size (n=22).

Adapted from Tiberti et al.

To further confirm the role of neutrophils in promoting GZMK production by CD8⁺ T cells, we increased intra-tumoral neutrophils infiltration by treating MC38 syngeneic mouse model of CRC with Granulocyte colony-stimulating factor (G-CSF), according to previous described protocols¹⁸⁶. As expected, we detected an increase in CD45⁺, CD11b⁺, Ly6g⁺ neutrophils (Figure 52 panel A) and in their expression of CXCR2 within the tumor (Figure

52 panel B), followed by an increase in the GZMK^{high} CD39⁻ population (Figure 52 panel C), as we described in humans.

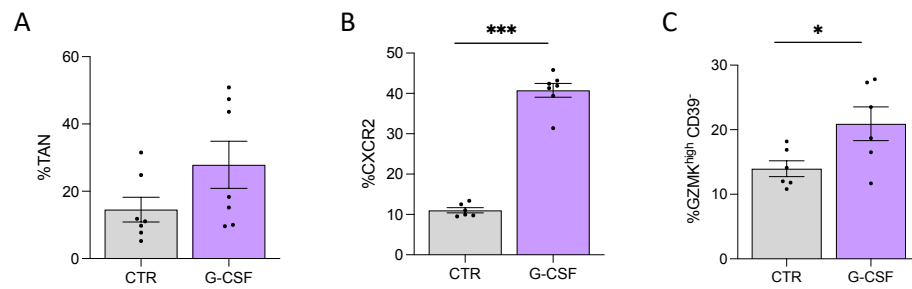


Figure 52. G-CSF-induced neutrophils enrichment within the tumor (T) favor GZMK^{high} CD39⁻ T cells accumulation.

A. Quantification of Tumor Associated Neutrophils (TAN) within T of MC38 syngeneic mouse model of colorectal cancer (CRC) with or without (CTR) Granulocyte colony-stimulating factor (G-CSF) treatment. Bars indicate mean \pm s.e.m. unpaired t test. **B.** Quantification of CXCR2⁺ TAN within T of MC38 CRC model in CTR versus G-CSF treatment. Bars indicate mean \pm s.e.m.; ***, $P < 0.001$; unpaired t test. **C.** Quantification of GZMK^{high} CD39⁻ CD8⁺ T cells within T of MC38 CRC model in CTR versus G-CSF treatment. Bars indicate mean \pm s.e.m.; *, $P < 0.05$; unpaired t test.

The association between tumor size, a higher infiltration of GZMK^{high} CD8⁺ T cells and CXCR2⁺ neutrophils (Figure 51 panel B), suggested us not only a specific crosstalk between these cell types, but also an important role in tumor progression. To address this hypothesis, we depleted neutrophils using anti-Ly6g antibody treatment daily from day 0 after tumor injection to 20, as described by Boivin et al²⁵⁴. Together with a decrease in the tumor associated neutrophils (Figure 53 panel A), we detected a decrease in tumor growth (Figure 53 panel B) and in GZMK expression by CD8⁺ T cells (Figure 53 panel C).

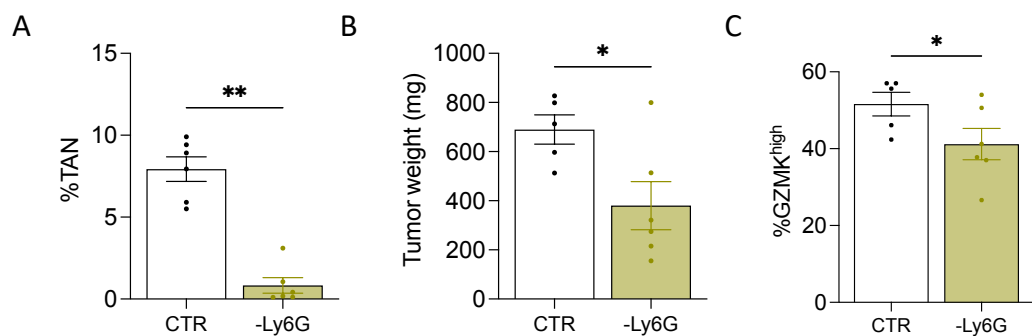


Figure 53. Neutrophils depletion improve tumor control and reduces CD8⁺ T cells' GZMK expression.

A. Quantification of Tumor Associated Neutrophils (TAN) within T of MC38 syngeneic mouse model of colorectal cancer (CRC) with or without (CTR, n=7) aLy6g (-Ly6G, n=7) treatment. Bars indicate mean \pm s.e.m. **, $P < 0.01$; Mann-Whitney test. **B.** Tumor weight of CTR (n=5) versus -Ly6G MC38 (n=6) CRC model. Bars indicate mean \pm s.e.m.; *, $P < 0.05$; unpaired t test. **C.** Quantification of GZMK^{high} CD8⁺ T cells within T of MC38 CRC model in CTR (n=5) versus -Ly6G (n=5). Bars indicate mean \pm s.e.m.; *, $P < 0.05$; Mann-Whitney test.

Adapted from Tiberti et al.

Additionally, based on the above results showing SDF1-dependent recruitment of neutrophil in HN tumors, we decided to prove if SDF-1 inhibition might counteract the GZMK^{high} CD8⁺ T cells, thus dumping tumor growth. Mice were systemically treated with AMD3100, a SDF-1 inhibitor (1mg/kg for 4 injections at day 5, 7, 9 and 11 after tumor injection) and immune infiltrate and tumor growth was assessed (Figure 54 panel A). AMD3100-treated mice showed a drastic reduction of the tumor growth which (Figure 54 panel B) was accompanied by a huge increase in the amount of CD8⁺ T cells infiltration in the tumor (Figure 54 panel C), as previously reported in literature. Interestingly, we reported here that AMD3100-treated mice experienced a significant decrease in mature (CXCR2⁺ CXCR4⁻)/immature (CXCR2⁻ CXCR4⁺) neutrophils ratio (Figure 54 panel D-E) followed by a decrease in the CD39⁻ GZMK⁺ population (Figure 54 panel F) which we have correlated with worst clinical outcome in humans.

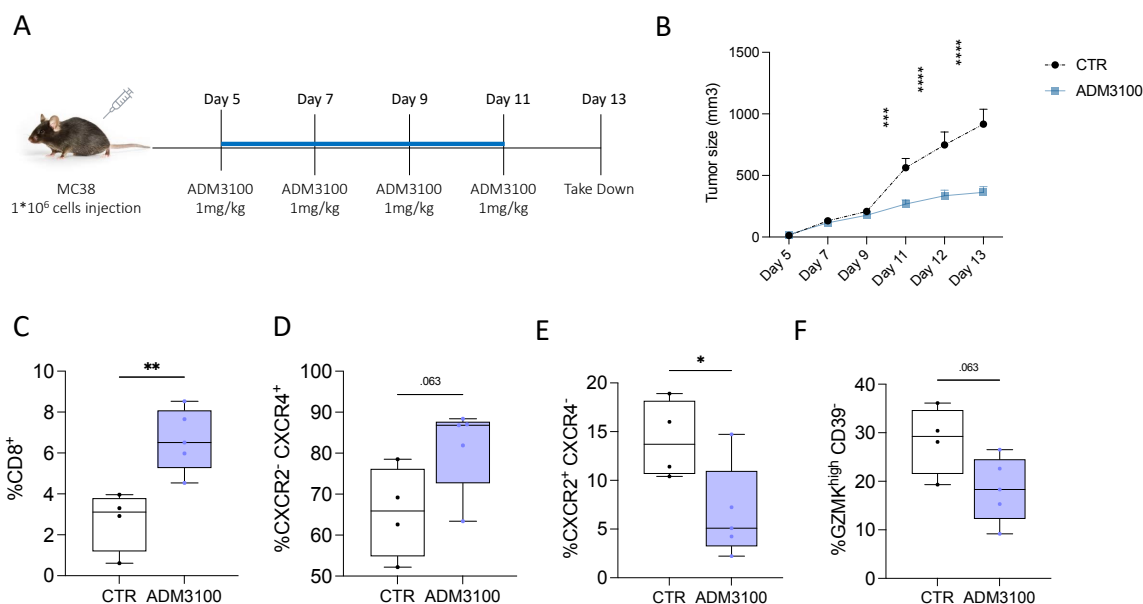


Figure 54. CXCR4 inhibitor (ADM3100) control tumor growth by increasing CD8⁺ T cells infiltrate and reducing GZMK^{high} CD39⁻ CD8⁺ T cells.

A. Experimental design. **B.** Growth curves of MC38 tumor bearing mice treated (n=5) and untreated (CTR, n=4) with ADM3100. Lines plot indicates mean \pm s.e.m. unpaired t test. **C-F.** Quantification of CD8⁺ T cells (C), CXCR2⁻CXCR4⁺ (D), CXCR2⁺CXCR4⁻ (E) neutrophils, and GZMK^{high} CD39⁻ CD8⁺ T cells (F) within tumor (T) of ADM3100 (n=5) and CTR (CTR, n=4). Box and whisker plot indicates Min to Max value; **, P < 0.01; *, P < 0.05; unpaired t test.

Thus, these results pinpointed an important role for SDF-1 in contributing to CRC relapse by causing neutrophils accumulation and thus favoring interaction with CD8⁺ T cells, which in turn are skewed to produce high levels of GZMK.

14. Direct neutrophil/CD8⁺ T cell interaction is required for skewing CD8⁺ T cell to produce high levels of GZMK

Having found evidence of an association between TAN and GZMK^{high} CD8⁺ T_{EM} also in a clinically relevant mouse model of CRC, we queried if neutrophils were directly involved in inducing a GZMK^{high} phenotype by co-culturing CD8⁺ T cells with neutrophils. When neutrophils were added to the culture, the frequencies of GZMK^{high} CD8⁺ T cells increased compared with CD8⁺ T cells alone from mice (Figure 55 panel A) and from humans (Figure 55 panel B). These data demonstrated that skewing of CD8⁺ T cells toward a GZMK^{high} phenotype can result from direct crosstalk between neutrophils and CD8⁺ T cells. We have also demonstrated that the direct contact between neutrophils and CD8⁺ T cells is required in order to have the maximal effect on GZMK production. Indeed, GZMK levels in CD8⁺ T cells are dramatically reduced when we performed the co-culture experiment using transwell (Figure 55 panel B). Moreover, the expression of GZMK in CD8⁺ T cells in coculture with neutrophils is higher as compared with freshly isolated CD8⁺ T cells (Figure 55 panel B) supporting that, despite we noticed a small decrease in the viability of CD8⁺ T cells in coculture (Figure 56 panel C), the enrichment of GZMK^{high} cells is not the result of a positive selection operated by neutrophils. Of notice, the coculture of CD8⁺ T cells with neutrophils induces an increase in T_{EM} cells with high expression of GZMK (Figure 55 panel D).

Importantly, using the mouse system, we were able to dissect that GZMK production in CD8⁺ T cells is induced in a stronger manner by neutrophils isolated from tumors compared both with BM derived neutrophils and PB derived neutrophils in mice (Figure 55 panel A). To further validates the role of TME in this contest, we treated CD8⁺ T cells with InF of CRC patients and we found a decrease in GZMK production in NAT compare with T (Figure 55 panel E), suggesting a role of soluble component present within T in the basal level of GZMK expression, while the NAT play an immunomodulatory role.

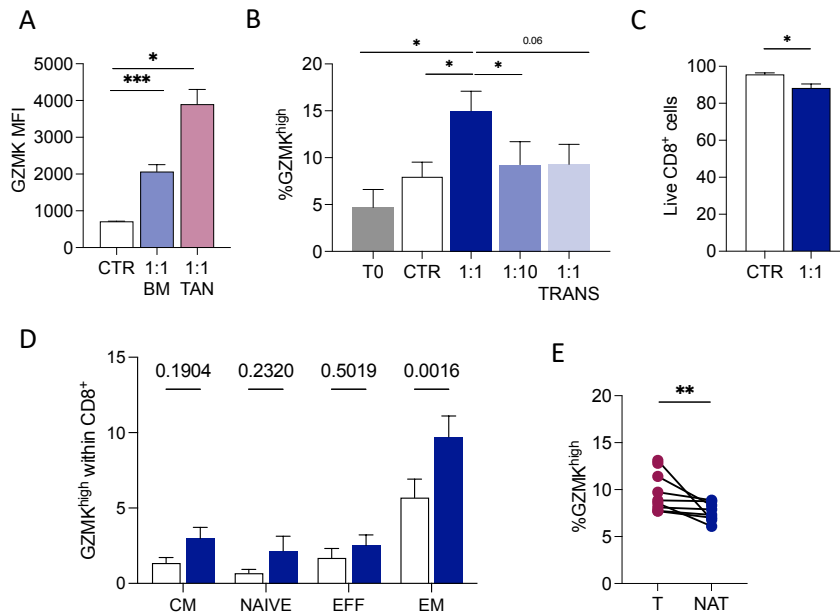


Figure 55. Neutrophils increase the basal production of GZMK in CD8⁺ T cells by direct contact in culture.

A. Quantification of GZMK expression within murine CD8⁺ T cells as mean fluorescence intensity (MFI) after 24h of culture alone or in contact with mouse Bone Marrow (BM) derived neutrophils or tumor associated neutrophils (TAN) isolated from the tumor (T) of MC38 CRC model in a 1:1 ratio. Bars indicate mean ± s.e.m.; ***, $P < 0.001$; *, $P < 0.05$; paired t test. **B.** Quantification of GZMK frequency within freshly isolated CD8⁺ T cells from healthy donors (HD) peripheral blood (PB) and after 24h of culture alone or in contact with PB derived neutrophils in a 1:1 and 1:10 ratio in contact and 1:1 ration in transwell. Bars indicate mean ± s.e.m.; *, $P < 0.05$; paired t test. **C.** Viability quantification of CD8⁺ T cells after 24h of culture alone or with neutrophils (1:1) Bars indicate mean ± s.e.m.; *, $P < 0.05$; paired t test. **D.** Frequency of GZMK^{high} central memory (CM), naïve, terminally effector (EFF) and effector memory (EM) T cells within CD8⁺ T cells after 24h of culture alone or with neutrophils (1:1) Bars indicate mean ± s.e.m.; *, $P < 0.05$; 2 way ANOVA. **E.** Frequency of GZMK in CD8⁺ T cells after 24h of culture with Interstitial fluid (InF) of tumor (T) and normal adjacent tissue (NAT). **, $P < 0.01$; paired t test.

Adapted from Tiberti et al.

Finally, despite the low number within human derived CRC sample, we were able to FACS-sort tumor infiltrating neutrophils from CRC patients and co-culture them with CD8⁺ T cells derived from PB of the same patient overnight, followed by the phenotypic analysis. Remarkably, neutrophils isolated from tumors present a higher capacity to induce GZMK in CD8⁺ T cells in comparison with matched neutrophils derived from PB of the same patient (Figure 56 panel A). Furthermore, to get a deep understanding of the impact of tumor infiltrating neutrophils on CD8⁺ T cell we FACS-sorted CD15^{high} and CD15^{low} CD66b⁺ neutrophils. We reported that the CD15^{high} population induced high GZMK production from CD8⁺ T cells as compared with the CD15^{low} counterpart (Figure 56 panel B).

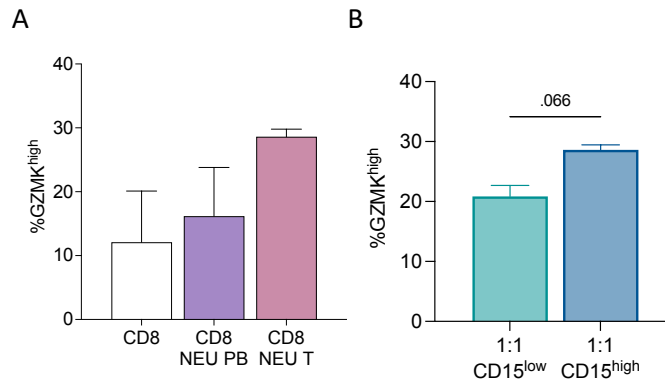


Figure 56. CD15^{high} neutrophils present within the tumor (T) induces higher production of GZMK in CD8⁺ T cells compared with peripheral neutrophils and the CD15^{low} counterpart.

A. Quantification of GZMK expression within CD8⁺ T cells overnight (O/N) culture alone or in contact with peripheral blood (PB) derived neutrophils or tumor derived neutrophils (NEU T) isolated from 3 CRC patients in a 1:1 ratio. Bars indicate mean \pm s.e.m. paired t test. **B.** Quantification of GZMK frequency within isolated CD8⁺ T cells from CRC patients PB after ON culture with tumor-derived neutrophils CD15^{low} and CD15^{high} respectively in a 1:1 ratio. Bars indicate mean \pm s.e.m. paired t test.

Adapted from Tiberti et al.

Overall, these data support a model where the direct interaction between neutrophils and CD8⁺ T cells skewed CD8⁺ T cells toward GZMK^{high} cells.

To further validate the crosstalk between neutrophils and CD8⁺ T cells and the capability of neutrophils to induce GZMK production in these cells, we analyzed the distance between CD66b⁺ neutrophils and CD8⁺ T cells GZMK⁺ directly on HN and LN tumors. We found that the production of GZMK is higher in CD8⁺ T cells close to neutrophils compared with other surrounding cell types (Figure 57 panel A). Likewise, the level of GZMK is higher in CD8⁺ T cells closer to neutrophils compared with the more distant ones (Figure 57 panel B).

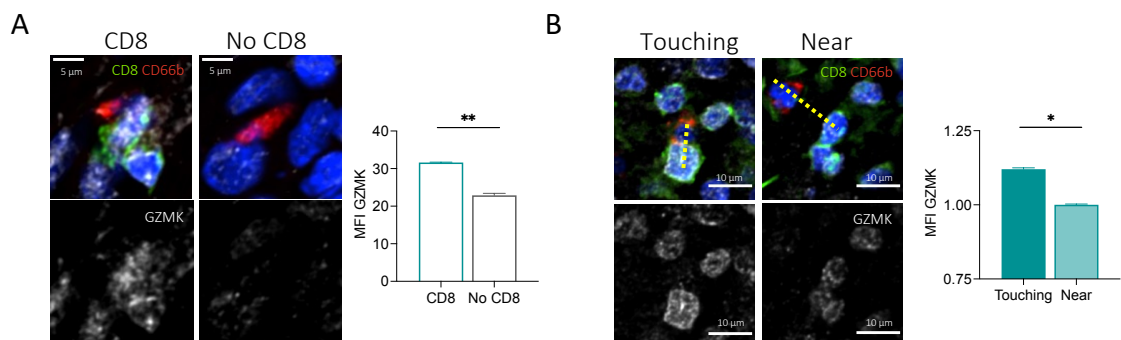


Figure 57. Neutrophils modulate GZMK within CD8⁺ T cells in a contact mediated manner.

A. Representative confocal images and relative quantification of GZMK MFI in CD8⁺ (in Green) and CD8⁻ (no CD8) cells within a 10 μ m distance from neutrophils (identified with CD66b⁺, in red). Scale bar 5 μ m. **, P < 0.01; unpaired t test. **B.** Representative confocal images and normalized quantification of GZMK MFI in CD8⁺ (Green) within 10 μ m (Touching, n=161) or between 10 and 20 μ m (Near, n=203) from neutrophils (CD66b⁺, in red). Yellow dotted lines represent 20 μ m (left) and 10 μ m (right). Scale bar 10 μ m. *, P < 0.05; unpaired t test.

Adapted from Tiberti et al.

These data corroborate once again the existence of a specific crosstalk between CD8⁺ T cells and neutrophils, which results in GZMK production by CD8⁺ T cells.

15. The GZMK produced by infiltrating CD8⁺ T_{EM} promotes relapse by reducing E-Cadherin expression in CRC tumors

We decided to understand the direct effect of GZMK on an *in vitro* model of intestine epithelium. To do this, we cocultured CACO2 and HT39 cell lines in a ratio 1:7 in a transwell device to allow the multilayer formation and the polarization of the epithelium. After 12 days of culture, we coculture CD8⁺ T cells and neutrophils isolated from HD PB on the epithelium and we observed a strong modulation in E-Cadherin (E-Cad) expression^{255,256} (Figure 58 panel A), without affecting the cell viability (Figure 58 panel B). This result suggested the development of an epithelial to mesenchymal transition process facilitating the tissue damage and metastasization.

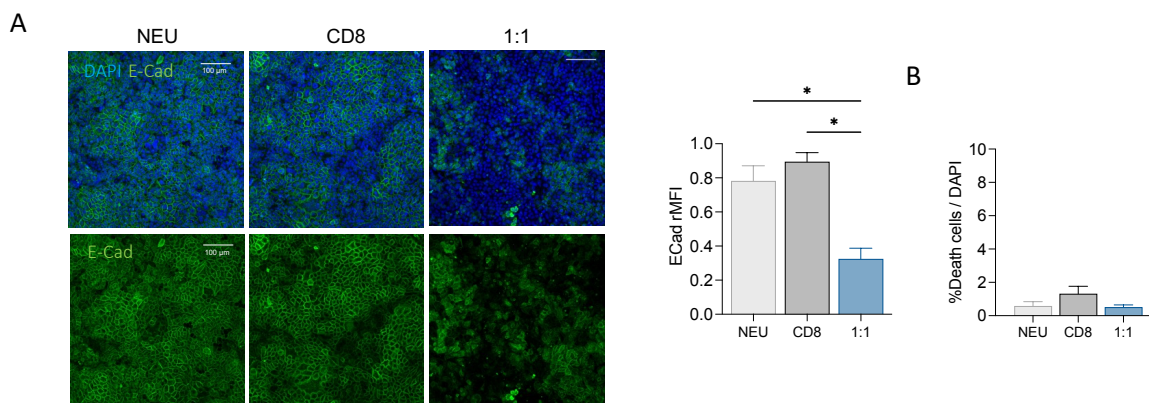


Figure 58. Coculture of CD8⁺ T cells and neutrophils induce a decrease in E-Cadherin (E-Cad) in an intestinal epithelial model.

A. Representative images and quantification of E-Cad expression on CACO-HT29 epithelial model on transwells in presence of neutrophils (NEU), CD8⁺ T cells (CD8) or neutrophils/CD8 (1:1 ratio) isolated from healthy donors (HD) peripheral blood (PB) for 24h (n=2). Multicolor confocal imaging. DAPI blue, E-Cad in green. Scale bar 50µm. Bars indicate mean ± s.e.m. *, P < 0.05; paired t test. **B.** Frequency of death cells within NEU, CD8 and 1:1. Bars indicate mean ± s.e.m. *, P < 0.05; paired t test.

Adapted from Tiberti et al.

To confirm the role of GZMK in this process we treated the transwell with or without rGZMK and we observed a strong decrease in E-Cad (Figure 59).

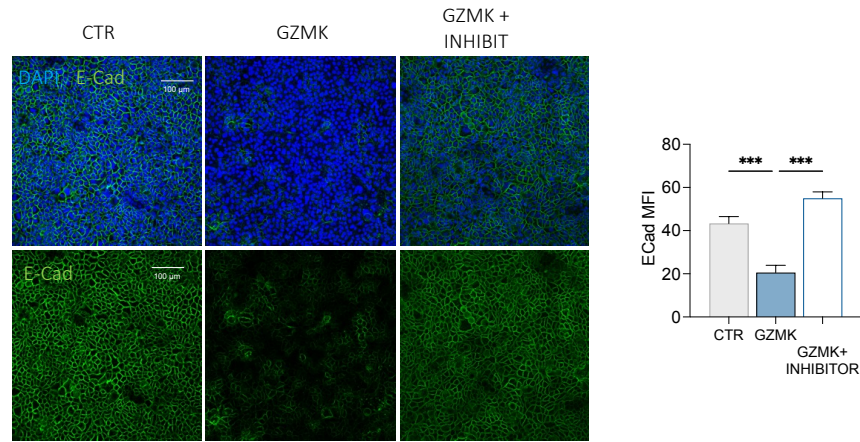


Figure 59. GZMK is responsible for E-Cadherin (E-Cad) decrease in intestinal epithelial model.

Representative images and quantification of E-Cad expression on CACO-HT29 epithelial model on transwells in treated with PBS (CTR) or recombinant active human GZMK, with (GZMK+INHIBIT) or without (GZMK) the PRO-321 GZMK's inhibitor Bikunin for 24h. DAPI blue, E-Cadherin green, n=10. Scale bar 100µm. Bars indicate mean ± s.e.m. ***, P < 0.001; paired t test.

Adapted from Tiberti et al.

Additionally, rGZMK induced a remodulation in the transcriptional profile of our intestinal epithelial model. Pathways involved in increase cell proliferation, DNA damage response and chromatin remodeling are strongly upregulated, suggesting us a progression toward an epithelial mesenchymal transition (EMT), which needs to be confirmed and investigated with further studies. (Figure 60).

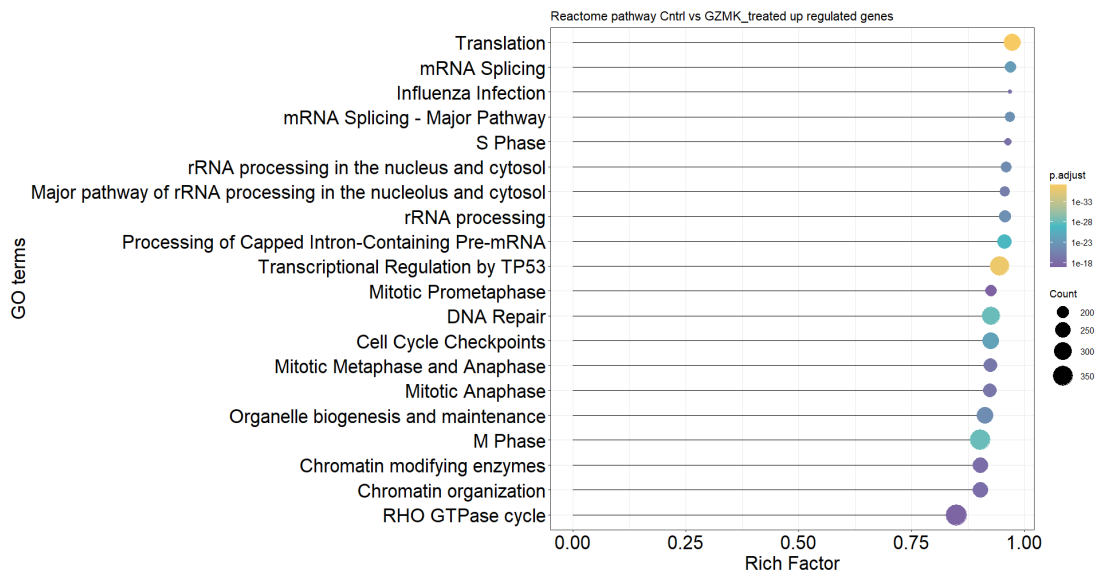


Figure 60. GZMK modulate transcriptional profile of an intestinal epithelial model.

Reactome pathways upregulated after treatment of CACO-HT29 epithelial model on transwells in treated with recombinant active human GZMK in respect to control with only media for 24h.

Adapted from Tiberti et al.

All these data support the pro-tumoral effect of GZMK produced by CD8⁺ T_{EM} into the TME of CRC patients. Remarkably, in line with the enrichment of GZMK^{high} CD8⁺ T_{EM} in HN patients, we detected a downregulation in E-Cad in their tumoral tissue (Figure 61).

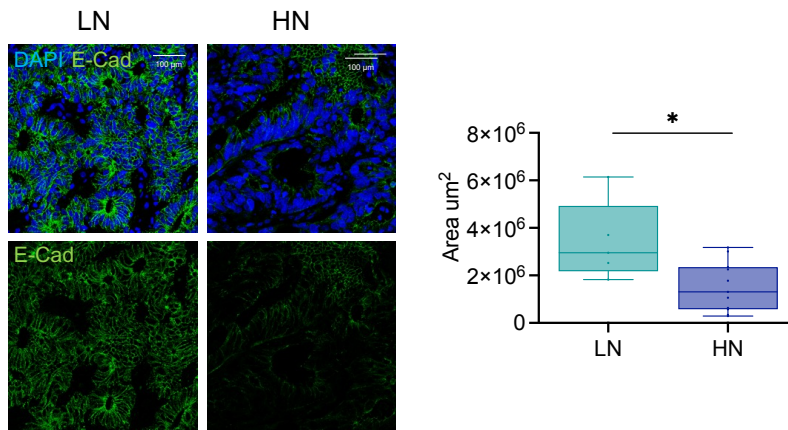


Figure 61. HN patients present lower E-Cadherin (E-Cad) expression.

Representative images and quantification of E-Cad expression by multicolor confocal imaging on FFPE sections within low (LN, n=5) and high (HN, n=12) neutrophils patients. DAPI blue, E-Cad green, n=10. Scale bar 100µm. Box and whisker plot indicates Min to Max value; *, P < 0.05; unpaired t test.

Adapted from Tiberti et al.

All these data support the development of a pro-metastatic TME and high risk of relapse in HN CRC patients.

Discussion

The tumor immune microenvironment is an important prognostic determinant in CRC. Here, we showed that tumor infiltrating neutrophils expressing high levels of CD15 interact with CD8⁺ T effector memory cells skewing them to produce GZMK, associated with tumor progression in CRC patients.

CRC possesses multiple histological subtypes that generate disparate immune responses²⁵⁷. However, genomic approaches alone were unable to translate them into solid prognostic biomarkers. While limiting the efficacy of therapy, immune heterogeneity offers an opportunity to develop novel diagnostics based on patient-specific immune biomarkers, instead. There have been recent attempts to profile the immune cell content of CRC and other solid tumor malignancies using transcriptional profiling data and Immune histochemistry (IHC)^{258–260}. Although informative, transcriptional signatures have not been clearly demonstrated to infer immune cell content, nor are they capable of delineating unique immune cell subtypes that require multiple markers to be identify. Alternatively, IHC provides critical information regarding the spatial relationships between immune and cancer cells, but only captures a small area of tumor and might not reliably represent tumor heterogeneity. Our study, instead, has provided a multilayered description of the immune landscape by combining scRNAseq profiling and MPFC to estimate the heterogeneity of immune cells within and across CRC patients while also obtaining functional information. Currently, the prognostic value of immune cell infiltration is not conclusive, especially regarding neutrophils²⁶¹. We provide evidence that neutrophils are the most abundant innate cell population infiltrating the tumor bed in early- stage CRC, revealing that CRC patients can be stratified based on high (HN) or low (LN) CD15^{high} neutrophil infiltration. Pro-tumorigenic roles have been ascribed to neutrophils across different tumor types^{262,263}, including promotion of angiogenesis and immunosuppression^{170,227}, but it is not clear whether distinct neutrophil populations gather the tumor or if phenotypic changes occur inside the TME. Also, the few functional studies available have led to conflicting conclusions on the impact of neutrophils on antitumor T cell responses^{196,198,264}. Our data supports the idea that neutrophils undergo phenotypic changes specifically within the TME. The majority of neutrophils in patient matched normal-adjacent tissues (NAT) and peripheral blood (PB) are characterized by CD15^{high} expression. Importantly, there are no differences in the expression of CD15 on PB-derived neutrophils from healthy donors (HD) and CRC patients. Once neutrophils are recruited to the site of inflammation, they are fated to programmed cell death, which is paralleled by downregulation of specific receptors, including CD15²⁶⁵. Our data show that also neutrophils recruited to the TME are subjected

to the same fate. Indeed, neutrophils gathering LN tumors significantly down-regulate CD15 compared to matched NAT and PB, likely to limit potentially harmful consequences of prolonged neutrophil activation. On the contrary, in HN tumors neutrophils maintain a high level of CD15 expression, likely remaining activated. This is consistent with the pro-tumoral phenotype exerted by CD15^{high} neutrophils, which have higher frequency of CXCR2⁺CXCR4⁺ and produce more total Ros (tROS) compared with CD15^{low}, in agreement with N2 type neutrophils^{175,253}. Likewise, exposure of neutrophil to the interstitial fluid (InF) from HN tumors pushes CD15 expression, implying that the TME has a direct role in polarizing neutrophils toward a CD15^{high} state. Moreover, InF from HN, differently from LN, did not foster neutrophil migration, suggesting that there might be some soluble factors in the HN TME which promote neutrophils retention, rather than increasing their recruitment to the tumor.

Neutrophils are recalled early to the site of inflammation, where they can provoke tissue damage if inappropriately retained²⁶⁶. To avoid it, neutrophils that migrate into tissues progressively lose CD15 and are phagocytosed by resident tissue macrophages²⁶⁷. Since HN tumors displayed an inverse correlation between macrophages and CD15 surface expression on neutrophils, we can speculate that the accumulation of CD15^{high} neutrophils in HN tumors might be due, at least in part, to inefficient clearance, as previously demonstrated in other tumor contexts²⁶⁸. M2 macrophages have a proven role in establishing an immunosuppressive TME; thus analysis to deeply characterize M1 or M2 macrophage phenotype in correlation with neutrophil abundance and GZMK^{high}CD8⁺ T cells in the CRC TME deserve further investigation.

On the other hand, SDF-1/CXCR4 signaling plays an important role in the retention of neutrophils at inflammatory sites²⁶⁹. Likewise, SDF-1 levels in CRC patients correlates with frequency of CD15^{high} neutrophils and, *in vitro*, with increased adhesion and release of TME's remodeling factors rather than driving chemotaxis. Overall, these data indicate that intratumoral high levels of SDF-1 promote neutrophil retention in HN tumors, favoring their accumulation.

Data presented here showed that most of the tumor infiltrating CD8⁺ T cells preserve their effector functions, while only a minority expressed co-inhibitory receptors, suggesting that other mechanisms besides canonical "T cell exhaustion" might contribute to the failure of tumor control in early CRC patients. Neutrophils can influence CD8⁺ T cell-mediated responses, however, results of different studies are controversial and debated^{169,186,196,198,249,250,264}. We reported that the direct crosstalk between neutrophils and CD8⁺ T cells leads to increased GZMK expression, which correlates with tumor relapse. Strikingly, the predominance of GZMK^{high} CD8⁺ T_{EM} cells in CRC patients that encountered

an early relapse suggested their detrimental role in favoring CRC progression. Indeed, GZMK^{high} CD8⁺ T_{EM} cell signature was effective in stratifying patients by overall survival (OS) in CRC and also lung carcinoma, supporting the hypothesis of GZMK^{high} CD8⁺ T_{EM} cells contributing to the establishment of a pro-tumoral TME. Further studies would be needed to address if CD8⁺ T cells recruited to the tumor and skewed toward a GZMK^{high} phenotype impacts neutrophil turnover and phenotype inside the tumor.

GZMK can be expressed by other cell types, including NK cells, plasma cells, mast cells, macrophages and fibroblasts, where its role has not been explored, yet. However, we have carefully evaluated the expression of GZMK by other identified T cell subpopulations by testing their association with the disease-free survival (DFS) in the external TCGA cohort, confirming that only the CD8_Tem-GZMK subpopulation is associated with a worse clinical outcome. These results imply that GZMK cannot be considered as an independent prognostic marker on CRC and that the increased risk of relapse is intimately linked to the presence of the CD8 Tem-GZMK subpopulation. It would be interesting to further investigate the regulation of GZMK expression in other cell types and its impact on tumor progression, eventually.

Nevertheless, it's worth to note that looking at the CD4 compartment, we found that conventional CD4⁺ T cells produce low amounts of GZMK without any significant correlation with neutrophils abundance. As opposed, we detected a negative correlation between Treg cells and CD15^{high} neutrophils, which deserves further investigation. In light of the recently identified immunosuppressive CD4⁺ GZMK⁺ EOMES⁺ Tr1-like subset¹²¹, it would be interesting to better profile the heterogeneity of the Treg compartment and address their role in relation to LN and HN status.

GZMK⁺ CD8⁺ T cell subpopulations have been recently identified and described as pre-dysfunctional^{44,45,60,223}. However, the here identified GZMK^{high} CD8⁺ T cell population harbored lower expression of co-inhibitory receptors, higher levels of activation markers and effector molecules like GZMB, compared to the GZMK⁻ counterpart, indicative of a functional and active phenotype. Moreover, their abundance in the TME was independent of tumor stage and aging, thus suggesting that these GZMK^{high} CD8⁺ T_{EM} cells are distinct from the one recently identified^{45,60}.

Tumor-specific CD8⁺ T cells could be distinguished from virus-specific CD8⁺ T cells based on the expression of specific surface protein, in particular CD39 and PD1^{75,223}, which have previously been associated with antitumor responses^{69,222}. It is worth it to emphasize that the GZMK^{high} CD8⁺ T_{EM} cell population enriched in HN lacked CD39 expression, suggesting that they are not specifically directed towards tumor associated antigens^{64,69} but rather towards irrelevant antigen⁷⁵. The enrichment of CD39⁻ virus-specific CD8⁺ T cells in the

TME is well described⁶⁷, however their contribution on cancer progression is yet to be underscored. Since they have been previously associated with inflammatory disease^{270,271}, the high proportion of GZMK^{high} CD39^{neg} CD8⁺ T_{EM} cells found in early CRC patients raises the possibility that they might mediate a cross-reactive response and favors cancer progression. Indeed, our transcriptomic analysis supports this model revealing that GZMK^{high} CD8⁺ T^{EM} cells harbor a peculiar alloreactive-like signature that might be controlled by *RORA*, *JUNB* and *HOPX*. In particular, *RORa*, which is down regulated specifically in the CD8 T_{EM} subset, has been previously associated with effector function and cytotoxicity rather than memory²⁷². On the other hand, the regulation of *JUNB* (which is a subunit of the AP-1 transcription complex together with *FOS*) and *HOPX* (which is a homeodomain-only cofactor involved in AP-1 function) go in opposite directions, in agreement with the role played by *HOPX* in inhibiting AP-1 expression both in nonlymphoid and, most importantly, immune cells. Indeed, work from Flavell's lab has demonstrated that *Hopx*-dependent downregulation of *Fos* and *Jun* expression upon rechallenge with an antigen under immunogenic conditions maintained Treg in a state of nonproliferation known as anergy²⁷³. In CD8⁺ T cells, this state of unresponsiveness can develop either in absence or following activation in the presence of co-stimulation, like on cells responding to a tumor. Anergy has been linked to mechanisms of suppression of acute T cell responses induced under strongly immunogenic conditions²⁷⁴ where it downregulates and prevents immunopathologic damage to the tissue in which it occurs²⁷⁵. Therefore, the antithetical regulation of *JUNB* and *HOPX* is consistent with a persistent acute activation in CD8⁺ T_{EM}, which may lead to tissue damage. Our study suggests that this might be due to the release of GZMK.

On the other hand, having found that the crosstalk between neutrophils and CD8⁺ T cells is fundamental for the skewing toward a GZMK^{high} cell population, it would be worth investigating if neutrophils directly mediate the “bystander” activation of CD8⁺ T cells.

The notion that GZMK is only a cytotoxic molecule have been challenged by evidence indicating that it might actually promote inflammation and tissue damage^{57,276}. This relates to its activity as extracellular protease and ability to promote epithelial-to-mesenchymal transition (EMT) by remodeling components of the extracellular matrix²⁷⁶. In line with this, compared to LN, HN CRC tumors showed reduced expression of E-Cadherin, which is a feature of EMT and tumor malignancy, establishing a potential link between infiltration of GZMK^{high} CD8⁺ T_{EM}, tumor progression and relapse. It is well established that cytotoxic CD8⁺ T cells are correlated with immunosurveillance and favorable prognosis. However, our study highlights the limitation of predicting clinical outcomes based on a CD8⁺ T cell's broad cytotoxic signature. Instead, different cytotoxic molecules might have diverse impacts

on tumor progression and combining signatures that match their specific expression with CD8⁺ T differentiation state could be instrumental to better stratify patients.

The association between neutrophil and CD8⁺ T cells identifies a unique immune signature in CRC patients, which might inform therapeutic decision making for standards as well as new immunotherapeutic strategies. Neoadjuvant checkpoint blockade therapy achieves deep or complete response in patients with mismatch-repair-deficient and mismatch-repair-proficient early colon cancer²⁴. These data open new opportunities for the treatment of inoperable CRC patients, as well as the potential to modify surgical practices toward less-radical resections. Our study supports the hypothesis that clinical outcome could tightly correlate with the crosstalk between innate and adaptive immune response at the tumor site. We posit that quantitative and qualitative analysis of the tumor immune infiltrates may serve as an effective approach to maximize ICB outcome, reduce the risk of toxicity in subjects that wouldn't benefit from the treatment and, overall, improve patient management while positively impacting the abatement cost for the health system. For instance, we speculate that in HN tumors, ICB-based therapies might potentially exacerbate the tumor promoting effect of GZMK^{high} CD8⁺ T cells in view of their alloreactive signature.

In conclusion, our data support the relevance of neutrophils in the regulation of CD8⁺ T cells infiltrating CRC tumors and improve CRC stratification based on which we could anticipate prognosis and/or response to ICB treatment.

This study demonstrates that functional information resulting from the crosstalk of CD8⁺ T cells with different components of the immune contexture and the stroma might implement the prognostic value of current biomarkers, which are mostly based on limited phenotypic or transcriptional CD8⁺ T cell characteristics and a possible prediction of response to the therapy.

Conclusions

Tumor infiltrating CD8⁺ T cells have emerged as a major determinant to establish prognosis in several solid tumors, including colorectal cancer (CRC). However, tumor contexture is highly heterogeneous and understanding how the interplay between different immune cell compartments impacts on the clinical outcome is still in its infancy. Here, we combined multiparametric flow cytometry (MPFC), multiplex enzyme-linked immunosorbent assay (ELISA), single cell RNA sequencing (scRNAseq) and confocal microscopy imaging to dissect the immune heterogeneity within the tumor microenvironment (TME). In a prospective cohort of early-stage non metastatic CRC patients, we describe a novel CD8⁺ T effector memory population, which is characterized by high levels of Granzyme K (GZMK^{high} CD8⁺ T_{EM}) and correlated with CD15^{high} tumor infiltrating neutrophils.

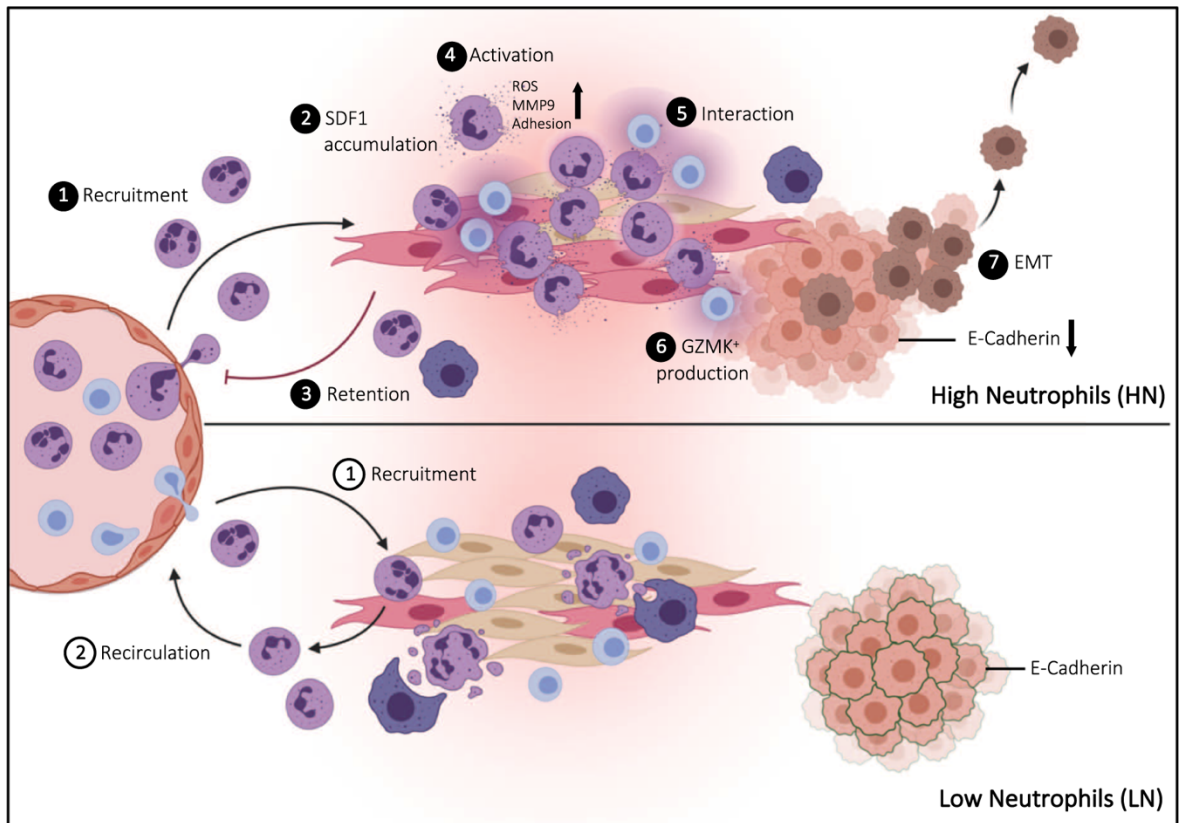
We provide both in vitro and in vivo evidence of the role of stromal cell-derived factor 1 (CXCL12/SDF-1) in driving functional changes on neutrophils at the tumor site shaping them toward an N2-like pro-tumoral phenotype, promoting their retention and increasing crosstalk with CD8⁺ T cells.

As a consequence of the interaction with neutrophils, CD8⁺ T cells are skewed towards a CD8⁺ T_{EM} phenotype, producing high levels of GZMK, which in turn contributes to remodeling the tumor microenvironment.

The following decrease in E-Cadherin expression is a well-known trait of malignancy, supported by the correlation of GZMK^{high} CD8⁺ T_{EM} and neutrophils with both tumor progression in a mouse model of colon carcinoma and early relapse in CRC patients.

Additionally, we generated by scRNAseq profiling a gene signature for GZMK^{high} CD8⁺ T_{EM} which was associated with worse prognosis on the Cancer Genome Atlas Colon Adenocarcinoma (TCGA-COAD) dataset, confirming effective stratification on an independent cohort of CRC patients and correlating GZMK^{high} CD8⁺ T cell signature to poor clinical outcome.

Overall, our results describe a new GZMK^{high} CD8⁺ T_{EM} population in early-stage CRC tumors as a hallmark of worst clinical outcome, driven by the interaction with neutrophils, which could implement current patient stratification and be targeted by novel therapeutics.



Graphical model.

The frequency of CD15^{high} neutrophils in the tumor identifies High (HN) and Low (LN) neutrophil subgroups of non-metastatic resectable CRC patients (1). Elevated SDF-1 levels in HN tumors remodel the functional state of infiltrating neutrophils in an N2-like pro-tumoral phenotype (2), promoting their retention (3) and activation (4) at the tumor site. The contact-mediated interaction with CD15^{high} neutrophils (5) skewed effector memory CD8⁺ T cells (T^{EM}) to produce high levels of Granzyme K (GZMK) (6), which in turn remodels the tumor microenvironment (TME) by decreasing E-Cadherin expression in the tissue and fostering epithelial to mesenchymal transition (EMT) (7). Created with BioRender.com.

Adapted from Tiberti et al.

Bibliography

1. Colorectal Cancer Screening Test Use* (%), Adults 50 Years and Older by State, 2018.
2. Keum, N. N. & Giovannucci, E. Global burden of colorectal cancer: emerging trends, risk factors and prevention strategies. *Nature Reviews Gastroenterology & Hepatology* 2019 16:12 **16**, 713–732 (2019).
3. Xi, Y. & Xu, P. Global colorectal cancer burden in 2020 and projections to 2040. *Transl Oncol* **14**, 101174 (2021).
4. Kinzler, K. W. *et al.* Identification of FAP Locus Genes from Chromosome 5q21. *Science* (1979) **253**, 661–665 (1991).
5. Groden, J. *et al.* Identification and characterization of the familial adenomatous polyposis coli gene. *Cell* **66**, 589–600 (1991).
6. Muzny, D. M. *et al.* Comprehensive molecular characterization of human colon and rectal cancer. *Nature* 2012 487:7407 **487**, 330–337 (2012).
7. Fearon, E. R. Molecular Genetics of Colorectal Cancer. <https://doi.org/10.1146/annurev-pathol-011110-130235> **6**, 479–507 (2011).
8. Colorectal Cancer Stages | Rectal Cancer Staging | Colon Cancer Staging. <https://www.cancer.org/cancer/colon-rectal-cancer/detection-diagnosis-staging/staged.html>.
9. Nelson, H. *et al.* Guidelines 2000 for Colon and Rectal Cancer Surgery. *JNCI: Journal of the National Cancer Institute* **93**, 583–596 (2001).
10. Guinney, J. *et al.* The consensus molecular subtypes of colorectal cancer. *Nature Medicine* 2015 21:11 **21**, 1350–1356 (2015).
11. Boland, C. R. & Goel, A. Microsatellite Instability in Colorectal Cancer. *Gastroenterology* **138**, 2073 (2010).
12. Gryfe, R. *et al.* Tumor microsatellite instability and clinical outcome in young patients with colorectal cancer. *N Engl J Med* **342**, 69–77 (2000).
13. Mlecnik, B. *et al.* Integrative Analyses of Colorectal Cancer Show Immunoscore Is a Stronger Predictor of Patient Survival Than Microsatellite Instability. *Immunity* **44**, 698–711 (2016).
14. Pagès, F. *et al.* In situ cytotoxic and memory T cells predict outcome in patients with early-stage colorectal cancer. *J Clin Oncol* **27**, 5944–5951 (2009).
15. Galon, J. *et al.* Towards the introduction of the ‘Immunoscore’ in the classification of malignant tumours. *J Pathol* **232**, 199 (2014).

16. Mlecnik, B., Bindea, G., Pagès, F. & Galon, J. Tumor immunosurveillance in human cancers. *Cancer and Metastasis Reviews* **30**, 5–12 (2011).
17. Mlecnik, B. *et al.* Histopathologic-based prognostic factors of colorectal cancers are associated with the state of the local immune reaction. *J Clin Oncol* **29**, 610–618 (2011).
18. Fridman, W. H., Pagès, F., Sauts-Fridman, C. & Galon, J. The immune contexture in human tumours: impact on clinical outcome. *Nat Rev Cancer* **12**, 298–306 (2012).
19. Broussard, E. K. & Disis, M. L. TNM staging in colorectal cancer: T is for T cell and M is for memory. *J Clin Oncol* **29**, 601–603 (2011).
20. Atreya, R. & Neurath, M. F. New therapeutic strategies for treatment of inflammatory bowel disease. *Mucosal Immunology 2008 1:3* **1**, 175–182 (2008).
21. Bindea, G. *et al.* Spatiotemporal dynamics of intratumoral immune cells reveal the immune landscape in human cancer. *Immunity* **39**, 782–795 (2013).
22. Pagès, F. *et al.* Effector Memory T Cells, Early Metastasis, and Survival in Colorectal Cancer. *New England Journal of Medicine* **353**, 2654–2666 (2005).
23. Mlecnik, B., Bindea, G., Angell, H. K., Valge-Archer, V. & Latouche, J.-B. Integrative Analyses of Colorectal Cancer Show Immunoscore Is a Stronger Predictor of Patient Survival Than Microsatellite Instability. *Immunity* **44**, 698–711 (2016).
24. Chalabi, M. *et al.* Neoadjuvant immunotherapy leads to pathological responses in MMR-proficient and MMR-deficient early-stage colon cancers. *Nature Medicine 2020 26:4* **26**, 566–576 (2020).
25. Edwards, S. C., Hoevenaar, W. H. M. & Coffelt, S. B. Emerging immunotherapies for metastasis. *British Journal of Cancer 2020 124:1* **124**, 37–48 (2020).
26. Nosho, K. *et al.* Tumour-infiltrating T-cell subsets, molecular changes in colorectal cancer, and prognosis: cohort study and literature review. *J Pathol* **222**, 350–366 (2010).
27. Ogino, S. *et al.* Lymphocytic reaction to colorectal cancer is associated with longer survival, independent of lymph node count, microsatellite instability, and CpG island methylator phenotype. *Clin Cancer Res* **15**, 6412–6420 (2009).
28. Frey, D. M. *et al.* High frequency of tumor-infiltrating FOXP3(+) regulatory T cells predicts improved survival in mismatch repair-proficient colorectal cancer patients. *Int J Cancer* **126**, 2635–2643 (2010).
29. Galon, J., Angell, H. K., Bedognetti, D. & Marincola, F. M. The Continuum of Cancer Immunoreveillance: Prognostic, Predictive, and Mechanistic Signatures. *Immunity* **39**, 11–26 (2013).

30. Angell, H. & Galon, J. From the immune contexture to the Immunoscore: the role of prognostic and predictive immune markers in cancer. *Curr Opin Immunol* **25**, 261–267 (2013).
31. Pagès, F. *et al.* International validation of the consensus Immunoscore for the classification of colon cancer: a prognostic and accuracy study. *The Lancet* **391**, 2128–2139 (2018).
32. Galon, J. *et al.* Type, density, and location of immune cells within human colorectal tumors predict clinical outcome. *Science (1979)* **313**, 1960–1964 (2006).
33. Suzuki, T. *et al.* Mutant KRAS drives metabolic reprogramming and autophagic flux in premalignant pancreatic cells. *Cancer Gene Therapy* *2021 29:5* **29**, 505–518 (2021).
34. Toda, K. *et al.* Metabolic Alterations Caused by KRAS Mutations in Colorectal Cancer Contribute to Cell Adaptation to Glutamine Depletion by Upregulation of Asparagine Synthetase. *Neoplasia* **18**, 654–665 (2016).
35. Liu, Y. H., Hu, C. M., Hsu, Y. S. & Lee, W. H. Interplays of glucose metabolism and KRAS mutation in pancreatic ductal adenocarcinoma. *Cell Death & Disease* *2022 13:9* **13**, 1–10 (2022).
36. Sadanandam, A. *et al.* A colorectal cancer classification system that associates cellular phenotype and responses to therapy. *Nature Medicine* *2013 19:5* **19**, 619–625 (2013).
37. Fessler, E. & Medema, J. P. Colorectal Cancer Subtypes: Developmental Origin and Microenvironmental Regulation. *Trends Cancer* **2**, 505–518 (2016).
38. Zheng, G. X. Y. *et al.* Massively parallel digital transcriptional profiling of single cells. *Nature Communications* *2017 8:1* **8**, 1–12 (2017).
39. Tirosh, I. *et al.* Dissecting the multicellular ecosystem of metastatic melanoma by single-cell RNA-seq. *Science (1979)* **352**, 189–196 (2016).
40. Savas, P. *et al.* Single-cell profiling of breast cancer T cells reveals a tissue-resident memory subset associated with improved prognosis. *Nature Medicine* *2018 24:7* **24**, 986–993 (2018).
41. Sade-Feldman, M. *et al.* Defining T Cell States Associated with Response to Checkpoint Immunotherapy in Melanoma. *Cell* **175**, 998-1013.e20 (2018).
42. Lavin, Y. *et al.* Innate Immune Landscape in Early Lung Adenocarcinoma by Paired Single-Cell Analyses. *Cell* **169**, 750-765.e17 (2017).
43. Azizi, E. *et al.* Single-Cell Map of Diverse Immune Phenotypes in the Breast Tumor Microenvironment. *Cell* **174**, 1293-1308.e36 (2018).

44. Guo, X. *et al.* Global characterization of T cells in non-small-cell lung cancer by single-cell sequencing. *Nature Medicine* 2018 24:7 **24**, 978–985 (2018).
45. Zhang, L. *et al.* Lineage tracking reveals dynamic relationships of T cells in colorectal cancer. *Nature* 2018 564:7735 **564**, 268–272 (2018).
46. Binnewies, M. *et al.* Understanding the tumor immune microenvironment (TIME) for effective therapy. *Nature Medicine* 2018 24:5 **24**, 541–550 (2018).
47. Peranzoni, E. *et al.* Macrophages impede CD8 T cells from reaching tumor cells and limit the efficacy of anti-PD-1 treatment. *Proc Natl Acad Sci U S A* **115**, E4041–E4050 (2018).
48. Tumeh, P. C. *et al.* PD-1 blockade induces responses by inhibiting adaptive immune resistance. *Nature* 2014 515:7528 **515**, 568–571 (2014).
49. Ling, A., Edin, S., Wikberg, M. L., Öberg, Å. & Palmqvist, R. The intratumoural subsite and relation of CD8+ and FOXP3+ T lymphocytes in colorectal cancer provide important prognostic clues. *British Journal of Cancer* 2014 110:10 **110**, 2551–2559 (2014).
50. Glaire, M. A. *et al.* Tumour-infiltrating CD8+ lymphocytes and colorectal cancer recurrence by tumour and nodal stage. *British Journal of Cancer* 2019 121:6 **121**, 474–482 (2019).
51. Waldman, A. D., Fritz, J. M. & Lenardo, M. J. A guide to cancer immunotherapy: from T cell basic science to clinical practice. *Nature Reviews Immunology* 2020 20:11 **20**, 651–668 (2020).
52. Jamal-Hanjani, M. *et al.* Tracking Genomic Cancer Evolution for Precision Medicine: The Lung TRACERx Study. *PLoS Biol* **12**, e1001906 (2014).
53. Ganesan, A. P. *et al.* Tissue-resident memory features are linked to the magnitude of cytotoxic T cell responses in human lung cancer. *Nature Immunology* 2017 18:8 **18**, 940–950 (2017).
54. Hamanishi, J. *et al.* Programmed cell death 1 ligand 1 and tumor-infiltrating CD8+ T lymphocytes are prognostic factors of human ovarian cancer. *Proc Natl Acad Sci U S A* **104**, 3360–3365 (2007).
55. Chowdhury, D. & Lieberman, J. Death by a Thousand Cuts: Granzyme Pathways of Programmed Cell Death. <https://doi.org/10.1146/annurev.immunol.26.021607.090404> **26**, 389–420 (2008).
56. Anthony, D. A., Andrews, D. M., Watt, S. v., Trapani, J. A. & Smyth, M. J. Functional dissection of the granzyme family: cell death and inflammation. *Immunol Rev* **235**, 73–92 (2010).
57. Joeckel, L. T. & Bird, P. I. Are all granzymes cytotoxic in vivo? *Biol Chem* **395**, 181–202 (2014).

58. Santiago, L. *et al.* Extracellular Granzyme A Promotes Colorectal Cancer Development by Enhancing Gut Inflammation. *Cell Rep* **32**, 107847 (2020).
59. Turner, C. T. *et al.* Granzyme K Expressed by Classically Activated Macrophages Contributes to Inflammation and Impaired Remodeling. *Journal of Investigative Dermatology* **139**, 930–939 (2019).
60. Mogilenko, D. A. *et al.* Comprehensive Profiling of an Aging Immune System Reveals Clonal GZMK⁺ CD8⁺ T Cells as Conserved Hallmark of Inflammaging. *Immunity* **54**, 99–115.e12 (2021).
61. Yan, M. *et al.* Dynamic regulatory networks of T cell trajectory dissect transcriptional control of T cell state transition. *Mol Ther Nucleic Acids* **26**, 1115–1129 (2021).
62. Galletti, G. *et al.* Two subsets of stem-like CD8⁺ memory T cell progenitors with distinct fate commitments in humans. *Nature Immunology* 2020 21:12 **21**, 1552–1562 (2020).
63. Zheng, C. *et al.* Landscape of Infiltrating T Cells in Liver Cancer Revealed by Single-Cell Sequencing. *Cell* **169**, 1342–1356.e16 (2017).
64. Scheper, W. *et al.* Low and variable tumor reactivity of the intratumoral TCR repertoire in human cancers. *Nature Medicine* 2018 25:1 **25**, 89–94 (2018).
65. Yost, K. E. *et al.* Clonal replacement of tumor-specific T cells following PD-1 blockade. *Nature Medicine* 2019 25:8 **25**, 1251–1259 (2019).
66. Li, H. *et al.* Dysfunctional CD8 T Cells Form a Proliferative, Dynamically Regulated Compartment within Human Melanoma. *Cell* **176**, 775–789.e18 (2019).
67. Duhén, T. *et al.* Co-expression of CD39 and CD103 identifies tumor-reactive CD8 T cells in human solid tumors. *Nature Communications* 2018 9:1 **9**, 1–13 (2018).
68. Gokuldass, A. *et al.* Qualitative Analysis of Tumor-Infiltrating Lymphocytes across Human Tumor Types Reveals a Higher Proportion of Bystander CD8⁺ T Cells in Non-Melanoma Cancers Compared to Melanoma. *Cancers* 2020, Vol. 12, Page 3344 **12**, 3344 (2020).
69. Simoni, Y. *et al.* Bystander CD8⁺ T cells are abundant and phenotypically distinct in human tumour infiltrates. *Nature* 2018 557:7706 **557**, 575–579 (2018).
70. Kvistborg, P. *et al.* TIL therapy broadens the tumor-reactive CD8⁺ T cell compartment in melanoma patients. *Oncoimmunology* **1**, 409 (2012).
71. Maurice, N. J., McElrath, M. J., Andersen-Nissen, E., Frahm, N. & Prlic, M. CXCR3 enables recruitment and site-specific bystander activation of memory CD8⁺ T cells. *Nat Commun* **10**, (2019).

72. Attrill, G. H. *et al.* Higher proportions of CD39⁺ tumor-resident cytotoxic T cells predict recurrence-free survival in patients with stage III melanoma treated with adjuvant immunotherapy. *J Immunother Cancer* **10**, (2022).
73. Meier, S. L., Satpathy, A. T. & Wells, D. K. Bystander T cells in cancer immunology and therapy. *Nature Cancer* **2022 3:2 3**, 143–155 (2022).
74. Rosato, P. C. *et al.* Virus-specific memory T cells populate tumors and can be repurposed for tumor immunotherapy. *Nature Communications* **2019 10:1 10**, 1–9 (2019).
75. Oliveira, G. *et al.* Phenotype, specificity and avidity of antitumour CD8⁺ T cells in melanoma. *Nature* **2021 596:7870 596**, 119–125 (2021).
76. X, G. *et al.* Global characterization of T cells in non-small-cell lung cancer by single-cell sequencing. *Nat Med* **24**, 978–985 (2018).
77. Hashimoto, M. *et al.* CD8 T Cell Exhaustion in Chronic Infection and Cancer: Opportunities for Interventions. *Annu Rev Med* **69**, 301–318 (2018).
78. Pauken, K. E. & Wherry, E. J. Overcoming T cell exhaustion in infection and cancer. *Trends Immunol* **36**, 265–276 (2015).
79. Wherry, E. J. & Kurachi, M. Molecular and cellular insights into T cell exhaustion. *Nat Rev Immunol* **15**, 486–499 (2015).
80. Thommen, D. S. *et al.* A transcriptionally and functionally distinct PD-1⁺ CD8⁺ T cell pool with predictive potential in non-small-cell lung cancer treated with PD-1 blockade. *Nat Med* **24**, 994–1004 (2018).
81. van der Leun, A. M., Thommen, D. S. & Schumacher, T. N. CD8⁺ T cell states in human cancer: insights from single-cell analysis. *Nature Reviews Cancer* **2020 20:4 20**, 218–232 (2020).
82. Blackburn, S. D., Shin, H., Freeman, G. J. & Wherry, E. J. Selective expansion of a subset of exhausted CD8 T cells by alphaPD-L1 blockade. *Proc Natl Acad Sci U S A* **105**, 15016–15021 (2008).
83. Pauken, K. E. *et al.* Epigenetic stability of exhausted T cells limits durability of reinvigoration by PD-1 blockade. *Science* **354**, 1160–1165 (2016).
84. Philip, M. *et al.* Chromatin states define tumour-specific T cell dysfunction and reprogramming. *Nature* **545**, 452–456 (2017).
85. Im, S. J. *et al.* Defining CD8⁺ T cells that provide the proliferative burst after PD-1 therapy. *Nature* **537**, 417–421 (2016).
86. Schietinger, A. *et al.* Tumor-Specific T Cell Dysfunction Is a Dynamic Antigen-Driven Differentiation Program Initiated Early during Tumorigenesis. *Immunity* **45**, 389 (2016).

87. Wherry, E. J., Blattman, J. N., Murali-Krishna, K., van der Most, R. & Ahmed, R. Viral Persistence Alters CD8 T-Cell Immunodominance and Tissue Distribution and Results in Distinct Stages of Functional Impairment. *J Virol* **77**, 4911–4927 (2003).
88. Dhatchinamoorthy, K., Colbert, J. D. & Rock, K. L. Cancer Immune Evasion Through Loss of MHC Class I Antigen Presentation. *Front Immunol* **12**, 469 (2021).
89. O'Donnell, J. S., Teng, M. W. L. & Smyth, M. J. Cancer immunoediting and resistance to T cell-based immunotherapy. *Nature Reviews Clinical Oncology* **2018 16:3** **16**, 151–167 (2018).
90. Cercek, A. *et al.* PD-1 Blockade in Mismatch Repair–Deficient, Locally Advanced Rectal Cancer. *New England Journal of Medicine* **386**, 2363–2376 (2022).
91. Le, D. T. *et al.* PD-1 Blockade in Tumors with Mismatch-Repair Deficiency. *New England Journal of Medicine* **372**, 2509–2520 (2015).
92. Miller, B. C. *et al.* Subsets of exhausted CD8⁺ T cells differentially mediate tumor control and respond to checkpoint blockade. *Nature Immunology* **2019 20:3** **20**, 326–336 (2019).
93. Manzo, T. *et al.* Accumulation of long-chain fatty acids in the tumor microenvironment drives dysfunction in intrapancreatic cd8⁺ t cells. *Journal of Experimental Medicine* **217**, (2020).
94. Scharping, N. E. *et al.* The Tumor Microenvironment Represses T Cell Mitochondrial Biogenesis to Drive Intratumoral T Cell Metabolic Insufficiency and Dysfunction. *Immunity* **45**, 374–388 (2016).
95. Yu, Y. R. *et al.* Disturbed mitochondrial dynamics in CD8⁺ TILs reinforce T cell exhaustion. *Nature Immunology* **2020 21:12** **21**, 1540–1551 (2020).
96. Platten, M., Wick, W. & van den Eynde, B. J. Tryptophan catabolism in cancer: beyond IDO and tryptophan depletion. *Cancer Res* **72**, 5435–5440 (2012).
97. Ma, E. H. *et al.* Metabolic Profiling Using Stable Isotope Tracing Reveals Distinct Patterns of Glucose Utilization by Physiologically Activated CD8⁺ T Cells. *Immunity* **51**, 856-870.e5 (2019).
98. Ho, P. C. *et al.* Phosphoenolpyruvate Is a Metabolic Checkpoint of Anti-tumor T Cell Responses. *Cell* **162**, 1217–1228 (2015).
99. Brand, A. *et al.* LDHA-Associated Lactic Acid Production Blunts Tumor Immunosurveillance by T and NK Cells. *Cell Metab* **24**, 657–671 (2016).
100. Zhang, Y. *et al.* Enhancing CD8⁺ T Cell Fatty Acid Catabolism within a Metabolically Challenging Tumor Microenvironment Increases the Efficacy of Melanoma Immunotherapy. *Cancer Cell* **32**, 377-391.e9 (2017).

101. Chang, C. H. *et al.* Metabolic Competition in the Tumor Microenvironment Is a Driver of Cancer Progression. *Cell* **162**, 1229–1241 (2015).
102. Al-Khami, A. A. *et al.* Exogenous lipid uptake induces metabolic and functional reprogramming of tumor-associated myeloid-derived suppressor cells. *Oncoimmunology* **6**, (2017).
103. Sasidharan Nair, V., Saleh, R., Toor, S. M., Cyprian, F. S. & Elkord, E. Metabolic reprogramming of T regulatory cells in the hypoxic tumor microenvironment. *Cancer Immunology, Immunotherapy* **2021 70:8 70**, 2103–2121 (2021).
104. Wang, H., Franco, F. & Ho, P. C. Metabolic Regulation of Tregs in Cancer: Opportunities for Immunotherapy. *Trends Cancer* **3**, 583–592 (2017).
105. Veglia, F., Sanseviero, E. & Gabrilovich, D. I. Myeloid-derived suppressor cells in the era of increasing myeloid cell diversity. *Nature Reviews Immunology* **2021 21:8 21**, 485–498 (2021).
106. Tay, R. E., Richardson, E. K. & Toh, H. C. Revisiting the role of CD4⁺ T cells in cancer immunotherapy—new insights into old paradigms. *Cancer Gene Therapy* **2020 28:1 28**, 5–17 (2020).
107. Bommireddy, R. & Doetschman, T. TGFβ1 and Treg cells: alliance for tolerance. *Trends Mol Med* **13**, 492–501 (2007).
108. Schlecker, E. *et al.* Tumor-infiltrating monocytic myeloid-derived suppressor cells mediate CCR5-dependent recruitment of regulatory T cells favoring tumor growth. *J Immunol* **189**, 5602–5611 (2012).
109. Chinen, T. *et al.* An essential role for the IL2 receptor in Treg cell function. *Nature Immunology* **2016 17:11 17**, 1322–1333 (2016).
110. Thornton, A. M. & Shevach, E. M. CD4⁺CD25⁺ Immunoregulatory T Cells Suppress Polyclonal T Cell Activation In Vitro by Inhibiting Interleukin 2 Production. *Journal of Experimental Medicine* **188**, 287–296 (1998).
111. Turnis, M. E. *et al.* Interleukin-35 Limits Anti-Tumor Immunity. *Immunity* **44**, 316–329 (2016).
112. Gunderson, A. J. *et al.* TGFβ suppresses CD8⁺ T cell expression of CXCR3 and tumor trafficking. *Nature Communications* **2020 11:1 11**, 1–13 (2020).
113. Chen, M. L. *et al.* Regulatory T cells suppress tumor-specific CD8 T cell cytotoxicity through TGF-β signals in vivo. *Proc Natl Acad Sci U S A* **102**, 419–424 (2005).
114. Togashi, Y., Shitara, K. & Nishikawa, H. Regulatory T cells in cancer immunosuppression — implications for anticancer therapy. *Nature Reviews Clinical Oncology* **2019 16:6 16**, 356–371 (2019).

115. Saleh, R. & Elkord, E. FoxP3+ T regulatory cells in cancer: Prognostic biomarkers and therapeutic targets. *Cancer Lett* **490**, 174–185 (2020).
116. Shang, B., Liu, Y., Jiang, S. J. & Liu, Y. Prognostic value of tumor-infiltrating FoxP3+ regulatory T cells in cancers: a systematic review and meta-analysis. *Scientific Reports* **2015 5:1 5**, 1–9 (2015).
117. Bergsland, C. H. *et al.* Spatial analysis and CD25-expression identify regulatory T cells as predictors of a poor prognosis in colorectal cancer. *Modern Pathology* **2022 35:9 35**, 1236–1246 (2022).
118. Saito, T. *et al.* Two FOXP3+CD4+ T cell subpopulations distinctly control the prognosis of colorectal cancers. *Nature Medicine* **2016 22:6 22**, 679–684 (2016).
119. Sinicrope, F. A. *et al.* Intraepithelial Effector (CD3+)/Regulatory (FoxP3+) T-Cell Ratio Predicts a Clinical Outcome of Human Colon Carcinoma. *Gastroenterology* **137**, 1270–1279 (2009).
120. Salama, P. *et al.* Tumor-infiltrating FOXP3+ T regulatory cells show strong prognostic significance in colorectal cancer. *Journal of Clinical Oncology* **27**, 186–192 (2009).
121. Bonnal, R. J. P. *et al.* Clonally expanded EOMES+ Tr1-like cells in primary and metastatic tumors are associated with disease progression. *Nature Immunology* **2021 22:6 22**, 735–745 (2021).
122. Laumont, C. M., Banville, A. C., Gilardi, M., Hollern, D. P. & Nelson, B. H. Tumour-infiltrating B cells: immunological mechanisms, clinical impact and therapeutic opportunities. *Nature Reviews Cancer* **2022 22:7 22**, 414–430 (2022).
123. Patel, A. J., Richter, A., Drayson, M. T. & Middleton, G. W. The role of B lymphocytes in the immuno-biology of non-small-cell lung cancer. *Cancer Immunology, Immunotherapy* **69**, 325–342 (2020).
124. Cabrita, R. *et al.* Tertiary lymphoid structures improve immunotherapy and survival in melanoma. *Nature* **2020 577:7791 577**, 561–565 (2020).
125. Helmink, B. A. *et al.* B cells and tertiary lymphoid structures promote immunotherapy response. *Nature* **2020 577:7791 577**, 549–555 (2020).
126. Castino, G. F. *et al.* Spatial distribution of B cells predicts prognosis in human pancreatic adenocarcinoma. *Oncoimmunology* **5**, (2016).
127. Petitprez, F. *et al.* B cells are associated with survival and immunotherapy response in sarcoma. *Nature* **2020 577:7791 577**, 556–560 (2020).
128. Edin, S. *et al.* The Prognostic Importance of CD20+ B lymphocytes in Colorectal Cancer and the Relation to Other Immune Cell subsets. *Scientific Reports* **2019 9:1 9**, 1–9 (2019).

129. Cui, C. *et al.* Neoantigen-driven B cell and CD4 T follicular helper cell collaboration promotes anti-tumor CD8 T cell responses. *Cell* **184**, 6101-6118.e13 (2021).
130. Sautès-Fridman, C., Petitprez, F., Calderaro, J. & Fridman, W. H. Tertiary lymphoid structures in the era of cancer immunotherapy. *Nature Reviews Cancer* **19**:6 **19**, 307–325 (2019).
131. Rodriguez, A. B. *et al.* Immune mechanisms orchestrate tertiary lymphoid structures in tumors via cancer-associated fibroblasts. *Cell Rep* **36**, 109422 (2021).
132. Fridman, W. H. *et al.* B cells and tertiary lymphoid structures as determinants of tumour immune contexture and clinical outcome. *Nature Reviews Clinical Oncology* **2022 19:7 19**, 441–457 (2022).
133. Zhu, W. *et al.* A high density of tertiary lymphoid structure B cells in lung tumors is associated with increased CD4+ T cell receptor repertoire clonality. *Oncoimmunology* **4**, (2015).
134. di Caro, G. *et al.* Occurrence of tertiary lymphoid tissue is associated with T-cell infiltration and predicts better prognosis in early-stage colorectal cancers. *Clinical Cancer Research* **20**, 2147–2158 (2014).
135. Raskov, H., Orhan, A., Christensen, J. P. & Gögenur, I. Cytotoxic CD8+ T cells in cancer and cancer immunotherapy. *British Journal of Cancer* **2020 124:2 124**, 359–367 (2020).
136. Broz, M. L. *et al.* Dissecting the Tumor Myeloid Compartment Reveals Rare Activating Antigen-Presenting Cells Critical for T Cell Immunity. *Cancer Cell* **26**, 638–652 (2014).
137. Fu, C. & Jiang, A. Dendritic Cells and CD8 T Cell Immunity in Tumor Microenvironment. *Front Immunol* **9**, 3059 (2018).
138. Gerhard, G. M., Bill, R., Messemaker, M., Klein, A. M. & Pittet, M. J. Tumor-infiltrating dendritic cell states are conserved across solid human cancers. *Journal of Experimental Medicine* **218**, (2021).
139. Pahne-Zeppenfeld, J. *et al.* Cervical cancer cell-derived interleukin-6 impairs CCR7-dependent migration of MMP-9-expressing dendritic cells. *Int J Cancer* **134**, 2061–2073 (2014).
140. Alshamsan, A. Induction of tolerogenic dendritic cells by IL6-secreting CT26 colon carcinoma. <http://dx.doi.org/10.3109/08923973.2011.625034> **34**, 465–469 (2012).
141. Qiao, J. *et al.* Targeting Tumors with IL10 Prevents Dendritic Cell-Mediated CD8+ T Cell Apoptosis. *Cancer Cell* **35**, 901-915.e4 (2019).

142. Tumor-induced interleukin 10 suppresses the ability of splenic dendritic cells to stimulate CD4 and CD8 T-cell responses - PubMed.
<https://pubmed.ncbi.nlm.nih.gov/12727833/>.
143. Peng, Q. *et al.* PD-L1 on dendritic cells attenuates T cell activation and regulates response to immune checkpoint blockade. *Nature Communications* 2020 11:1 **11**, 1–8 (2020).
144. Wang, Y. *et al.* Dendritic cell biology and its role in tumor immunotherapy. *J Hematol Oncol* **13**, 1–18 (2020).
145. Wykes, M. N. & Lewin, S. R. Immune checkpoint blockade in infectious diseases. *Nature Reviews Immunology* 2017 18:2 **18**, 91–104 (2017).
146. Mills, C. D., Lenz, L. L. & Harris, R. A. A Breakthrough: Macrophage-Directed Cancer Immunotherapy. *Cancer Res* **76**, 513–516 (2016).
147. Anderson, N. R., Minutolo, N. G., Gill, S. & Klichinsky, M. Macrophage-Based Approaches for Cancer Immunotherapy. *Cancer Res* **81**, 1201–1208 (2021).
148. Duan, Z. & Luo, Y. Targeting macrophages in cancer immunotherapy. *Signal Transduction and Targeted Therapy* 2021 6:1 **6**, 1–21 (2021).
149. Yuan, R. *et al.* Reversing the polarization of tumor-associated macrophages inhibits tumor metastasis. *Int Immunopharmacol* **49**, 30–37 (2017).
150. Ma, J. *et al.* The M1 form of tumor-associated macrophages in non-small cell lung cancer is positively associated with survival time. *BMC Cancer* **10**, 1–9 (2010).
151. Guilliams, M., Mildner, A. & Yona, S. Developmental and Functional Heterogeneity of Monocytes. *Immunity* **49**, 595–613 (2018).
152. López-Janeiro, Á., Padilla-Ansala, C., de Andrea, C. E., Hardisson, D. & Melero, I. Prognostic value of macrophage polarization markers in epithelial neoplasms and melanoma. A systematic review and meta-analysis. *Mod Pathol* **33**, 1458–1465 (2020).
153. Allison, E., Edirimanne, S., Matthews, J. & Fuller, S. J. Breast Cancer Survival Outcomes and Tumor-Associated Macrophage Markers: A Systematic Review and Meta-Analysis. *Oncol Ther* (2022) doi:10.1007/S40487-022-00214-3.
154. Guo, Z. *et al.* M2 macrophages promote NSCLC metastasis by upregulating CRYAB. *Cell Death & Disease* 2019 10:6 **10**, 1–11 (2019).
155. Sumitomo, R. *et al.* M2 tumor-associated macrophages promote tumor progression in non-small-cell lung cancer. *Exp Ther Med* **18**, (2019).
156. Li, W. *et al.* Gastric cancer-derived mesenchymal stromal cells trigger M2 macrophage polarization that promotes metastasis and EMT in gastric cancer. *Cell Death & Disease* 2019 10:12 **10**, 1–16 (2019).

157. Martinek, J. *et al.* Transcriptional profiling of macrophages in situ in metastatic melanoma reveals localization-dependent phenotypes and function. *Cell Rep Med* **3**, (2022).
158. Edin, S. *et al.* The distribution of macrophages with a M1 or M2 phenotype in relation to prognosis and the molecular characteristics of colorectal cancer. *PLoS One* **7**, (2012).
159. Tsukamoto, M. *et al.* PD-L1 expression enhancement by infiltrating macrophage-derived tumor necrosis factor- α leads to poor pancreatic cancer prognosis. *Cancer Sci* **110**, 310–320 (2019).
160. Kuo, I. Y. *et al.* Converged Rab37/IL6 trafficking and STAT3/PD-1 transcription axes elicit an immunosuppressive lung tumor microenvironment. *Theranostics* **11**, 7029–7044 (2021).
161. Harbaum, L. *et al.* Peritumoral eosinophils predict recurrence in colorectal cancer. *Modern Pathology* 2015 28:3 **28**, 403–413 (2014).
162. Prizment, A. E. *et al.* Tumor eosinophil infiltration and improved survival of colorectal cancer patients: Iowa Women’s Health Study. *Modern Pathology* 2016 29:5 **29**, 516–527 (2016).
163. Carretero, R. *et al.* Eosinophils orchestrate cancer rejection by normalizing tumor vessels and enhancing infiltration of CD8⁺ T cells. *Nature Immunology* 2015 16:6 **16**, 609–617 (2015).
164. Villanueva, M. T. Eosinophils — T cells’ little helpers. *Nature Reviews Cancer* 2015 15:6 **15**, 320–320 (2015).
165. Cheng, J. N. *et al.* Radiation-induced eosinophils improve cytotoxic T lymphocyte recruitment and response to immunotherapy. *Sci Adv* **7**, 7609–7638 (2021).
166. Lingblom, C., Andersson, J., Andersson, K. & Wennerås, C. Regulatory Eosinophils Suppress T Cells Partly through Galectin-10. *The Journal of Immunology* **198**, 4672–4681 (2017).
167. Mackey, J. B. G., Coffelt, S. B. & Carlin, L. M. Neutrophil maturity in cancer. *Front Immunol* **10**, 1912 (2019).
168. Pillay, J., Tak, T., Kamp, V. M. & Koenderman, L. Immune suppression by neutrophils and granulocytic myeloid-derived suppressor cells: Similarities and differences. *Cellular and Molecular Life Sciences* **70**, 3813–3827 (2013).
169. Jaillon, S. *et al.* Neutrophil diversity and plasticity in tumour progression and therapy. *Nature Reviews Cancer* 2020 20:9 **20**, 485–503 (2020).
170. Coffelt, S. B., Wellenstein, M. D. & de Visser, K. E. Neutrophils in cancer: neutral no more. *Nature Reviews Cancer* 2016 16:7 **16**, 431–446 (2016).

171. Montaldo, E. *et al.* Cellular and transcriptional dynamics of human neutrophils at steady state and upon stress. *Nature Immunology* 2022 23:10 **23**, 1470–1483 (2022).
172. Hedrick, C. C. & Malanchi, I. Neutrophils in cancer: heterogeneous and multifaceted. *Nature Reviews Immunology* 2021 22:3 **22**, 173–187 (2021).
173. Gentles, A. J. *et al.* The prognostic landscape of genes and infiltrating immune cells across human cancers. *Nature Medicine* 2015 21:8 **21**, 938–945 (2015).
174. Finisguerra, V. *et al.* MET is required for the recruitment of anti-tumoural neutrophils. *Nature* 2015 522:7556 **522**, 349–353 (2015).
175. Fridlender, Z. G. *et al.* Polarization of Tumor-Associated Neutrophil Phenotype by TGF- β : ‘N1’ versus ‘N2’ TAN. *Cancer Cell* **16**, 183–194 (2009).
176. van Egmond, M. & Bakema, J. E. Neutrophils as effector cells for antibody-based immunotherapy of cancer. *Semin Cancer Biol* **23**, 190–199 (2013).
177. Brinkmann, V. *et al.* Neutrophil extracellular traps kill bacteria. *Science* **303**, 1532–1535 (2004).
178. Munir, H. *et al.* Stromal-driven and Amyloid β -dependent induction of neutrophil extracellular traps modulates tumor growth. *Nature Communications* 2021 12:1 **12**, 1–16 (2021).
179. Demers, M. *et al.* Priming of neutrophils toward NETosis promotes tumor growth. *Oncoimmunology* **5**, (2016).
180. Xia, X. *et al.* Neutrophil extracellular traps promote metastasis in gastric cancer patients with postoperative abdominal infectious complications. *Nature Communications* 2022 13:1 **13**, 1–14 (2022).
181. Yang, L. *et al.* DNA of neutrophil extracellular traps promotes cancer metastasis via CCDC25. *Nature* 2020 583:7814 **583**, 133–138 (2020).
182. Bekes, E. M. *et al.* Tumor-Recruited Neutrophils and Neutrophil TIMP-Free MMP-9 Regulate Coordinately the Levels of Tumor Angiogenesis and Efficiency of Malignant Cell Intravasation. *Am J Pathol* **179**, 1455–1470 (2011).
183. Kennel, K. B. & Greten, F. R. Immune cell - produced ROS and their impact on tumor growth and metastasis. *Redox Biol* **42**, 101891 (2021).
184. Houghton, A. M. G. *et al.* Neutrophil elastase-mediated degradation of IRS-1 accelerates lung tumor growth. *Nature Medicine* 2010 16:2 **16**, 219–223 (2010).
185. Albregues, J. *et al.* Neutrophil extracellular traps produced during inflammation awaken dormant cancer cells in mice. *Science* (1979) **361**, (2018).
186. Li, P. *et al.* Dual roles of neutrophils in metastatic colonization are governed by the host NK cell status. *Nature Communications* 2020 11:1 **11**, 1–14 (2020).

187. Xiao, Y. *et al.* Cathepsin C promotes breast cancer lung metastasis by modulating neutrophil infiltration and neutrophil extracellular trap formation. *Cancer Cell* **39**, 423–437.e7 (2021).
188. Wculek, S. K. & Malanchi, I. Neutrophils support lung colonization of metastasis-initiating breast cancer cells. *Nature* *2015 528:7582* **528**, 413–417 (2015).
189. Calzetti, F. *et al.* CD66b–CD64dimCD115– cells in the human bone marrow represent neutrophil-committed progenitors. *Nature Immunology* *2022 23:5* **23**, 679–691 (2022).
190. Aarts, C. E. M. *et al.* Activated neutrophils exert myeloid-derived suppressor cell activity damaging T cells beyond repair. *Blood Adv* **3**, 3562–3574 (2019).
191. Germann, M. *et al.* Neutrophils suppress tumor-infiltrating T cells in colon cancer via matrix metalloproteinase-mediated activation of TGF β . *EMBO Mol Med* **12**, (2020).
192. Coffelt, S. B. *et al.* IL17-producing $\gamma\delta$ T cells and neutrophils conspire to promote breast cancer metastasis. *Nature* *2015 522:7556* **522**, 345–348 (2015).
193. Teijeira, Á. *et al.* CXCR1 and CXCR2 Chemokine Receptor Agonists Produced by Tumors Induce Neutrophil Extracellular Traps that Interfere with Immune Cytotoxicity. *Immunity* **52**, 856–871.e8 (2020).
194. Wang, H. *et al.* Regulatory T-cell and neutrophil extracellular trap interaction contributes to carcinogenesis in non-alcoholic steatohepatitis. *J Hepatol* **75**, 1271–1283 (2021).
195. Oberg, H. H., Wesch, D., Kalyan, S. & Kabelitz, D. Regulatory interactions between neutrophils, tumor cells and T Cells. *Front Immunol* **10**, 1690 (2019).
196. Singhal, S. *et al.* Origin and Role of a Subset of Tumor-Associated Neutrophils with Antigen-Presenting Cell Features in Early-Stage Human Lung Cancer. *Cancer Cell* **30**, 120–135 (2016).
197. Pylaeva, E. *et al.* During early stages of cancer, neutrophils initiate anti-tumor immune responses in tumor-draining lymph nodes. *Cell Rep* **40**, (2022).
198. Governa, V. *et al.* The Interplay Between Neutrophils and CD8+ T Cells Improves Survival in Human Colorectal Cancer. *Clin Cancer Res* **23**, 3847–3858 (2017).
199. Schena, M., Shalon, D., Davis, R. W. & Brown, P. O. Quantitative monitoring of gene expression patterns with a complementary DNA microarray. *Science* (1979) **270**, 467–470 (1995).
200. Stark, R., Grzelak, M. & Hadfield, J. RNA sequencing: the teenage years. *Nature Reviews Genetics* *2019 20:11* **20**, 631–656 (2019).

201. de Simone, M., Rossetti, G. & Pagani, M. Single Cell T Cell Receptor Sequencing: Techniques and Future Challenges. *Front Immunol* **9**, (2018).
202. Cusanovich, D. A. *et al.* A Single-Cell Atlas of In Vivo Mammalian Chromatin Accessibility. *Cell* **174**, 1309-1324.e18 (2018).
203. Buenrostro, J. D. *et al.* Integrated Single-Cell Analysis Maps the Continuous Regulatory Landscape of Human Hematopoietic Differentiation. *Cell* **173**, 1535-1548.e16 (2018).
204. Rotem, A. *et al.* Single-cell ChIP-seq reveals cell subpopulations defined by chromatin state. *Nat Biotechnol* **33**, 1165–1172 (2015).
205. Ramani, V. *et al.* Sci-Hi-C: A single-cell Hi-C method for mapping 3D genome organization in large number of single cells. *Methods* **170**, 61–68 (2020).
206. Belton, J. M. *et al.* Hi-C: A comprehensive technique to capture the conformation of genomes. *Methods* **58**, 268–276 (2012).
207. Botta, C. *et al.* FlowCT for the analysis of large immunophenotypic data sets and biomarker discovery in cancer immunology. *Blood Adv* **6**, 690–703 (2022).
208. Gadalla, R. *et al.* Validation of CyTOF against flow cytometry for immunological studies and monitoring of human cancer clinical trials. *Front Oncol* **9**, 415 (2019).
209. Wang, F. *et al.* RNAscope: a novel in situ RNA analysis platform for formalin-fixed, paraffin-embedded tissues. *J Mol Diagn* **14**, 22–29 (2012).
210. Amir, E. A. D. *et al.* viSNE enables visualization of high dimensional single-cell data and reveals phenotypic heterogeneity of leukemia. *Nature Biotechnology* **2013** 31:6 **31**, 545–552 (2013).
211. Becht, E. *et al.* Dimensionality reduction for visualizing single-cell data using UMAP. *Nature Biotechnology* **2018** 37:1 **37**, 38–44 (2018).
212. Lugli, E., Zanon, V., Mavilio, D. & Roberto, A. FACS analysis of memory T lymphocytes. *Methods in Molecular Biology* **1514**, 31–47 (2017).
213. Quintelier, K. *et al.* Analyzing high-dimensional cytometry data using FlowSOM. *Nature Protocols* **2021** 16:8 **16**, 3775–3801 (2021).
214. Levine, J. H. *et al.* Data-Driven Phenotypic Dissection of AML Reveals Progenitor-like Cells that Correlate with Prognosis. *Cell* **162**, 184–197 (2015).
215. Tiberti, S. *et al.* GZMK^{high} CD8⁺ T effector memory cells are associated with CD15^{high} neutrophil abundance in non-metastatic colorectal tumors and predict poor clinical outcome. *Nature Communications* **2022** 13:1 **13**, 1–20 (2022).

216. Butler, A., Hoffman, P., Smibert, P., Papalexi, E. & Satija, R. Integrating single-cell transcriptomic data across different conditions, technologies, and species. *Nature Biotechnology* 2018 36:5 **36**, 411–420 (2018).
217. Trapnell, C. *et al.* The dynamics and regulators of cell fate decisions are revealed by pseudotemporal ordering of single cells. *Nat Biotechnol* **32**, 381–386 (2014).
218. Romero, P. *et al.* Four Functionally Distinct Populations of Human Effector-Memory CD8⁺ T Lymphocytes. *The Journal of Immunology* **178**, 4112–4119 (2007).
219. Godfrey, D. I., Koay, H. F., McCluskey, J. & Gherardin, N. A. The biology and functional importance of MAIT cells. *Nature Immunology* 2019 20:9 **20**, 1110–1128 (2019).
220. Lee, Y. J. *et al.* CD39⁺ tissue-resident memory CD8⁺ T cells with a clonal overlap across compartments mediate antitumor immunity in breast cancer. *Sci Immunol* **7**, eabn8390 (2022).
221. Chow, A. *et al.* The ectonucleotidase CD39 identifies tumor-reactive CD8⁺ T cells predictive of immune checkpoint blockade efficacy in human lung cancer. *Immunity* **56**, 93-106.e6 (2023).
222. Caushi, J. X. *et al.* Transcriptional programs of neoantigen-specific TIL in anti-PD-1-treated lung cancers. *Nature* 2021 596:7870 **596**, 126–132 (2021).
223. Hornburg, M. *et al.* Single-cell dissection of cellular components and interactions shaping the tumor immune phenotypes in ovarian cancer. *Cancer Cell* **39**, 928-944.e6 (2021).
224. Bengsch, B. *et al.* Epigenomic-Guided Mass Cytometry Profiling Reveals Disease-Specific Features of Exhausted CD8 T Cells. *Immunity* **48**, 1029-1045.e5 (2018).
225. van Aalderen, M. C. *et al.* Label-free Analysis of CD8⁺ T Cell Subset Proteomes Supports a Progressive Differentiation Model of Human-Virus-Specific T Cells. *Cell Rep* **19**, 1068–1079 (2017).
226. Gustafson, M. P. *et al.* A Method for Identification and Analysis of Non-Overlapping Myeloid Immunophenotypes in Humans. *PLoS One* **10**, e0121546 (2015).
227. Bronte, V. *et al.* Recommendations for myeloid-derived suppressor cell nomenclature and characterization standards. *Nature Communications* 2016 7:1 **7**, 1–10 (2016).
228. Marini, O. *et al.* Mature CD10⁺ and immature CD10[−] neutrophils present in G-CSF-treated donors display opposite effects on T cells. *Blood* **129**, 1343–1356 (2017).

229. Zhong, J., Li, Q., Luo, H. & Holmdahl, R. Neutrophil-derived reactive oxygen species promote tumor colonization. *Communications Biology* 2021 4:1 **4**, 1–7 (2021).
230. Uhl, B. *et al.* Aged neutrophils contribute to the first line of defense in the acute inflammatory response. *Blood* **128**, 2327 (2016).
231. Cox, G., Crossley, J. & Xing, Z. Macrophage engulfment of apoptotic neutrophils contributes to the resolution of acute pulmonary inflammation in vivo. *Am J Respir Cell Mol Biol* **12**, 232–237 (1995).
232. Grigg, J. M., Silverman, M., Savill, J. S., Sarraf, C. & Haslett, C. Neutrophil apoptosis and clearance from neonatal lungs. *The Lancet* **338**, 720–722 (1991).
233. Buckley, C. D. *et al.* Identification of a phenotypically and functionally distinct population of long-lived neutrophils in a model of reverse endothelial migration. *J Leukoc Biol* **79**, 303–311 (2006).
234. Robertson, A. L. *et al.* A zebrafish compound screen reveals modulation of neutrophil reverse migration as an anti-inflammatory mechanism. *Sci Transl Med* **6**, (2014).
235. Wang, J. *et al.* Visualizing the function and fate of neutrophils in sterile injury and repair. *Science* (1979) **358**, 111–116 (2017).
236. Woodfin, A. *et al.* The junctional adhesion molecule JAM-C regulates polarized transendothelial migration of neutrophils in vivo. *Nature Immunology* 2011 12:8 **12**, 761–769 (2011).
237. Senra, L. *et al.* IL17E (IL25) Enhances Innate Immune Responses during Skin Inflammation. *Journal of Investigative Dermatology* **139**, 1732-1742.e17 (2019).
238. Fort, M. M. *et al.* IL25 Induces IL4, IL5, and IL13 and Th2-associated pathologies in vivo. *Immunity* **15**, 985–995 (2001).
239. Caruso, R. *et al.* Interleukin-25 Inhibits Interleukin-12 Production and Th1 Cell-Driven Inflammation in the Gut. *Gastroenterology* **136**, 2270–2279 (2009).
240. Moore, K. W., de Waal Malefyt, R., Coffman, R. L. & O’Garra, A. Interleukin-10 and the Interleukin-10 Receptor. <https://doi.org/10.1146/annurev.immunol.19.1.683> **19**, 683–765 (2003).
241. Kyo, S., Kanaya, T., Takakura, M. & Inoue, M. A Case of Cervical Cancer with Aggressive Tumor Growth: Possible Autocrine Growth Stimulation by G-CSF and IL6. *Gynecol Oncol* **78**, 383–387 (2000).
242. Joshita, S. *et al.* Granulocyte-Colony Stimulating Factor-Producing Pancreatic Adenosquamous Carcinoma Showing Aggressive Clinical Course. *Internal Medicine* **48**, 687–691 (2009).

243. Gholamin, M. *et al.* Overexpression and interactions of interleukin-10, transforming growth factor β , and vascular endothelial growth factor in esophageal squamous cell carcinoma. *World J Surg* **33**, 1439–1445 (2009).
244. Gerlini, G. *et al.* Metastatic melanoma secreted IL10 down-regulates CD1 molecules on dendritic cells in metastatic tumor lesions. *American Journal of Pathology* **165**, 1853–1863 (2004).
245. Vallböhmer, D. & Lenz, H. J. Epidermal growth factor receptor as a target for chemotherapy. *Clin Colorectal Cancer* **5**, S19–S27 (2005).
246. Kojima, Y. *et al.* Autocrine TGF- β and stromal cell-derived factor-1 (SDF-1) signaling drives the evolution of tumor-promoting mammary stromal myofibroblasts. *Proc Natl Acad Sci U S A* **107**, 20009–20014 (2010).
247. Suratt, B. T. *et al.* Role of the CXCR4/SDF-1 chemokine axis in circulating neutrophil homeostasis. *Blood* **104**, 565–571 (2004).
248. Silvestre-Roig, C., Hidalgo, A. & Soehnlein, O. Neutrophil heterogeneity: implications for homeostasis and pathogenesis. *Blood* **127**, 2173–2181 (2016).
249. Sangaletti, S. *et al.* Defective stromal remodeling and neutrophil extracellular traps in lymphoid tissues favor the transition from autoimmunity to lymphomas. *Cancer Discov* **4**, 110–129 (2014).
250. Eruslanov, E. B. *et al.* Tumor-associated neutrophils stimulate T cell responses in early-stage human lung cancer. *J Clin Invest* **124**, 5466–5480 (2014).
251. Li, P. *et al.* Lung mesenchymal cells elicit lipid storage in neutrophils that fuel breast cancer lung metastasis. *Nature Immunology* **21**, 1444–1455 (2020).
252. Seddiki, N. *et al.* Expression of interleukin (IL)-2 and IL7 receptors discriminates between human regulatory and activated T cells. *Journal of Experimental Medicine* **203**, 1693–1700 (2006).
253. Capucetti, A., Albano, F. & Bonecchi, R. Multiple Roles for Chemokines in Neutrophil Biology. *Front Immunol* **11**, 1259 (2020).
254. Boivin, G. *et al.* Durable and controlled depletion of neutrophils in mice. *Nature Communications* **11**, 1–9 (2020).
255. Zeisberg, M. & Neilson, E. G. Biomarkers for epithelial-mesenchymal transitions. *J Clin Invest* **119**, 1429–1437 (2009).
256. Huber, M. A., Kraut, N. & Beug, H. Molecular requirements for epithelial–mesenchymal transition during tumor progression. *Curr Opin Cell Biol* **17**, 548–558 (2005).

257. Roelands, J. *et al.* Immunogenomic Classification of Colorectal Cancer and Therapeutic Implications. *Int J Mol Sci* **18**, (2017).
258. Zhang, L. *et al.* Single-Cell Analyses Inform Mechanisms of Myeloid-Targeted Therapies in Colon Cancer. *Cell* **181**, 442-459.e29 (2020).
259. Lee, H. O. *et al.* Lineage-dependent gene expression programs influence the immune landscape of colorectal cancer. *Nature Genetics* **2020 52:6 52**, 594–603 (2020).
260. Pelka, K. *et al.* Spatially organized multicellular immune hubs in human colorectal cancer. *Cell* **184**, 4734-4752.e20 (2021).
261. Shaul, M. E. & Fridlender, Z. G. Tumour-associated neutrophils in patients with cancer. *Nature Reviews Clinical Oncology* **2019 16:10 16**, 601–620 (2019).
262. Mantovani, A., Cassatella, M. A., Costantini, C. & Jaillon, S. Neutrophils in the activation and regulation of innate and adaptive immunity. *Nature Reviews Immunology* **2011 11:8 11**, 519–531 (2011).
263. Galdiero, M. R., Varricchi, G., Loffredo, S., Mantovani, A. & Marone, G. Roles of neutrophils in cancer growth and progression. *J Leukoc Biol* **103**, 457–464 (2018).
264. Wu, P. *et al.* $\gamma\delta$ T17 cells promote the accumulation and expansion of myeloid-derived suppressor cells in human colorectal cancer. *Immunity* **40**, 785–800 (2014).
265. Hart, S. P., Ross, J. A., Ross, K., Haslett, C. & Dransfield, I. Molecular characterization of the surface of apoptotic neutrophils: Implications for functional downregulation and recognition by phagocytes. *Cell Death & Differentiation* **2000 7:5 7**, 493–503 (2000).
266. Rock, K. L., Latz, E., Ontiveros, F. & Kono, H. The Sterile Inflammatory Response. <https://doi.org/10.1146/annurev-immunol-030409-101311> **28**, 321–342 (2010).
267. Lawrence, S. M., Corriden, R. & Nizet, V. The Ontogeny of a Neutrophil: Mechanisms of Granulopoiesis and Homeostasis. *Microbiology and Molecular Biology Reviews* **82**, (2018).
268. Peng, Z. *et al.* Tumors exploit CXCR4^{hi}CD62L^{lo} aged neutrophils to facilitate metastatic spread. *Oncoimmunology* **10**, (2021).
269. Isles, H. M. *et al.* The CXCL12/CXCR4 Signaling Axis Retains Neutrophils at Inflammatory Sites in Zebrafish. *Front Immunol* **10**, 1784 (2019).
270. Chiou, S. H. *et al.* Global analysis of shared T cell specificities in human non-small cell lung cancer enables HLA inference and antigen discovery. *Immunity* **54**, 586-602.e8 (2021).
271. Corridoni, D. *et al.* Single-cell atlas of colonic CD8⁺ T cells in ulcerative colitis. *Nature Medicine* **2020 26:9 26**, 1480–1490 (2020).

272. Doering, T. A. *et al.* Network Analysis Reveals Centrally Connected Genes and Pathways Involved in CD8⁺ T Cell Exhaustion versus Memory. *Immunity* **37**, 1130–1144 (2012).
273. Hawiger, D., Wan, Y. Y., Eynon, E. E. & Flavell, R. A. The transcription cofactor Hopx is required for regulatory T cell function in dendritic cell–mediated peripheral T cell unresponsiveness. *Nature Immunology* *2010 11:10* **11**, 962–968 (2010).
274. Gavin, M. A., Clarke, S. R., Negrou, E., Gallegos, A. & Rudensky, A. Homeostasis and anergy of CD4⁺CD25⁺ suppressor T cells in vivo. *Nature Immunology* *2001 3:1* **3**, 33–41 (2001).
275. Alpan, O., Bachelder, E., Isil, E., Arnheiter, H. & Matzinger, P. ‘Educated’ dendritic cells act as messengers from memory to naive T helper cells. *Nature Immunology* *2004 5:6* **5**, 615–622 (2004).
276. Wensink, A. C., Hack, C. E. & Bovenschen, N. Granzymes Regulate Proinflammatory Cytokine Responses. *The Journal of Immunology* **194**, 491–497 (2015).

ARTICLE

Accumulation of long-chain fatty acids in the tumor microenvironment drives dysfunction in intrapancreatic CD8⁺ T cells

Teresa Manzo^{1,2}, Boone M. Prentice³, Kristin G. Anderson^{4,5}, Ayush Raman², Aislyn Schalck⁶, Gabriela S. Codreanu⁷, Carina B. Nava Lauson¹, Silvia Tiberti¹, Andrea Raimondi⁸, Marissa A. Jones³, Michelle Reyzer³, Breanna M. Bates^{4,5}, Jeffrey M. Spraggins³, Nathan H. Patterson³, John A. McLean⁷, Kunal Rai², Carlo Tacchetti⁸, Sara Tucci¹⁰, Jennifer A. Wargo^{2,11}, Simona Rodighiero¹, Karen Clise-Dwyer⁹, Stacy D. Sherrod⁷, Michael Kim¹¹, Nicholas E. Navin⁶, Richard M. Caprioli³, Philip D. Greenberg^{4,5}, Giulio Draetta², and Luigi Nezi^{1,2}

CD8⁺ T cells are master effectors of antitumor immunity, and their presence at tumor sites correlates with favorable outcomes. However, metabolic constraints imposed by the tumor microenvironment (TME) can dampen their ability to control tumor progression. We describe lipid accumulation in the TME areas of pancreatic ductal adenocarcinoma (PDA) populated by CD8⁺ T cells infiltrating both murine and human tumors. In this lipid-rich but otherwise nutrient-poor TME, access to using lipid metabolism becomes particularly valuable for sustaining cell functions. Here, we found that intrapancreatic CD8⁺ T cells progressively accumulate specific long-chain fatty acids (LCFAs), which, rather than provide a fuel source, impair their mitochondrial function and trigger major transcriptional reprogramming of pathways involved in lipid metabolism, with the subsequent reduction of fatty acid catabolism. In particular, intrapancreatic CD8⁺ T cells specifically exhibit down-regulation of the very-long-chain acyl-CoA dehydrogenase (VLCAD) enzyme, which exacerbates accumulation of LCFAs and very-long-chain fatty acids (VLCFAs) that mediate lipotoxicity. Metabolic reprogramming of tumor-specific T cells through enforced expression of *ACADVL* enabled enhanced intratumoral T cell survival and persistence in an engineered mouse model of PDA, overcoming one of the major hurdles to immunotherapy for PDA.

Introduction

The advent of immunotherapy has revolutionized cancer treatment by inducing, providing, and/or reactivating antitumor T cells. Therapeutic results have been heterogeneous, with better outcomes generally correlating with the ability of tumor-specific T cells to infiltrate the tumor, persist, and retain effector functions. Complete and durable clinical responses have been achieved in patients whose cancers were resistant to available standard treatments (Mellman et al., 2011). Yet, it has met with limited success in most patients with solid tumors (Joyce and Fearon, 2015; Menon et al., 2016), including pancreatic ductal adenocarcinoma (PDA; Guo et al., 2017). Although the overall survival rate in PDA patients appears to correlate with CD8⁺

T cell infiltration (Ene-Obong et al., 2013; Fukunaga et al., 2004; Ino et al., 2013), our knowledge of the mechanisms that regulate the function of these infiltrating T cells in the context of the tumor microenvironment (TME) is still limited.

CD8⁺ T cells are key effectors of antitumor immunity. However, tumor-infiltrating CD8⁺ T cells often acquire an altered state of differentiation referred to as “exhaustion” (Wherry and Kurachi, 2015) and, as a result, fail to control tumor outgrowth. Several studies in both murine models of pancreatic cancer and PDA patients have demonstrated that CD8⁺ T cells are often scarce and, if present, have become dysfunctional (Bailey et al., 2016; Beatty et al., 2015; Clark et al., 2007; Stromnes et al.,

¹Department of Experimental Oncology, IRCCS European Institute of Oncology, Milano, Italy; ²Department of Genomic Medicine, The University of Texas MD Anderson Cancer Center, Houston, TX; ³Department of Biochemistry, Mass Spectrometry Research Center, Department of Chemistry, Department of Pharmacology and Medicine, Vanderbilt University, Nashville, TN; ⁴Clinical Research Division and Program in Immunology, Fred Hutchinson Cancer Research Center, Seattle, WA; ⁵Departments of Medicine/Oncology and Immunology, University of Washington School of Medicine, Seattle, WA; ⁶Department of Genetics and Department of Bioinformatics and Computational Biology, The University of Texas MD Anderson Cancer Center, Houston, TX; ⁷Center for Innovative Technology, Vanderbilt University, Nashville, TN; ⁸Experimental Imaging Center, IRCCS San Raffaele Scientific Institute, San Raffaele Vita-Salute University, Milano, Italy; ⁹Department of Stem Cell Transplantation, The University of Texas MD Anderson Cancer Center, Houston, TX; ¹⁰Laboratory of Clinical Biochemistry and Metabolism Center for Pediatrics and Adolescent Medicine, University of Freiburg, Freiburg, Germany; ¹¹Department of Surgical Oncology, The University of Texas MD Anderson Cancer Center, Houston, TX.

Correspondence to Luigi Nezi: luigi.nezi@ieo.it; Teresa Manzo: teresa.manzo@ieo.it; B.M. Prentice's present address is Department of Chemistry, University of Florida, Gainesville, FL; A. Raman's present address is Broad Institute of MIT and Harvard, Cambridge, MA.

© 2020 Manzo et al. This article is distributed under the terms of an Attribution-Noncommercial-Share Alike-No Mirror Sites license for the first six months after the publication date (see <http://www.rupress.org/terms/>). After six months it is available under a Creative Commons License (Attribution-Noncommercial-Share Alike 4.0 International license, as described at <https://creativecommons.org/licenses/by-nc-sa/4.0/>).

Rockefeller University Press

J. Exp. Med. 2020 Vol. 217 No. 8 e20191920



<https://doi.org/10.1084/jem.20191920> 1 of 22

GZMK^{high} CD8⁺ T effector memory cells are associated with CD15^{high} neutrophil abundance in non-metastatic colorectal tumors and predict poor clinical outcome

Received: 1 December 2021

Accepted: 26 October 2022

Published online: 08 November 2022

 Check for updates

Silvia Tiberti¹, Carlotta Catozzi¹, Ottavio Croci², Mattia Ballerini¹, Danilo Cagnina¹, Chiara Soriani¹, Caterina Scirgolea³, Zheng Gong⁴, Jiatai He^{4,5}, Angeli D. Macandog¹, Amir Nabinejad¹, Carina B. Nava Lauson¹, Arianna Quinte¹, Giovanni Bertalot⁶, Wanda L. Petz⁷, Simona P. Ravenda⁸, Valerio Licursi⁹, Paola Paci¹⁰, Marco Rasponi¹¹, Luca Rotta¹, Nicola Fazio⁷, Guangwen Ren⁴, Uberto Fumagalli-Romario⁷, Martin H. Schaefer¹, Stefano Campaner², Enrico Lugli³, Luigi Nezi^{1,12} ✉ & Teresa Manzo^{1,12} ✉

CD8⁺ T cells are a major prognostic determinant in solid tumors, including colorectal cancer (CRC). However, understanding how the interplay between different immune cells impacts on clinical outcome is still in its infancy. Here, we describe that the interaction of tumor infiltrating neutrophils expressing high levels of CD15 with CD8⁺ T effector memory cells (T_{EM}) correlates with tumor progression. Mechanistically, stromal cell-derived factor-1 (CXCL12/SDF-1) promotes the retention of neutrophils within tumors, increasing the crosstalk with CD8⁺ T cells. As a consequence of the contact-mediated interaction with neutrophils, CD8⁺ T cells are skewed to produce high levels of GZMK, which in turn decreases E-cadherin on the intestinal epithelium and favors tumor progression. Overall, our results highlight the emergence of GZMK^{high} CD8⁺ T_{EM} in non-metastatic CRC tumors as a hallmark driven by the interaction with neutrophils, which could implement current patient stratification and be targeted by novel therapeutics.

Colorectal cancer (CRC) is the third most commonly diagnosed tumor worldwide and a leading cause of cancer related death. Efficacy of treatment and survival are largely dictated by the tumor-node-metastasis (TNM) stage at diagnosis. Tumor contexture has emerged as a major prognostic determinant and a guide to implement therapy outcome^{1,2}. However, 30–40% of surgically resected CRC relapse despite favorable TNM staging and significant lymphocyte infiltration³, become metastatic and patients ultimately die⁴, demonstrating the inadequacy of current stratification.

In this regard, cytotoxic CD8⁺ T cell infiltration has been associated with a better prognosis in CRC and other solid tumors^{5,6} and high levels of memory CD8⁺ T cells prevent early metastatic invasion and are associated with better survival⁷. However, the tumor immune infiltrate is highly heterogeneous and, although the influence of various myeloid cell populations on T cell activity has been reported^{8–10}, the interplay between different cell compartments at the tumor site and their impact on the clinical outcome is just starting being exposed. In particular, tumor-associated neutrophils represent a significant

A full list of affiliations appears at the end of the paper. ✉ e-mail: luigi.nezi@ieo.it; teresa.manzo@ieo.it

The tumor microenvironment drives NK cell metabolic dysfunction leading to impaired antitumor activity

Nicola Tumino¹ | Carina B. Nava Lauson² | Silvia Tiberti² | Francesca Besi³ |
Stefania Martini⁴ | Piera Filomena Fiore³ | Francesca Scodamaglia⁵ |
Maria Cristina Mingari⁴ | Lorenzo Moretta³ | Teresa Manzo² | Paola Vacca¹

¹Immunology Research Area, Innate Lymphoid Cells Unit, Bambino Gesù Children's Hospital IRCCS, Rome, Italy

²Immunometabolism and Cancer Immunotherapy Unit, IRCCS Istituto Europeo di Oncologia, Milan, Italy

³Tumor Immunology, Bambino Gesù Children's Hospital IRCCS, Rome, Italy

⁴UO Immunology, IRCCS Ospedale Policlinico San Martino, Genoa, Italy

⁵SC Pneumologia Ospedale Villa Scassi, ASL3 Genovese, Genoa, Italy

Correspondence

Teresa Manzo, Immunometabolism and Cancer Immunotherapy Unit, IRCCS Istituto Europeo di Oncologia, Milan, Italy.
Email: teresa.manzo@ieo.it

Paola Vacca, Immunology Research Area, Innate Lymphoid Cells Units, Bambino Gesù Children's Hospital IRCCS, Rome, Italy.
Email: paola.vacca@opbg.net

Funding information

Associazione Italiana per la Ricerca sul Cancro, Grant/Award Numbers: 19920, 21147, 21474, Fellowship; Ministero della Salute, Grant/Award Numbers: 5 per mille, Ricerca corrente 2022

Abstract

NK cells represent key players capable of driving antitumor immune responses. However, the potent immunosuppressive activity of the tumor microenvironment (TME) may impair their effector function. Here, we strengthen the importance of metabolic interactions between NK cells and TME and propose metabolic dysfunction as one of the major mechanisms behind NK failure in cancer treatment. In particular, we described that TME has a direct negative impact on NK cell function by disrupting their mitochondrial integrity and function in pediatric and adult patients with primary and metastatic cancer. Our results will help to design new strategies aimed at increasing the NK cell antitumor efficacy by their metabolic reprogramming. In this regard, we reveal an unprecedented role of IL15 in the metabolic reprogramming of NK cells enhancing their antitumor functions. IL15 prevents the inhibitory effect of soluble factors present in TME and restores both the metabolic characteristics and the effector function of NK cells inhibited by exposure to malignant pleural fluid. Thus, we propose here that IL15 may be exploited as a new strategy to metabolically reprogram NK cells with the aim of increasing the efficacy of NK-based immunotherapy in a wide range of currently refractory adult and pediatric solid tumors.

KEYWORDS

metabolic dysfunction, NK cells, tumor immunology, tumor microenvironment

What's new

The tumor microenvironment may hamper the functional activities of tumor-infiltrating immune effector cells by affecting both their antitumor cytotoxicity and metabolic fitness. This study shows that the tumor microenvironment exerts a direct negative impact on NK cells in pediatric and adult patients with primary and metastatic cancer by disrupting the integrity and function of

Abbreviations: ASL, azienda sanitaria locale; ATP, adenosine triphosphate; ECAR, extracellular acidification rate; HD, healthy donors; IL, interleukin; MFI, mean fluorescence intensity; mPE, malignant pleural effusions; NK, natural killer cells; OCR, oxygen consumption rate; OXPHOS, mitochondrial oxidative phosphorylation; PBMC, peripheral blood mononuclear cells; TIGIT, T cell immune receptor with Ig and ITIM domains; TME, tumor microenvironment.

Silvia Tiberti and Carina B. Nava Lauson contributed equally to this work.
Teresa Manzo and Paola Vacca are joint senior authors.

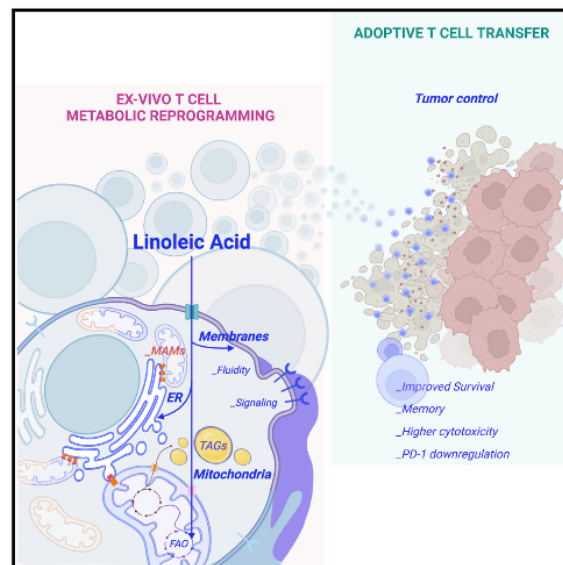
This is an open access article under the terms of the [Creative Commons Attribution-NonCommercial-NoDerivs](https://creativecommons.org/licenses/by-nc-nd/4.0/) License, which permits use and distribution in any medium, provided the original work is properly cited, the use is non-commercial and no modifications or adaptations are made.

© 2022 The Authors. *International Journal of Cancer* published by John Wiley & Sons Ltd on behalf of UICC.

Cell Metabolism

Linoleic acid potentiates CD8⁺ T cell metabolic fitness and antitumor immunity

Graphical abstract



Authors

Carina B. Nava Lauson, Silvia Tiberti, Paola A. Corsetto, ..., Simona Rodighiero, Luigi Nezi, Teresa Manzo

Correspondence

teresa.manzo@ieo.it

In brief

Nava-Lauson et al. report that linoleic acid potentiates antitumor function of CD8⁺ T cells by operating a profound metabolic reprogramming that protects from exhaustion and pushes toward a memory phenotype with superior cytotoxic functions. LA-redirection CD8⁺ T cells are empowered with an improved metabolic and functional fitness within the TME, thereby improving efficacy of ACT-based therapy.

Highlights

- Linoleic acid (LA) improves “quality” and “quantity” of CTL mitochondria
- LA redirects CTL away from exhaustion and toward a memory-like phenotype
- LA fosters MERC formation and harnesses CTL with superior effector functions
- LA potentiates antitumor CTL response and improves ACT efficacy

Nava Lauson et al., 2023, Cell Metabolism 35, 1–18
 April 4, 2023 © 2023 The Author(s). Published by Elsevier Inc.
<https://doi.org/10.1016/j.cmet.2023.02.013>